Tuning oxidation states of terbium and europium towards high purity terbium-161 and samarium-153 for medical applications

MERYEM ÖZGE ARMAN

Supervisors:

Prof. Dr. Koen Binnemans
Prof. Dr. Thomas Cardinaels

Mentors:

Dr. Ing. Bart Geboes
Dr. Karen Van Hecke

Examination committee:

Prof. Dr. Erik Nies
Prof. Dr. Annelies Delabie
Prof. Dr. Edward Matthijs
Dr. Sofía Riaño Torres
Prof. Dr. Ing. Tom Breugelmans

Dissertation presented in partial fulfilment of the requirements for the degree of Doctor of Science (PhD): Chemistry

September 2023

© 2023 KU Leuven - Faculty of Science Uitgegeven in eigen beheer, Meryem Özge Arman, Leuven

Alle rechten voorbehouden. Niets uit deze uitgave mag worden vermenigvuldigd en/of openbaar gemaakt worden door middel van druk, fotokopie, microfilm, elektronisch of op welke andere wijze ook zonder voorafgaande schriftelijke toestemming van de uitgever.

All rights reserved. No part of the publication may be reproduced in any form by print, photoprint, microfilm, electronic or any other means without written permission from the publisher.

Acknowledgements

This PhD dissertation is the result of the research that was performed in a project that was collaborated between SCK CEN and KU Leuven. The project was funded by the SCK CEN Academy, and Research Foundation – Flanders (FWO) – SBO project Terbium Isotopes for Medical Applications in Flanders (Tb – IRMA – V, Grant number S005019N).

First of all, I would like to sincerely thank my supervisors Prof. Dr. Koen Binnemans and Prof. Dr. Thomas Cardinaels for making it possible to work on this research project, their support, guidance and understanding throughout these years. I really appreciate all the scientific contributions, and feel fortunate to had the opportunity to work with you and learn from you.

I also feel grateful to work with my mentors Dr. Ing. Bart Geboes and Dr. Karen Van Hecke along this challenging road. Bart, thank you very much for putting up with me, not only scientifically but also mentally supporting me all these years. I feel extremely lucky to have you as my mentor, and really envy your knowledge and enthusiasm on electrochemistry. I wish one day I would reach just a quarter of your level. Karen, thank you so much for your support especially in the separation chemistry part of my thesis. I really appreciate your all help and also moral support.

I would also like to thank all the jury members of the Examination Committee, Prof. Dr. Erik Nies, Prof. Dr. Annelies Delabie, Prof. Dr. Edward Matthijs, Dr. Sofia Riaño Torres and Prof. Dr. Ing. Tom Breugelmans for their time to read the thesis, for their valuable inputs and advices to improve the quality of this thesis.

Within these years I had a lot of colleagues and friends come and go, that I would like to show my gratitude for making me achieve this accomplishment today. To start with, I would like to thank my first office-mates Michiel, Peter, Christian and Liliane for helping me survive my first year at SCK, for all the discussions, coffee breaks and fun moments. You all were very understanding, helpful, kind and welcoming, creating a very nice office environment. Now that I have seen all you guys finishing your PhDs one by one, and Liliane being retired, I can finally join the team! I would also like to thank Bart Verlinden, aka my buddy Bart, that helped me even before I had to move to Mol, and being such a nice friend since then, listening all my complaints.

I would also like to thank the RCY and NURA colleagues, Steven, Ken, Jolan, Marijke, Karen, Maarten, Tomas, Adrien, Wendy - especially Michiel, Stijn, and `the other` Michiel, for helping me with the experiments with activity, letting me share the fumehood and instruments, and Stijn – many thanks for arranging the irradiations. Sorry for being such a pain in the last months, and thanks a lot for helping me out. Now that `activity` is mentioned, great thanks to Eddy and Job, for helping me out with all the troubles I encounter and being so patient with my non-stop requests.

I would also thank to the PhD colleagues that understand and share the suffer: Irwin, Diana, Tom, Filip, Hilde, Hongshan and Cedric. Although we have known each other for a limited time, I really enjoyed your accompany and the social activities – that I should`ve attended more often. Han-Hung, thanks a lot for being so helpful and such a kind office-mate. I wish you the best in finishing your PhD as well. Wout and Robin, you guys were the dream team – I can`t thank enough for your help in the gamma measurements and for the moral support in the failures. Since most of my work was full of downs, downs, downs and barely some ups – which I blame you Wout for bringing the bad luck to the lab – I really appreciate all your efforts in helping me. You were such good listeners, and even better complainers about me, but I know you both love me so much and cried a lot after I left :P But don`t worry, I will keep my promise and we will have a raki night soon enough!

Many thanks should also go to my rather new colleagues, the members of SOLVOMET group. Thanks a lot for creating such a welcoming environment, being so helpful and supportive, and making the work so much fun! Although it was a pretty tough year for me, feeling your support helped me a lot to go through things. I feel so lucky to be the part of this group, and also would like to thank Sofia for giving me the opportunity and believing in me as my mentor. Although we spent limited time together, I learned a lot from you, and hope to be such a brilliant scientist like you. I also really appreciate your kindness and helpfulness during the tough times, being so understanding and listening all my troubles.

My lovely friends Canan, Elif, Irmak and Muge aka `pideler`, it is unreal that we know each other since 2009, and still be able to share the same laughter all together. I feel extremely lucky to have you all as my friends, even more than my friends, my sisters. You were always there for me, even though I suck at sharing. But I believe I improved, or after this many years, you just accepted me like that. I don`t say it often, but I love you all, and hope to be

the same old gang in future, celebrating our retirements with you! I wouldn`t be able to cope with all the stress without you, thanks a lot for all your support no matter what!

I wouldn`t be able to be here without the endless support of my family. Annem, benim buradaki başarımda büyük katkın var. Beni desteklediğin için sonsuz teşekkürler. Emeklerini bundan sonra da boşa çıkarmam umuyorum. Abicim, hem maddi hem de manevi desteklerini ödeyemem, her şey için çok çok teşekkürler. Beni her zaman desteklediğin için, her türlü yardıma koştuğun için ve burada okumama vesile olduğun için minnettarım. Senin kadar zeki olamasam da, biraz zorlayarak bu diplomayı almayı başardım. Daha da iyileri Toprak ve Nehir'in olsun. Nazlı abla, desteklerin için sana da çok teşekkür ederim. Burada kalabilmemde senin de payın büyük, bana evini açtığın için ve her türlü desteği sağladığın için çok sağol. Canım Toprak'ım ve Nehir'im, dünyanın en tatlı çocukları, farkında olmasanız da sizinle oyun oynamak ve vakit geçirmek benim en keyif aldığım şey. Sizi çok seviyorum! Umarım her istediğinizi başarırsınız ve hep mutlu olursunuz.

Lastly, I would like to thank my former boyfriend (haha no heart attack please) and now husband Laurens, for his endless support and believing in me. You do deserve the most credit here, making me feel in a safe place, giving me peace of mind whenever I need and helping me to be a better person. I do believe that I wouldn`t be achieving this today without your constant help and motivation. Even now you woke me up to finish this part, so I literally wouldn`t make this without you :P Thank you so much to put up with me, listening all my complaints and be there the moment I need you. You have such a nice heart, and I am so lucky to have you in my life.

Abstract

Radionuclides have a variety of medical applications as radiopharmaceuticals. The most significant and frequent use is in diagnostic imaging to visualize infected, cancerous or damaged areas (e.g. after a heart attack) in the body. More recently, therapeutic radiopharmaceuticals have gained more interest, particularly in cancer treatment, as the ionizing radiation can target and destroy harmful tumor cells in a precise and selective manner. In recent years, various radionuclides from the lanthanide series have been utilized and are investigated in nuclear medicine. Radiolanthanides are highly promising for use in nuclear medicine due to their chemical similarities, allowing for coordination compounds of the same type to be used in a range of diagnostic and therapeutic applications. Terbium, for instance, has four radioisotopes with distinct decay properties, energies, and half-lives that can be utilized in non-invasive theranostic applications. To produce carrier-free terbium-161, highly enriched gadolinium-160 targets are neutron-irradiated in the Belgian Reactor 2 (BR2). Terbium-161 emits low-energy beta (β^-) particles along with gamma (γ) photons, and possesses properties similar to lutetium-177. Moreover, the co-emission of Auger electrons makes terbium-161 even more attractive for β^- and Auger electron therapy.

Another example, samarium-153, is a radiolanthanide that can be effectively used in medicine due to its favorable half-life and stable daughter isotope europium-153, which ensures no significant additional side effects in the human body. It is often coordinated by EDTMP (ethylenediamine tetramethylene phosphonate), sold commercially as Quadramet® and Lexidronam®, used for treatment of painful bone metastases caused by various cancers. The β^- emission of samarium-153 is utilized to destroy harmful cancer cells, and its γ emission is also used in imaging to visualize infected areas in the human skeleton. Like many other medical radioisotopes, samarium-153 can be most efficiently produced in a nuclear research reactor by irradiating a highly enriched target with neutrons in a high thermal neutron flux, resulting in a product with high yield, purity, and specific activity.

In addition to their dominant trivalent oxidation state, some lanthanides can also exist in the divalent or tetravalent oxidation states. This change in valence state alters their chemical properties and make intragroup

lanthanide separations easier. Although hydrated terbium(III) ions typically have a highly positive reduction potential, they can be electrochemically oxidized to their tetravalent state and stabilized in highly concentrated carbonate solutions. Terbium(III) can be oxidized to terbium(IV) in aqueous carbonate, nitrate, and periodate media. To examine the stability of terbium(III) complexes in aqueous electrolytes, spectroscopic and elemental analyses were conducted, with a parametric study focusing on pH, terbium concentration, salt concentration, and applied electrical potentials. The lowest applied potential value to oxidize terbium(III) was +0.9 V vs. Ag/AgCl in periodate medium, while nitrate and periodate media offered poor terbium(IV) stabilization compared to a carbonate medium. Therefore, an aqueous carbonate medium appears to be the most promising medium for developing a separation process based on terbium oxidation state change. Successful separation of terbium(IV) from trivalent lanthanides was achieved performing ion exchange chromatography with the carbonate form of the Dowex-IX8 resin. Sufficient characterization and remarkable reproducibility of the methodology demonstrates the potential of this methodology as a new separation process for the purification of terbium(IV).

Finally, the divalent oxidation state of europium was investigated based on the electrochemical reduction of europium(III) to europium(II) in aqueous nitrate, chloride and perchlorate media. The kinetic parameters were studied using a rotating disk electrode. As a next step, separation of samarium from europium was achieved using a TEVA column in nitrate form. The feasibility of this separation method was tested using the samarium-153 and europium-152 radioisotopes in the same concentration ratio as the concentration ratio of these elements present in a dissolved irradiated enriched samarium-152 target.

Beknopte samenvatting

Radionucliden hebben verschillende medische toepassingen als radiofarmaca. Het belangrijkste en meest frequente gebruik is voor diagnostische doeleinden om geïnfecteerde, kankerachtige of beschadigde weefsels (vb. na een hartaanval) in beeld te brengen. Meer recent is de belangstelling voor therapeutische radiofarmaca toegenomen, in het bijzonder voor de behandeling van kanker, omdat de ioniserende straling op een precieze en selectieve manier schadelijke tumorcellen kan treffen en vernietigen. In de nucleaire geneeskunde worden de afgelopen jaren verschillende isotopen uit de lanthanidenreeks gebruikt. Radiolanthaniden zijn veelbelovend voor gebruik in de nucleaire geneeskunde vanwege hun gelijkaardige chemische eigenschappen, waardoor coördinatieverbindingen van hetzelfde type kunnen worden gebruikt in een reeks diagnostische en therapeutische toepassingen. Terbium heeft bijvoorbeeld vier radio-isotopen met verschillende vervaleigenschappen, energieën en halfwaardetijden die kunnen worden gebruikt in niet-invasieve theranostische toepassingen. Om dragervrij terbium-161 te produceren, worden hoogaangerijkte gadolinium-160-targets met neutronen bestraald in de Belgian Reactor 2 (BR2). Dit radionuclide zendt beta (β) deeltjes met lage energie uit samen met gamma (γ) fotonen en heeft eigenschappen die vergelijkbaar zijn met lutetium-177. Bovendien maakt de co-emissie van Auger-elektronen terbium-161 nog aantrekkelijker voor β- en Auger-elektronentherapie.

Samarium-153 is een ander voorbeeld van een radiolanthanide die effectief kan worden gebruikt in de geneeskunde vanwege de gunstige halfwaardetijd en het stabiele dochternuclide europium-153, dat niet zorgt voor significante extra bijwerkingen in het menselijk lichaam. Het wordt vaak gecoördineerd door EDTMP (ethyleendiaminetetramethyleenfosfonaat), commercieel verkocht als Quadramet® en Lexidronam®, en wordt toegepast voor de behandeling van pijnlijke botmetastasen veroorzaakt door verschillende vormen van kanker. De β-emissie van samarium-153 wordt gebruikt om schadelijke kankercellen te vernietigen, en de γ-emissie wordt ook gebruikt bij beeldvorming om geïnfecteerde gebieden in het menselijk skelet zichtbaar te maken. Net als veel andere medische radio-isotopen kan samarium-153 het meest efficiënt worden geproduceerd in een nucleaire

onderzoeksreactor door een sterk aangerijkt target te bestralen met neutronen in een hoge thermische neutronenflux, wat resulteert in een product met een hoge opbrengst, zuiverheid en specifieke activiteit.

Naast hun dominante driewaardige oxidatietoestand, kunnen sommige lanthaniden ook voorkomen in de tweewaardige of vierwaardige oxidatietoestand. Deze verandering in valentietoestand kan hun chemische eigenschappen veranderen en lanthanidenscheidingen binnen de groep gemakkelijker maken. Hoewel gehydrateerde terbium(III) ionen doorgaans een zeer positief reductiepotentieel hebben, kunnen ze elektrochemisch worden geoxideerd tot hun vierwaardige toestand en worden gestabiliseerd in sterk geconcentreerde carbonaatoplossingen. Terbium(III) kan worden geoxideerd tot terbium(IV) in waterige carbonaat-, nitraat- en perjodaatmedia. Om de stabiliteit van terbium(IV) complexen in waterige elektrolyten te onderzoeken, werden spectroscopische en elementaire analyses uitgevoerd, met een parameterstudie gericht op pH, terbiumconcentratie, zoutconcentratie en toegepaste elektrische potentialen. De laagste toegepaste potentiaal om terbium(III) te oxideren was +0.9 V vs. Ag/AgCl in perjodaatmedium, terwijl nitraat- en perjodaatmedia een slechte stabilisatie van terbium(IV) opleverden in vergelijking met het carbonaatmedium. Daarom lijkt waterig carbonaatmedium het meest veelbelovende medium te zijn voor het ontwikkelen van een scheidingsproces op basis van oxidatietoestandsverandering van terbium. Succesvolle scheiding van terbium (IV) van driewaardige lanthaniden werd bereikt door ionenuitwisselingschromatografie uit te voeren met de carbonaatvorm van Dowex-IX8-hars. De volledige karakterisering en opmerkelijke reproduceerbaarheid van de methodologie demonstreert het potentieel van deze methodologie als een nieuw scheidingsproces voor de opzuivering van terbium(IV).

Verder werd de tweewaardige oxidatietoestand onderzocht op basis van een elektrochemische reductie van europium(III) naar europium(II) in waterige nitraat-, chloride- en perchloraatmedia. De kinetische parameters werden bestudeerd met behulp van een roterende schijfelektrode. Als volgende stap werd de scheiding van Sm van Eu bereikt met behulp van een TEVA-kolom in nitraatvorm. De haalbaarheid van deze scheidingsmethode is getest met behulp van de Sm-153 en Eu-152 isotopen in dezelfde verhouding van de kernreactoromstandigheden.

List of abbreviations

α-HIBA	α-hydroxy isobutyric acid
BDD	boron-doped diamond
BFC	bifunctional chelators
BR2	Belgian Reactor 2
CA	carrier-added
CAN	ceric ammonium nitrate
CGE	conducting glass electrode
cGMP	current good manufacturing practices
DEPA	7-[2-(biscarboxymethylamino)ethyl]-4,10-biscarboxy-methyl-1,4,7,10-tetraazacyclododec-1-yl-acetic acid
DGA	diglycolamide
DNA	deoxyribonucleic acid
DOTA	1,4,7,10-tetraazacyclododecane-1,4,7,10-tetraacetic acid
DOTMP	1,4,7,10-tetraazacyclododecane tetramethylene phosphonic acid
DTPA	diethylenetriamine-pentaacetic acid
EDTMP	ethylenediamine tetramethylene phosphonate
EPD	electronic personal dosimeter
HDEHP	di-(2-ethylhexyl) phosphoric acid
HEH[EHP]	2-ethylhexyl phosphonic acid mono-2-ethylhexyl ester
HER	hydrogen evolution reaction
HPIC	high-pressure ion chromatography
HPLC	high performance liquid chromatography
ICP-MS	inductively coupled plasma mass spectrometry
ISCD	inorganic crystal structure database
LCF	linear combination fitting

LET	linear energy transfer
LINAC	linear accelerator
mCRPC	metastatic castration-resistant prostate cancer
MEK	methyl ethyl ketone
NCA	non-carrier-added
NOTA	1,4,7-triazacyclononane-1,4,7-triacetic acid
OSL	optically stimulated luminescence
PET	positron emission tomography
PSMA	prostate-specific membrane antigen
RDE	rotating disk electrode
RVC	reticulated vitreous carbon
SCE	standard calomel electrode
SCK CEN	Studiecentrum voor Kernenergie Centre d'Etude de l'Energy Nucléaire (Belgian Nuclear Research Center)
SHE	standard hydrogen electrode
SILP	solid ionic liquid phase
SPECT	single-photon emission computed tomography
TAT	targeted alpha therapy
TBP	tri-*n*-butyl phosphate
TEAP	tetraethylammonium perchlorate
TETA	1,4,8,11-tetraazacyclotetradecane-1,4,8,11-tetraacetic acid
TEVA	tetravalent actinide
TODGA	N,N,N',N'-tetraoctyldiglycolamide
UV-Vis	ultraviolet-visible
WHO	World Health Organization
XANES	X-ray absorption near Edge structure
XAS	X-ray absorption spectroscopy
XRD	X-ray diffractometry

List of symbols

$t_{1/2}$	half-life
A	electrode surface area
(n, y)	neutron irradiation followed by gamma decay
σ_{th}	cross section for interaction with thermal neutrons
α	charge transfer coefficient
Bq	becquerel
BV	bed volume
C	concentration
^0C	Celsius
D	diffusion coefficient
ΔE_p	peak separation potential
e^-	electron
$E_\beta{}^{max}$	maximum beta energy
E_0	standard reduction potential
$E_{p/2}{}^c$	cathodic half-peak potential
$E_p{}^c$	cathodic peak potential
F	Faraday`s constant
I	current
i_k	kinetic current
i_l	limiting current
i_{pc}	cathodic peak current
K	Kelvin
k	rate constant
Ln(III)	trivalent lanthanide

n	number of exchanged electrons (electrochemistry)
n	neutron (radiation chemistry)
nα	the number of electrons transferred in the rate determining step
ø	diameter
Φ_{th}	thermal neutron flux
Q	charge
R	universal gas constant
t	time
T	temperature
v	potential sweep rate
ν	kinematic viscosity
α	alpha particle
β^-	beta particle (beta minus particle)
β^+	beta plus particle (positron)
γ	gamma radiation
ω	angular frequency

List of figures

Figure 1.1. Schematic representation of the design of a radiopharmaceutical. 1
Figure 1.2. Chemical structures of representative chelators used in radiopharmaceuticals. 2
Figure 1.3. Examples of lanthanides coordinating with chelators a) trivalent lanthanide ion coordination with DOTA b) ^{153}Sm-EDTMP complex, known as Quadramet®. 4
Figure 1.4. Overview of the different steps in the production route of a radiopharmaceutical. 5
Figure 1.5. Representation of LET of different emissions on DNA strand. 6
Figure 1.6. Radiolanthanides used in nuclear medicine. Adapted from Kostelnik *et al.*[5] 10
Figure 1.7. Non-carrier added production route of ^{161}Tb from ^{160}Gd target. 16
Figure 1.8. Production route of ^{153}Sm via neutron capture using ^{152}Sm target. 17
Figure 1.9. Structure of α-hydroxy isobutyric acid. 22
Figure 1.10. Standard reduction potentials of lanthanides. 25
Figure 3.1. UV-Vis absorption spectra of 0.1 mol.L^{-1} Tb(III) in 5.5 mol.L^{-1} K_2CO_3 solution at pH = 14 at electrolysis times 0 min – 270 min. Tb(IV) formation was followed by the peak characterized with 365 nm. Electrolysis was at constant potential +1.15 V vs. Ag/AgCl, applied for 270 min. Blank solution was used as reference sample for baseline correction. The cell path length was 1 mm. 43
Figure 3.2. UV-Vis absorption spectra of 0.1 mol.L^{-1} Tb(III) in 5.5 mol.L^{-1} K_2CO_3 solution at pH = 14 at electrolysis times 0 min – 270 min. Tb(IV) formation was followed by the peak characterized with 365 nm. Electrolysis was constant potential +1.3 V vs. Ag/AgCl, applied for 270 min. Blank solution was used as reference sample for baseline correction. The cell path length was 1 mm. 44
Figure 3.3. Correlation between the absorbance values at 365 nm and electrolysis times at potentials +1.15 V and +1.3 V vs. Ag/AgCl. 44
Figure 3.4. UV-Vis absorption spectra of solutions electrolyzed 2 h at +1.3 V vs Ag/AgCl containing 0.05 – 0.15 mol.L^{-1} Tb(III) in (a) 4 mol.L^{-1} (b) 5 mol.L^{-1} of K_2CO_3 at pH = 14. Tb(IV) formation was followed by the peak characterized

with 365 nm. Blank solution was used as reference sample for baseline correction. The cell path length was 1 mm. 47
Figure 3.5. Correlation between absorbance values measured at 365 nm and electrolysis time. UV-Vis absorption spectra of 0.07 mol.L^{-1} Tb(III) in 4 mol.L^{-1} K_2CO_3 solution at pH = 14 is recorded in 1 h intervals. Blank solution was used as reference sample for baseline correction. The path length was 0.1 mm. The measurement was done triplicate. The uncertainty ranges from 0.001 – 0.04 a.u. At 11 hours of electrolysis, absorbance value is measured as 0.38 ± 0.04. 48
Figure 3.6. (a) UV-Vis absorption spectra of 0.04 – 0.2 mol.L^{-1} Tb(III) in 4 mol.L^{-1} K_2CO_3 solution at pH = 14. Blank solution was used as reference sample for baseline correction. The path length was 0.1 mm **(b)** Correlation between absorbance values measured at 365 nm and initial Tb(III) concentration... 49
Figure 3.7. UV-Vis absorption spectra of 0.010 mol.L^{-1} Tb(III) in 4.5 mol.L^{-1} $Ca(NO_3)_2$ solution, followed up with increasing electrolysis time up to 210 min with samples taken in every 30 min, electrolyzed at constant potential of +2.1 V vs. Ag/AgCl. Tb(IV) formation was followed by the peak characterized with 369 nm. Blank solution was used as reference sample for baseline correction. The cell path length was 10 mm. 51
Figure 3.8. UV-Vis absorption spectra of blank in 3 mol.L^{-1} $Ca(NO_3)_2$ and 0.01 mol.L^{-1} Tb(III) in 3 mol.L^{-1} $Ca(NO_3)_2$ solution electrolyzed for 2 hours at +2.1 V vs. Ag/AgCl. Tb(IV) formation was followed by the peak characterized with 365 nm. Blank solution without terbium was used as reference sample for baseline correction. The cell path length was 10 mm. 52
Figure 3.9. UV-Vis absorption spectra of 0.004 mol.L^{-1} Tb(III) in 0.09 mol.L^{-1} KIO_4 solution at pH 12.9, electrolyzed for 1 h at constant potential of +1.3 V vs. Ag/AgCl. Tb(IV) formation was followed by the absorbance peak at 369 nm. Blank solution without terbium was used as reference sample for baseline correction. The cell path length was 10 mm. 54
Figure 3.10. (a) Stability measurement of Tb(IV). UV-Vis absorbance values at 365 nm of 0.07 mol.L^{-1} Tb(III) in 4 mol.L^{-1} K_2CO_3 solution at pH 14 at varying electrolysis times (90 min – 360 min) during and certain time frames after the electrolysis at constant potential of +1.3 V vs. Ag/AgCl. **(b)** Correlation of data sets at various electrolysis times with absorbance measured during (0 day) and after the electrolysis (1 day, 10 days, 20 days and 30 days). 57
Figure 3.11. UV-Vis absorption spectra of 0.01 mol.L^{-1} Tb(III) in 4.5 mol.L^{-1} $Ca(NO_3)_2$ solution at different times after electrolysis at constant potential of +1.3 V vs. Ag/AgCl and centrifugation. Tb(IV) formation was followed by

the absorbance peak at 369 nm. Blank solution without terbium was used as reference sample for baseline correction. The cell path length was 10 mm. 58
Figure 4.1. UV–Vis absorption spectra of the fractions collected at different feed volumes of 0.07 mol.L^{-1} Tb(IV) in 4 mol.L^{-1} K_2CO_3 solution at pH = 14. Electrolysis is performed at constant potential +1.3 V vs. Ag/ AgCl for 3h. The formation of Tb(IV) was followed by the absorbance peak at 365 nm. Blank carbonate solution is used as the reference sample for baseline correction. The cell path length was 1 mm..... 70
Figure 4.2. UV–Vis absorption spectra of undiluted 0.07 mol.L^{-1} Tb(IV) in 4 mol.L^{-1} K_2CO_3 solution at pH = 14, 1:1 (v:v) dilution and 1:2 (v:v) dilution. Electrolysis was performed on the undiluted sample at constant potential +1.3 V vs. Ag/ AgCl during 30 min. The formation of Tb(IV) was followed by the absorbance peak at 365 nm. Blank carbonate solution is used as the reference sample for baseline correction. The path length of the quartz cuvette is 1 mm. 71
Figure 4.3. Schematic representation of the proposed purification method using Dowex 1-X8 resin packed column. 73
Figure 4.4. Elution curve of tracer spiked Tb(III) solution using a Dowex 1-X8 resin filled cartridge (ø: 1 cm, h: 2.5 cm, BV: 2 mL). Feed: 0.4 mL of a solution containing 0.018 mol.L^{-1} Tb(III) in 1 mol.L^{-1} K_2CO_3 solution (pH ≈ 12). The vertical dashed line denotes the change of mobile phase from water to 2 mol.L^{-1} K_2CO_3 . Flow rate: 0.3 mL min^{-1}. 74
Figure 4.5. Elution curve of tracer spiked and electrolysed Tb(IV) solution using a Dowex 1-X8 resin filled cartridge (ø: 1 cm, h: 2.5 cm, BV: 2 mL). Feed: 0.4 mL of a solution containing 0.018 mol.L^{-1} Tb(III)/Tb(IV) in 1 mol.L^{-1} K_2CO_3 solution (pH≈12). The vertical dashed line denotes the change of mobile phase from water to 2 mol.L^{-1} K_2CO_3. Flow rate: 0.3 mL min^{-1}. 75
Figure 4.6. UV–Vis absorption spectra of 0.05 mol.L^{-1} Tb(III) , 0.05 mol.L^{-1} Gd(III) and 0.05 mol.L^{-1} Dy(III) in 4 mol.L^{-1} K_2CO_3 at pH = 14, before and after the electrolysis. Electrolysis is performed at constant potential +1.3 V vs. Ag/ AgCl for 2h. The formation of Tb(IV) was followed by the absorbance peak at 365 nm. Blank carbonate solution is used as the reference sample for baseline correction. The path length is 1 mm. 77
Figure 4.7. Elution curve of tracer spiked electrolyzed lanthanide mixture solution (0.05 mol.L^{-1} Tb(III) , 0.05 mol.L^{-1} Gd(III) and 0.05 mol.L^{-1} Dy(III) in 4 mol.L^{-1}) solution using a Dowex 1-X8 resin filled cartridge (ø: 1 cm, h: 2.5 cm, BV: 2 mL). Feed: 0.2 mL of a solution containing 0.018 mol.L^{-1}

Ln(III) in 1 mol.L^{-1} K_2CO_3 solution (pH ≈ 12). The vertical dashed line denotes the change of mobile phase from water to 2 mol.L^{-1} K_2CO_3. Flow rate: 0.3 mL min^{-1}. 78
Figure 4.8. Suggested process flowsheet for terbium-161 purification..... 80
Figure 4.9. Normalized XANES spectra of the oxidation of Tb(III) (0.07 mol.L^{-1}) in a 4 mol.L^{-1} K_2CO_3 solution as a function of time (15 min – 120 min). White line of terbium was observed with a maximum at 7519 eV..... 81
Figure 4.10. Simulated L3-edge spectra for reference structures ICSD-7183 and ICSD-422736 and comparison with experimental XANES traces of 0h and 24h electrolysis. 83
Figure 4.11. Molecular structure (ISCD 7183) adapted from Dixey and Saines et al.[182] 84
Figure 5.1. a) Cyclic voltammograms (second cycles) of 10 mmol.L^{-1} Eu(III) in 1 mol.L^{-1} $NaClO_4$ at various scan rates between 10 – 1000 mV/s b) Linear correlation of anodic and cathodic peak densities with respect to the square root at these scan rates. 94
Figure 5.2. a) Cyclic voltammograms (second cycles) of 10 mmol.L^{-1} Eu(III) in 0.1 mol.L^{-1} $Ca(NO_3)_2$ at various scan rates between 10 – 1000 mV/s b) Linear correlation of anodic and cathodic peak densities with respect to the square root at these scan rates. 95
Figure 5.3. a) Cyclic voltammograms (second cycles) of 10 mmol.L^{-1} Eu(III) in 0.1 mol.L^{-1} $CaCl_2$ at various scan rates between 10 – 1000 mV/s b) Linear correlation of anodic and cathodic peak densities with respect to the square root at these scan rates. 96
Figure 5.4. Peak separation potentials of 10 mmol.L^{-1} Eu(III) in 1 mol.L^{-1} perchlorate, 0.1 mol.L^{-1} chloride and 0.1 mol.L^{-1} nitrate media as a function of scan rate in logarithmic scale. 97
Figure 5.5. a) Linear sweep voltammogram on a glassy carbon rotating disk electrode in 0.01 mol.L^{-1} Eu(III) in 0.1 mol.L^{-1} $CaCl_2$ solution at a scan rate of 50 mV s^{-1} for rotation speeds 175 – 1600 rpm b) Levich plot at -1.2 V vs. Ag/AgCl and c) Koutecký – Levich plot at various potentials (-0.65 V to -0.9 V vs. Ag/AgCl) d) Tafel plot deducted from the Koutecký–Levich analysis. .. 101
Figure 5.6. a) Linear sweep voltammogram on a glassy carbon rotating disk electrode in 0.01 mol.L^{-1} Eu(III) in 0.1 mol.L^{-1} $Ca(NO_3)_2$ solution at a scan rate of 50 mV s^{-1} for rotation speeds 175 – 1600 rpm b) Levich plot at -1.2 V vs. Ag/AgCl and c) Koutecký – Levich plot at various potentials (-0.65 V to -0.9 V vs. Ag/AgCl) d) Tafel plot deducted from the Koutecký–Levich analysis. .. 104

Figure 5.7. a) Linear sweep voltammogram on a glassy carbon rotating disk electrode in 0.01 mol.L^{-1} Eu in 1 mol.L^{-1} $NaClO_4$ solution at a scan rate of 50 mV s^{-1} for rotation speeds 175 – 1600 rpm b) Levich plot at -1.2 V vs. Ag/AgCl and c) Koutecký – Levich plot at various potentials (-0.65 V to -0.9 V vs. Ag/AgCl) d) Tafel plot deducted from the Koutecký–Levich analysis. 105
Figure 6.1. Chronoamperograms of blank (6.6 mmol.L^{-1} Sm(III) in 3 mol.L^{-1} $Ca(NO_3)_2$) and Eu(III) solution (6.6 mmol.L^{-1} Eu(III) and Sm(III) in 3 mol.L^{-1} $Ca(NO_3)_2$) recorded during 3h of electrolysis. 115
Figure 6.2. UV-Vis absorption spectra of 10 mmol.L^{-1} Sm(III) and 10 mmol.L^{-1} Eu(III) in 6 mol.L^{-1} NH_4NO_3 (top) and 3 mol.L^{-1} $Ca(NO_3)_2$ (bottom) measured before and after 2h of electrolysis at -0.75 V vs. Ag/AgCl. Blank solution of the electrolyte is used for background correction and 1 mm path length is used. 117
Figure 6.3. UV-Vis absorption spectra of the feed consist of 10 mmol.L^{-1} Eu(III) and 10 mmol.L^{-1} Sm(III) in 3 mol.L^{-1} $Ca(NO_3)_2$ and the first fraction collected from the column. Blank solution of the electrolyte is used for background correction and 1 mm path length is used. 119
Figure 6.4. Elution curves of Sm(III) (a) and Eu(II) (b) using a TEVA resin filled cartridge (ø: 1 cm, h: 2.5 cm, BV: 2 mL) based on the radiotracer activities. Feed: 1 mL of a spiked solution containing 6.6 mmol.L^{-1} Eu(III) and 6.6 mmol.L^{-1} Sm(III) in 3 mol.L^{-1} $Ca(NO_3)_2$. The vertical dashed line indicates the switch of mobile phase from 3 mol.L^{-1} $Ca(NO_3)_2$ to water. Flow rate: 1 mL.min^{-1}. 121
Figure 6.5. Elution curves of Sm(III) (a) and Eu(II) (b) using a TEVA resin filled cartridge (ø: 1 cm, h: 2.5 cm, BV: 2 mL) based on the radiotracer activities. Feed: 1 mL of a spiked solution containing 6.6 mmol.L^{-1} Eu(III) and 6.6 mmol.L^{-1} Sm(III) in 3 mol.L^{-1} $Ca(NO_3)_2$. The vertical dashed line indicates the switch of mobile phase from 3 mol.L^{-1} $Ca(NO_3)_2$ to water. Flow rate: 0.2 mL.min^{-1}. 122
Figure 6.6. Elution curves of Sm(III) (a) and Eu(II) (b) using a TEVA resin filled cartridge (ø: 1 cm, h: 2.5 cm, BV: 2 mL) based on the radiotracer activities. Feed: 1 mL of a spiked solution containing 6.6 mmol.L^{-1} Eu(III) and 6.6 mmol.L^{-1} Sm(III) in 6 mol.L^{-1} NH_4NO_3. The vertical dashed line indicates the switch of mobile phase from 6 mol.L^{-1} NH_4NO_3 to water. Flow rate: 1 mL.min^{-1}. 123
Figure 6.7. Elution curves of Sm(III) (a) and Eu(II) (b) using a DGA resin filled cartridge (ø: 1 cm, h: 2.5 cm, BV: 2 mL) based on the radiotracer activities. Feed: 1 mL of a spiked solution containing 6.6 mmol.L^{-1} Eu(III) and 6.6 mmol.L^{-1} Sm(III) in 6 mol.L^{-1} NH_4NO_3. The vertical dashed line indicates the switch of mobile phase from 6 mol.L^{-1} NH_4NO_3 to water. Flow rate: 1 mL.min^{-1}. 125

Figure 6.8. Elution curves of Sm(III) (a) and Eu(III) (b) using a DGA resin filled cartridge (ø: 1 cm, h: 2.5 cm, BV: 2 mL) based on the radiotracer activities. Feed: 0.7 mL of a spiked solution containing 0.86 mmol.L^{-1} Eu(III) and 21.5 mmol.L^{-1} Sm(III) in 3 mol.L^{-1} $Ca(NO_3)_2$. The vertical dashed line indicates the switch of mobile phase from in 3 mol.L^{-1} $Ca(NO_3)_2$ to water. Flow rate: 1 mL.min^{-1} 127

List of tables

Table 1.1. Properties of particles used for therapeutic purposes[14] 7
Table 1.2. Decay characteristic of Tb radioisotopes.[22,39] 14
Table 5.1. Difference in anodic and cathodic potentials at 50 mV/s and diffusion coefficients of Eu(III)/Eu(II) reaction at different electrolytes. 97
Table 5.2. D, α and k values calculated based on Levich and Koutecký-Levich analysis. 106

Table of contents

Acknowledgements i
Abstract v
Beknopte samenvatting vii
List of abbreviations xi
List of symbols xiii
List of figures xv
List of tables xxi
Table of contents xxii
Outline xxvi
Chapter 1. 1
Introduction 1
1.1. Medical radiolanthanides 9
1.1.1. Production routes 11
1.1.1.1. Terbium-161 13
1.1.1.2. Samarium-153 17
1.2. Separation methods for radiolanthanides 18
1.3. Redox chemistry of lanthanides 24
1.3.1. Tetravalent oxidation state 25
1.3.2. Divalent oxidation state 27
Chapter 2. 32
Objectives 32
Chapter 3. 35
Electrochemical oxidation of terbium(III) in aqueous media: influence of supporting electrolyte on oxidation potential and stability 35
3.1. Abstract 36
3.2. Introduction 36

3.3. Experimental 38
3.3.1. Materials 38
3.3.2. Bulk electrolysis 39
3.3.3. UV-Vis spectroscopy 39
3.3.4. Inductive coupled plasma mass spectrometry 40
3.3.5. X-ray powder diffraction 40
3.4. Results and Discussion 41
3.4.1. Electrochemical oxidation of Tb(III) in various aqueous media 41
3.4.2. Carbonate medium 42
3.4.3. Nitrate media 50
3.4.4. Periodate medium 53
3.4.5. Stability studies 54
3.5. Conclusions 59
Chapter 4. 61
Separation of terbium as a first step towards high purity terbium-161 for medical applications 61
4.1. Abstract 62
4.2. Introduction 62
4.3. Experimental 64
4.3.1. Chemicals 64
4.3.2. Production of ^{161}Tb 65
4.3.3. Electrochemical oxidation of terbium 66
4.3.4. UV-Vis Spectroscopy 66
4.3.5. Extraction chromatography 66
4.3.6. Gamma spectrometry 67
4.3.7. X-Ray absorption spectroscopy 67
4.4. Results and Discussion 68
4.4.1. Stability of Tb(IV) complex 68
4.4.2. Column separation using Dowex 1X-8 resin 74

4.4.3. XANES measurements 81
4.5. Conclusions 84
Chapter 5. 87
Kinetics of electrochemical Eu(III) to Eu(II) reduction in aqueous media 87
5.1. Abstract 88
5.2. Introduction 88
5.3. Experimental 91
5.3.1. Materials 91
5.3.2. Instruments and electrodes 91
5.4. Results and discussion 92
5.4.1. Cyclic voltammetry 92
5.4.2. Linear sweep voltammetry at rotating disk electrode 99
5.5. Conclusions 107
Chapter 6. 109
Samarium-153 purification using electrochemistry and column separation techniques 109
6.1. Abstract 110
6.2. Introduction 110
6.3. Materials and methods 112
6.3.1. Chemicals 112
6.3.2. Electrochemical reduction of Eu(III) 113
6.3.3. Extraction chromatography 113
6.3.4. Gamma spectrometry 114
6.4. Results and Discussion 114
6.4.1. Electrochemical reduction of Eu(III) 114
6.4.2. UV-Vis absorption spectroscopy 116
6.4.3. Extraction chromatography using radiotracers 118
6.4.3.1. TEVA resin 118
6.4.3.2. DGA Resin 124

6.4.3.3. BR2 irradiation experimental conditions 126
6.5. Conclusions 128
Chapter 7. 130
Conclusions and Outlook 130
Chapter 8. 136
Health, Safety and Environment (HSE) 136
Appendices 139
Scientific output 150
References 152

Outline

This dissertation entitled “Tuning oxidation states of terbium and europium towards high purity terbium-161 and samarium-153 for medical applications” is the result of research on the redox chemistry and separation of the lanthanides terbium and europium, towards applications in nuclear medicine. It consists of 8 chapters:

Chapter 1 covers detailed background information on radiolanthanides and their use in nuclear medicine, the unusual oxidation states of the lanthanides, and the purification processes established for these isotopes.

Chapter 2 describes the main objectives of this PhD thesis.

Chapter 3 presents the first research chapter, where the investigation of the electrochemical oxidation of terbium is performed in aqueous electrolytes. A qualitative analysis is performed in order to evaluate the stability of tetravalent terbium and the electrolysis conditions are optimized to obtain the maximum yield.

In **Chapter 4**, the purification of terbium using anion exchange chromatography is demonstrated. The electrochemical process optimized in the previous chapter is used prior to the separation process in order to change the valence state of terbium to obtain a selective separation for medical terbium-161. X-ray absorption spectroscopy is also used to determine these oxidation states as well as to describe the complexation of trivalent and tetravalent terbium ions in potassium carbonate electrolyte.

Chapter 5 covers the redox chemistry of divalent europium, using electrochemical techniques such as cyclic voltammetry and linear sweep voltammetry using a rotating disk electrode. A more fundamental study is conducted to investigate the kinetics of europium reduction reaction in nitrate, chloride and perchlorate media. As opposed to terbium, a more easily reachable reduction potential enables to do the kinetic analysis for the first time using these techniques.

The focus in **Chapter 6** is the column separation of the adjacent lanthanides europium and samarium towards the purification of the samarium-153 radionuclide. The mixture of samarium-153 and europium-152 in highly concentrated calcium nitrate solution is first electrolysed to obtain stable

divalent europium. This is followed by extraction chromatography using TEVA or DGA resins. A selective separation based on the valence change is aimed for, and conditions similar to the conditions expected after dissolution of an irradiated samarium-152 target are also applied to evaluate the applicability of the method.

The research findings from earlier chapters are summarized in **Chapter 7**, which also offers a preview of potential future studies.

The PhD thesis concludes with a discussion of Health, Safety and Environment (SHE) issues that were taken into account when conducting the tests, a list of references, a list of publications, and a list of conferences that the author of this PhD thesis attended.

Chapter 1.

Introduction

Today, cancer is still a leading cause of death worldwide, and according to the World Health Organization (WHO), nearly 10 million deaths were caused by cancer in 2020, which is one of the six death events.[1] Unfortunately, the numbers of new cancer cases are expected only to increase in the future. However, many cancers can be diagnosed in early stages and can be treated effectively. In fact, a significant improvement can be achieved in a patient`s condition by early detection and this can result in less mortality rates due to higher chances of responding to the treatment. Every year, over 10,000 hospitals around the world use radioisotopes for *in-vivo* diagnosis or treatment of approximately 35 million patients, 9 million of whom are in Europe.[2] Current cancer treatments include various approaches: surgery, radiation therapy or anticancer drugs in chemotherapy, immunotherapy, hormone therapy and targeted therapy.[3] Nuclear medicine uses ionizing radiation for diagnosis and therapy, not only for cancer but also for brain disorders or cardiovascular diseases. To illustrate, technetium-99m (^{99m}Tc) is the most commonly used radionuclide in diagnosis, accounting for approximately 80% of all nuclear medicine procedures and 85% of diagnostic scans in nuclear medicine worldwide.[4]

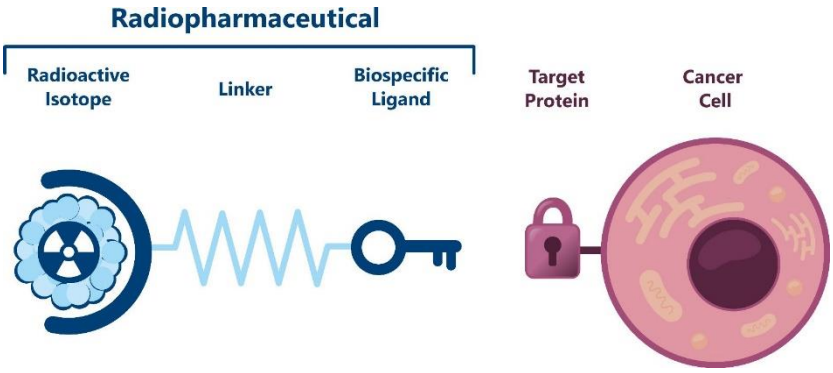

Figure 1.1. Schematic representation of the design of a radiopharmaceutical.

Radiopharmaceuticals consist of three parts: a radionuclide, linker and a targeting biomolecule (e.g. monoclonal antibodies, nanobodies, small peptides) determining the uptake of the drug in a specific location, for example a tumor site (**Figure 1.1**). The targeting molecules have usually to be modified with a covalently bound bifunctional chelator (BFC) such as DOTA (1,4,7,10-tetraazacyclododecane-1,4,7,10-tetraacetic acid) which selectively complexes the radionuclide (**Figure 1.2**). According to Kostelnik *et al.*, this type of drug design is favored since it gives the ability to modify individual components to fine-tune, opening possibilities for "plug and play" drug discovery.[5]

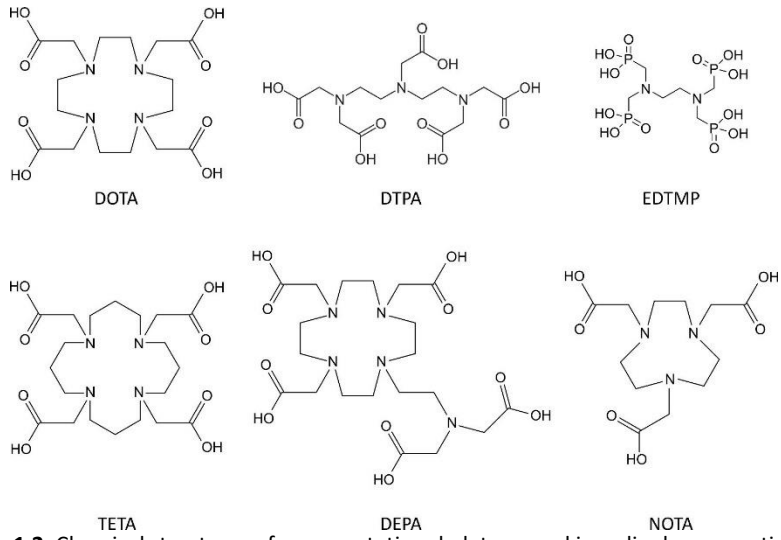

Figure 1.2. Chemical structures of representative chelators used in radiopharmaceuticals.

Bifunctional chelators are ligands having dual functionality; binding to the radionuclide and forming a stable conjugation with a biological targeting vector via a linker.[6] Some examples of these functional groups are amines, carboxylic acids, esters, isothiocyanates or isocyanates. In coordination chemistry, multidentate neutral amine ligands are by far the most effective family of ligands. These ligands have adjustable steric profiles, thermodynamically stable backbones, and varied coordination modes.[7] The coordination chemistry of the radionuclides to the chelators covers some criteria like charge, the cavity size of the chelating agent, and the number of donor binding groups. The cavity of the chelating agent should be matching with the ionic radius of the radionuclide, and therefore the donor groups are

aligned for optimal binding to the metal ion. This would lead to a high stability and therefore limited dissociation. For the metal ion – ligand complex stability, hard and soft acids and bases (HSAB) principle applies. Most of the radionuclides, like Lu^{3+} or Ga^{3+}, are hard Lewis acids, that can be paired with hard donor atoms as oxygen or nitrogen in the ligands, ensuring a strong interaction with the central metal ion and the coordination sphere, resulting in stable complexes.[8] The selection and design of the chelators are not only based on the binding properties but also the yield, temperature and the reaction time required for the radiolabelling process. The isotopes with short half-life like ^{68}Ga ($t_{1/2}$: 68 min) should be paired with chelators that have fast binding kinetics, whereas the isotope with rather longer half-lives as ^{161}Tb ($t_{1/2}$: 6.98d) or ^{177}Lu ($t_{1/2}$: 6.65d) would allow slow kinetics. However, the most convenient reaction times for radiolabelling should be in either case ideally less than 10 – 15 minutes.[9] Temperature also plays an important role in these reactions; room temperature would be ideal for antibodies, eliminating the degradation of these vectors. For example, while DOTA requires elevated temperatures for radiolabelling reactions with metals, DOTA and its derivatives provides exceptional in vivo stability and inertness, making them the most often used chelator. High stability is crucial to ensure that the radiolanthanide is delivered to the malignant cancer cells without detaching, which would cause severe damage to healthy cells.[9]

Lanthanides have a dominant trivalent oxidation state, and therefore the chelators for radiolanthanides need to be suitable for binding trivalent ions. Because the 4f electrons of the lanthanide cations are not participating in bond formation, the interactions between the lanthanide ions and chelators are mainly electrostatic. Polydentate chelators, having many coordinating sites and composed of entropically favored complex structures, are usually preferred for the radiolanthanides.[10] The majority of these complexes are derivatives of acyclic and macrocyclic (poly)aminophosphonic acids, (poly)aminocarboxylic acids and porphyrins. Whereas the macrocyclic chelators are requiring minimal manipulation during metal ion coordination, thanks to their pre-organized geometry, acyclic chelators must undergo changes in their orientation and geometry to achieve the coordination in a more thermodynamically more favorable way. However the advantage of the acyclic ligands is their ability to quantitatively radiolabel a metal with rather faster kinetics and less harsh conditions compared to the macrocyclic ligands. This can be especially useful when working with heat-sensitive molecules like

antibodies, as well as working with short half-life isotopes.[9] Some examples can be seen in **Figure 1.3**, where the coordination of lanthanide ions with DOTA and EDTMP are presented.

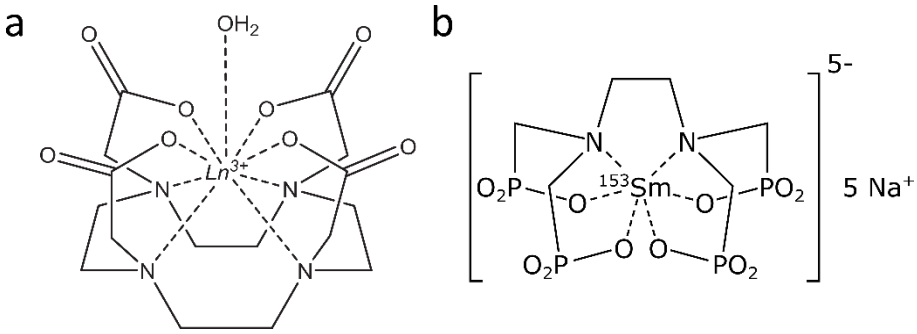

Figure 1.3. Examples of lanthanides coordinating with chelators a) trivalent lanthanide ion coordination with DOTA b) ^{153}Sm-EDTMP complex, known as Quadramet®.

In **Figure 1.4**, an overview of the production route for a radiopharmaceutical is shown. As a first step, the radionuclide should be produced either via cyclotron, a nuclear reactor or a generator route. This involves handling large amounts of radioactive isotopes and further chemical processing of it to have high chemical and radiochemical purities. The import and manufacturing should comply with the codes of current good manufacturing practices (cGMP). Then it can be followed by radiolabeling of the targeting biomolecules, ending up in the hospitals in individual patient doses.

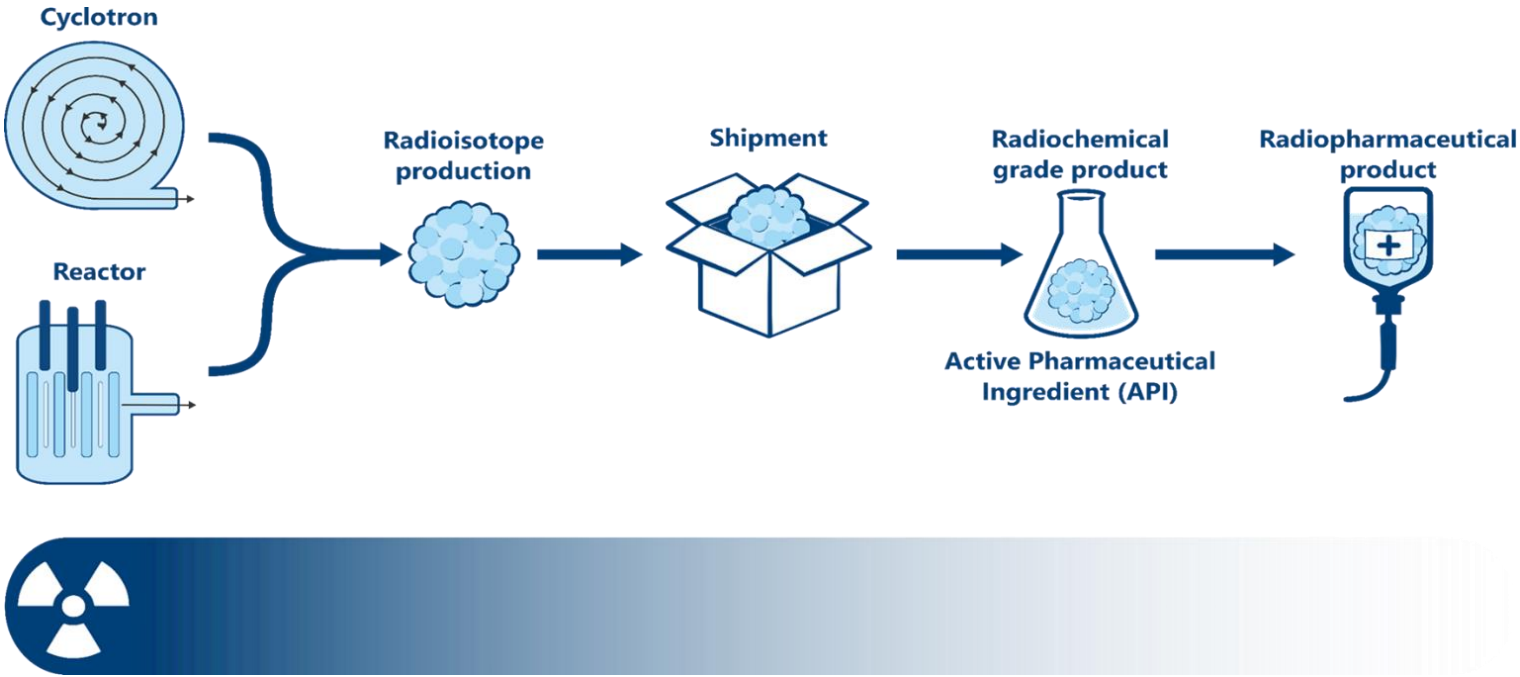

Figure 1.4. Overview of the different steps in the production route of a radiopharmaceutical.

Radiopharmaceuticals can be used either for diagnosis or therapy purposes based on the decay properties of the isotope being used. For diagnosis use, short-lived radionuclides emitting positrons (β^+) or gamma (γ) - rays are used whereas for therapeutic use alpha (α), beta minus (β^-) or Auger electron emitters are preferred.[6,11,12] While diagnostic agents release high energy photons that can be detected externally, the decay of the therapeutic agents can result in damage of the cells e.g. breaking of the DNA strands.

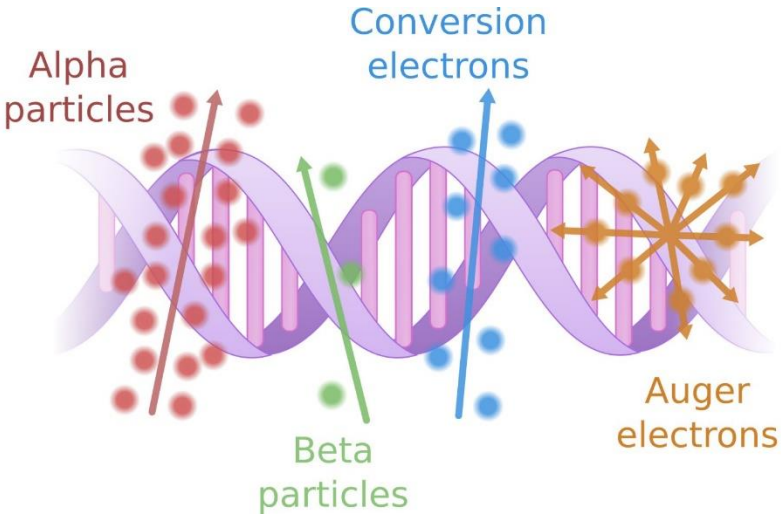

Figure 1.5. Representation of LET of different emissions on DNA strand.

In addition to the decay characteristics and resulting effect range and potency, the feasibility of chemistry and the availability of the nuclide should be taken into consideration as well. For treatment purposes, an important characteristic is represented in **Figure 1.5**; the linear energy transfer (LET) of different ionizing radiation. LET is defined as the amount of energy transferred per unit path length of the particle's track through a tissue.[13] Depending on the therapeutic effect, the isotope can be determined by comparison of LET of the respective emitted ionizing radiation (**Table 1.1**). High LET causes energy deposition in a highly concentrated area, resulting in reduced toxicity

in nearby healthy cells, whereas lower LET, due to its wider range, can be advantageous in larger malignancies.[14] As a result, β^- - emitters are prone to cause single-strand DNA breaks and due to their range leading to a more evenly distributed dose, while α- or Auger e^- - emitters, are more likely to cause double-strand DNA breaks, increasing their effectiveness in small range. Because of their limited range within cells, Auger e^- emitters must be located within or very close to the nucleus.[15,16]

Table 1.1. Properties of particles used for therapeutic purposes[14]

Particle	Energy	Range	LET
Beta (β^-)	50–2300 keV	0.05–12 mm	0.2 keV.mm^{-1}
Alpha (α)	5–9 MeV	40–100 µm	80 keV.mm^{-1}
Auger electron (e^-)	< 25 keV	2–500 nm	14–26 keV.mm^{-1}

When we move to the diagnostics, the emitted radiation can be detected externally by an instrument. Molecular imaging techniques allow non-invasive visualization in two or three dimensional images, by using tracers. This can be accomplished in two distinct ways: with γ rays or with annihilation photons from β^+. One of the most sensitive techniques is *single photon emission computed tomography* (SPECT); which utilizes radiopharmaceuticals labeled with single-photon emitters, radioisotopes that emits one gamma-ray photon for each instance of radioactive decay, such as technetium-99m (^{99m}Tc) or iodine-123 (^{123}I).[17,18] As mentioned earlier, ^{99m}Tc has been the most widely used radionuclide in imaging, due to its short half-life of 6.03 h, photon emission at 140 keV, availability via ^{99}Mo/^{99m}Tc generator route and its rich chemistry.[4,15]

The other technique, *positron emission tomography* (PET) requires the labeling isotope to be a β^+ emitter. Upon emission from the nucleus, β^+ particles only travel a short distance in the tissue. By annihilation

with an electron, 511 keV γ-rays are emitted simultaneously at approximately 180° to each other, which are detected by surrounding detectors. The most common radionuclides used for PET are fluor-18 (^{18}F) and gallium-68 (^{68}Ga). However, an advantage of PET is that it applies isotopes of carbon-11 (^{11}C), nitrogen-13 (^{13}N), and oxygen-15 (^{15}O), allowing the synthesis of radiopharmaceuticals that are chemically identical to their nonradioactive counterparts.[18,19]

With the advances in drug developments that are target specific, a new approach with the use of the same ligand for both imaging and therapy using different radionuclides has emerged. Theranostics – the combination of therapy and diagnostics - is a systematic approach offering simultaneous diagnosis and therapy components, leading to the development of personalized medicine, and as a result, increasing the effectiveness of the therapy.[6,10,15,20] While with therapy, the aim would be killing the tumor cells without any side effects, prediction of the therapeutic response of the patient to the radiation dose as well as the progress of the treatment can be determined via nuclear imaging.[21] For this purpose, a suitable radionuclide pair should be formed, in ideal case using the same element to minimize the differences in biological behavior.[22] Radioiodine was the first theranostic radiopharmaceutical in nuclear medicine history used for thyroid diseases.[23,24] Other theranostic pairs that are being developed, of which some of them have found its application in clinical research, are ^{86}Y/^{90}Y, ^{83}Sr/^{89}Sr, ^{152}Tb/^{161}Tb, ^{152}Tb/^{149}Tb, ^{68}Ga/^{177}Lu and ^{90}Y/^{177}Lu.[13,25]

As briefly discussed, there are several requirements to be fulfilled for the radionuclides to be used in radiopharmaceuticals for various purposes, such as suitable decay characteristics and half-life, availability & ease of production, compatible chemistry and pharmacokinetics. There, radiolanthanides step in thanks to their similar chemical properties yet different nuclear properties.

1.1. Medical radiolanthanides

Lanthanides typically exist in the trivalent (+3) oxidation state, which results in a similar coordination chemistry. This versatility allows the flexibility to select the radiolanthanide with the most suitable half-life, decay mode and decay energy for a certain application (diagnosis or therapy) from a range of possible radiolanthanides that are all compatible with the same carrier molecule.[5,10,16,26–28] In aqueous media, radiolanthanides are stabilized by chelation of multidentate ligands providing hard donors. Because lanthanide complexes form ionic bonds, multidentate chelates are required to form complexes that are resistant to ligand substitution reactions. In vivo, dissociation of the lanthanide from the chelate may result in undesirable bone and liver uptake since they have the ability to mimic calcium in biological systems.[5] As can be seen in **Figure 1.6**, the radiolanthanides can be used in various applications thanks to their diverse nuclear properties, both in therapy and diagnostics. Among the radiolanthanides, most radiotherapeutic studies focus on β^- – emitters such as ^{149}Pm, ^{153}Sm, ^{161}Tb, ^{165}Dy, ^{166}Ho, ^{169}Er, ^{170}Tm and ^{177}Lu. In addition, there are therapeutic Auger e^- emitters like ^{161}Tb, ^{165}Er and ^{135}La, as well as isotopes that are suitable for diagnostics as ^{152}Tb, ^{155}Tb, ^{135}La or ^{177}Lu. ^{149}Tb is the sole radionuclide suitable for α- therapy.

The most important therapeutic and best known radionuclide among the lanthanides is lutetium-177 (^{177}Lu), with a half live of 6.65 days. It emits low to medium energy β^--particles with a maximum of 0.49 MeV, accompanied by low abundance γ-photon emissions, making it a suitable candidate for theranostics. In order to develop a variety of potential radiopharmaceuticals with ^{177}Lu, radiolabelling of antibodies, peptides, phosphonate ligands, monoclonal antibodies, steroids, and other small molecules are being investigated.[29] Favorable nuclear properties and accessible chemistry of ^{177}Lu results in stable compounds with good *in-vivo* properties, and its ease of manufacturing in high activity levels with high specific activity in many nuclear reactors globally makes it attractive.[30] Furthermore, the Food and Drug Administration (FDA) approved ^{177}Lu-DOTATATE (DOTA:

1,4,7,10-tetraazacyclododecane-1,4,7,10-tetraacetic acid; TATE: tyrosine-3-octreotate) (LUTATHERA®), a radiolabelled somatostatin analog, for the treatment of neuroendocrine tumors in adults. It is reported that ^{177}Lu-labelled somatostatin analogs can achieve tumor response rates of up to 30 – 35%.[31] More recently, ^{177}Lu-PSMA-617 (PSMA - prostate-specific membrane antigen) (PLUVICTO®) has been approved for metastatic prostate cancer treatment in March 2022.[30] These developments in ^{177}Lu-based radiopharmaceuticals stimulate a growth in research in targeted nuclear therapy and thanks to their similar chemistry, further investigation on other radiolanthanides can bring new opportunities and expand the current research on radiopharmaceuticals.

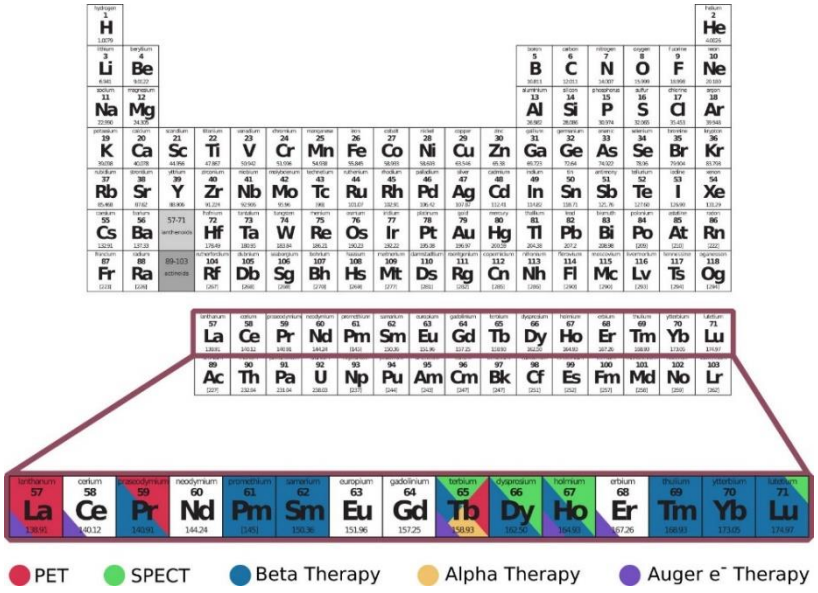

Figure 1.6. Radiolanthanides used in nuclear medicine. Adapted from Kostelnik *et al.*[5]

This PhD thesis focuses on terbium-161 (^{161}Tb) and samarium-153 (^{153}Sm), two β$^-$-emitting therapeutic radiolanthanides. Terbium offers 4 radioisotopes that can serve various combinations of therapy and diagnosis; among which ^{161}Tb ($t_{1/2}$: 6.98d) emits low-energy β$^-$-

particles with a maximum of 0.59 MeV. In contrast to ^{177}Lu, it emits a significant quantity of conversion and Auger electrons that can end up in higher effectiveness. Besides, the comparable chemistry could lead to similar approaches for carrier molecules. ^{153}Sm ($t_{1/2}$: 46.7h) complexes are effective in treating bone metastases and can be used in radionuclide bone scan due to the accompanying emission of γ photons of 103.2 keV (28%), which can be used for imaging, providing efficacious theranostic concept.[22] ^{153}Sm - EDTMP (ethylenediamine tetramethylene phosphonic acid) (Quadramet®) is clinically approved and used in bone palliations.[32] Apart from their medical importance, their unique redox chemistries could introduce some advantages in their separation from the neighboring lanthanides, which will be explained in the following sections.

1.1.1. Production routes

The choice of production method for radiolanthanides depends on various factors, such as the required specific activity, radionuclidic purity, target material availability, and cost-effectiveness. Nuclear reactors are still the most commonly used method for producing radiolanthanides due to their high yield and production capacity, but cyclotrons and radionuclide generator systems are becoming more prevalent in medical applications.[26] Another method is using linear accelerators (LINACS) for medical radionuclide production, yet this method is much less common.[33,34] Based on the production route, the product can either be carrier-added (ca) or non-carrier-added (nca) as explained here below.

To start with, three reaction types can occur due to neutron irradiation in nuclear research reactors: neutron capture, neutron capture with particle emission and fission. Among them, the mostly used one is the neutron capture (n,γ) reaction with thermal neutrons, known as the direct reaction route. High yields can be achieved with this straightforward production route, yet to avoid radioimpurities or

chemical impurities, highly enriched, and thus expensive, target materials must be used. Lanthanide oxides or inorganic salts have been used as a target material due to their commercial availability and chemical stability. For instance, ^{153}Sm, ^{166}Ho and ^{177}Lu can be produced via single neutron capture route; e.g. in the case of using an ^{152}Sm-enriched samarium(III) oxide target (99%), the production of impurities such as ^{154}Sm or ^{151}Sm will be minimized. However, the end product is *carrier-added* (ca) since it cannot be separated from the target material.[16,35]

The indirect reaction route with neutron capture (n,γ) can lead to *non-carrier-added* (nca) radiolanthanides, which are desirable for certain medical applications. This route involves the use of a target material that consists of the isotope of the element with one atomic number lower than that of the desired radionuclide and with one mass number lower as well that can be activated by neutron capture to produce the desired isotope through β-decay of a short-lived intermediate. This process can result in higher radionuclidic purity and specific activity, as well as a lower risk of chemical impurities. Several radiolanthanides can be produced via this indirect route, including ^{177}Lu, ^{143}Pr, ^{149}Pm, and ^{161}Tb. For example, for production of ^{177}Lu, ^{176}Yb can be used as a target material, where the final products contains no ^{177m}Lu, referring to nca route. The choice of target material and the parameters of the irradiation process can affect the yield, specific activity, and purity of the resulting radionuclide, so careful optimization is necessary to achieve the desired product. Reactors with high thermal neutron flux, such as the BR2 reactor at SCK CEN, are often used for the production of medical radionuclides via neutron capture reactions.

Production of medical radiolanthanides can be done in cyclotrons as well. In general, the reactor produced radionuclides are neutron-excess ones mostly decaying by β^--emission, whereas the cyclotron produced ones are usually neutron-deficient nuclides decaying by electron capture or β^+-emission. However, α- and β^- -emitting radionuclides can be produced via a cyclotron too. To illustrate, ^{149}Tb

($t_{1/2}$: 4.12h) is an α- emitter candidate for immunotherapeutic use. It can be produced using ^{152}Gd as a target material with (p, 4n) reaction at an energy higher than 30 MeV. Further mass separation is necessary to isolate ^{149}Tb from other terbium isotopes produced via (p, xn) reactions.[36]

A radionuclide generator is based on a long-lived parent/ short-lived daughter radionuclide pair; e.g. ^{99}Mo($t_{1/2}$: 66h) and ^{99m}Tc($t_{1/2}$: 6h), where the parent nuclide is introduced to the generator after irradiation in a nuclear reactor. It is then followed by a regular separation and extraction of the daughter from the parent which can be referred as 'milking the generator'.[37] Nuclide generators offer several advantages in the production of radiolanthanides. They allow for on-site production of short-lived radiopharmaceuticals without the need for a nuclear reactor or cyclotron. This significantly reduces the cost and complexity of the production process. In addition, the generator system provides a constant source of the desired radionuclide, allowing for a continuous supply of the radiopharmaceutical. However, radionuclide generators have some limitations as well. To achieve high radionuclidic purity, the impurities should be removed. This often requires separation of two lanthanides, which is very challenging. In addition, the separation is done in between macro amounts of lanthanides and micro amounts of desired lanthanide. Also, the available quantity of the parent radionuclide is limited by its half-life, and frequent replacement of the generator may be required.[37,38]

1.1.1.1. Terbium-161

Terbium offers 4 different radioisotopes that are interesting for nuclear medicine: ^{149}Tb, ^{152}Tb, ^{155}Tb and ^{161}Tb which are having complementary decay characteristics.[39] ^{149}Tb emits short range α particles making it suitable for targeted alpha therapy (TAT), whereas ^{152}Tb and ^{155}Tb could be used for diagnosis via PET and SPECT imaging, respectively, without high dose rates administrated to the patient.

Finally, ^{161}Tb is suitable for therapeutic use due to the emission of low-energy β^- particles, conversion and Auger electrons. In addition, γ rays are emitted which can be used for SPECT imaging. The matched terbium radionuclide quadruplet enables the use of biologically and chemically identical radioconjugates for various purposes. So-called "matched pairs" of diagnostic and therapeutic radioisotopes of the same chemical element are particularly useful because they allow the preparation of radiopharmaceuticals that are absorbed and distributed in identical ways in the body. This is the reason that terbium is called a `Swiss army knife` for nuclear medicine.[40]

Table 1.2. Decay characteristic of Tb radioisotopes.[22,39]

Nuclide	Decay mode	Half-life	Average particle decay energy (MeV)	Main γ-rays (keV)	Applications
^{149}Tb	α(16.7%) β^+(4.3%) EC(79%)	4.12h	3.97 (α)	165 (26%) 352.2 (29%) 388.6 (18%)	α-therapy
^{152}Tb	EC(82%) β^+(18%)	17.5h	1.08 (β^+)	344 (65%)	PET
^{155}Tb	EC(100%)	5.32d	-	87 (32%) 105 (25%)	SPECT
^{161}Tb	β^- (100 %)	6.98d	0.154 (β^-)	25.7 (23%) 48.9 (17%) 74.6 (10.2%)	β^- / Auger therapy

In **Table 1.2**, an overview of the decay characteristics of these terbium isotopes is given. Among these isotopes, ^{161}Tb has a half-life of 6.98 d and emission of low-energy β^--particles with maximum energy (E^{β}_{max}) of 0.59 MeV accompanied by γ photons, showing similar properties to ^{177}Lu($t_{1/2}$: 6.65 d, E^{β}_{max}:0.49 MeV). In addition, ^{161}Tb offers higher local damage on tumor cells thanks to the simultaneously emitted Auger and conversion electrons with energies between 3–50 keV. Therefore, the similar chemical and decay properties to ^{177}Lu, make similar approaches of radiolabelling possible. For example, in the study of Grünberg *et al.*, the same radiolabelling protocols of ^{177}Lu with DOTA conjugated antibodies were applied to ^{161}Tb and *in-vivo* biodistribution and therapeutic efficacy is investigated. It is reported that when compared to ^{177}Lu, ^{161}Tb radioimmunotherapy is more efficacious in an ovarian cancer model.[41] In study of *Müller et al.*, *in-vivo* experiments using radiotracers of ^{161}Tb-DOTA-folate and ^{177}Lu-DOTA-folate are performed.[42] The SPECT images during in vivo experiments are taken for both radiotracers, and it was observed that tumor growth was reduced more efficiently using the ^{161}Tb analogue. Another very recent investigation is on therapeutic potential of ^{161}Tb-PSMA-617 on metastatic castration-resistant prostate cancer (mCRPC).[43,44] Based on the success of ^{177}Lu-PSMA treatment in patients with prostate cancer, ^{161}Tb is considered as an alternative as well. Moreover, recently the first-ever patient images obtained with ^{161}Tb have shown that its γ-radiation can be used for both whole-body planar and SPECT/CT imaging, even with low injected activity of the radioisotope. The ^{161}Tb-DOTATOC ((DOTA^0-Phe^1-Tyr^3) octreotide) conjugate is found to be tolerated by the patients, meaning the use is safe and indeed can be a suitable alternative for ^{177}Lu-DOTATOC.[45] These findings provide a foundation for future studies involving ^{161}Tb-based radiopharmaceuticals, where the activity of ^{161}Tb administered to patients can be gradually increased to achieve therapeutic effectiveness.

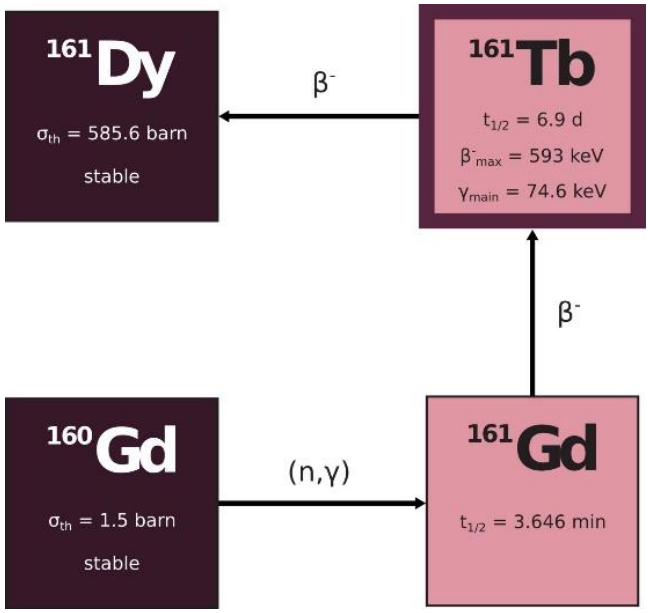

Figure 1.7. Non-carrier added production route of ^{161}Tb from ^{160}Gd target.

^{161}Tb is commonly produced through the non-carrier-added reactor production route (**Figure 1.7**), which involves neutron irradiation (n,γ) of an enriched ^{160}Gd target. ^{160}Gd has a rather low thermal neutron capture cross-section of 1.5 barns, therefore a high-flux reactor like BR2 is required. The neutron capture of ^{160}Gd produces short-lived ^{161}Gd, which decays through β^--emission into ^{161}Tb. When a highly enriched ^{160}Gd target material is used, radionuclidically pure ^{161}Tb can be obtained at the end of the irradiation.[46] However, when ^{161}Tb decays, stable ^{161}Dy is formed, which can interfere with radiolabeling due to the chemical similarity. As a result, besides separating ^{161}Tb from ^{160}Gd, it is crucial to separate ^{161}Tb and ^{161}Dy in order to maintain the high specific activity. The currently used methods, which are only dealing with the separation of micro-amounts of ^{161}Tb from a macro-amount of ^{161}Gd target material, will be explained in more detail in section 1.2.

1.1.1.2. Samarium-153

^{153}Sm is a β$^-$-emitting radionuclide with a mean energy of 233 keV, having 46.7h half-life. As mentioned previously, ^{153}Sm-EDTMP complex is clinically used in the USA, commercially known as Lexidronam® and Quadramet®, as a palliative agent for skeletal metastasis. A high local dose can be administered without damaging the healthy surrounding tissues and normal bone marrow. The skeletal metastases are usually due to different types of cancers such as lung, breast or prostate cancer. Despite its relatively short half-life, in recent studies the possibility of using ^{153}Sm-labeled microparticles in other types of cancers has been studied.[16,47–49]

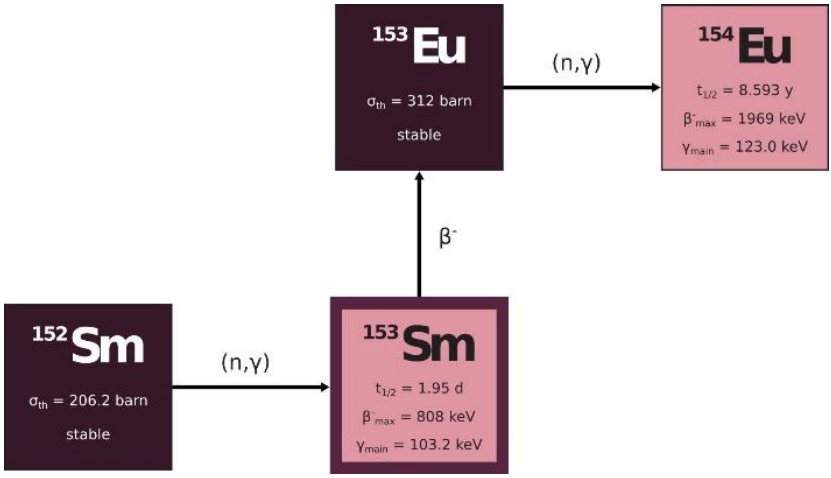

Figure 1.8. Production route of ^{153}Sm via neutron capture using ^{152}Sm target.

Additionally, ^{153}Sm has accompanying γ-rays at 103 keV (29.14%) which could be used in SPECT imaging. When it is compared to ^{99m}Tc, the bone uptake is both more than 50% of the administered dose, resulting in very comparable results.[50] Due to the combination of β$^-$-particle emission and γ-emission theranostic applications and targeted treatment possibilities has drawn attention, thanks to the

appropriate tissue penetration of medium-energy β^--particles (2–3 mm effective range).[22] A new radiopharmaceutical with an alternative ligand,^{153}Sm–DOTMP-(1,4,7,10-tetraazacyclododecane tetramethylene phosphonic acid) is looking more promising and favorable for chelator to metal ratio, is now being tested in clinical studies for the treatment of bone cancer and related metastases.[51,52]

^{153}Sm is typically produced through the carrier-added method, which involves the thermal neutron activation of isotopically enriched ^{152}Sm (**Figure 1.8**). During the production, a small amount of long-lived ^{154}Eu is also formed, which limits the shelf life of the product due to strict regulations on the maximum amount of ^{154}Eu that can be administered to a patient. Additionally, trace amounts of long-lived ^{152}Eu($t_{1/2}$: 8.593 y) and ^{156}Eu($t_{1/2}$: 15.19 d) may also be present in the irradiated targets.[53–55] Therefore, a separation method should be developed that enables an efficient purification allowing safe administration to the patient and to increase the shelf-life.

1.2. Separation methods for radiolanthanides

In the lanthanides series, inner 4f orbitals are filled and shielded by filled 5s and 5p shells. Furthermore, the 4f electrons behave like a core and neither they participate in bond formation nor they are affected by the surrounding ligands. The most prominent oxidation state of the lanthanides is the +3 one. Therefore, adjacent lanthanides show similar chemical properties which makes separation challenging. There are exceptions such as Ce or Eu, that can have other valence states, that can allow selective separation, which will be discussed later. Lanthanide separation can be accomplished using standard chemistry techniques such as solvent extraction,[56–61] chromatography, [62–66] precipitation,[67] or crystallization.[68–70] However, for medical radiolanthanide separation a rapid, efficient and robust separation procedure is required because of the short half-life of the radionuclides. Another requirement is that the separation method should allow the separation of micro amounts from the bulk target material. Furthermore, while similar chemical properties are

advantageous in the development of radiolanthanides for radiolabelling reactions, they are a major disadvantage in the separation process. In addition, to minimize radiation exposure of the staff, a separation method that is easy to automate is preferred.

Solvent extraction is one of the methods used for separation of lanthanides, where soluble species are distributed between two immiscible liquid phases based on their affinity to each phase. For example, an ionic liquid based liquid-liquid extraction experiments have been conducted in the separation of ^{225}Ac/^{227}Th.[71] Ionic liquids have been investigated as diluent, where N,N,N',N'-tetraoctyldiglycolamide (TODGA) or di(2-ethylhexyl)phosphoric acid (HDEHP) were used as extractants.[71] TODGA was quite efficient at extracting both metals from the aqueous phase, however it did not result in an acceptable separation in any of the conditions that are studied. TODGA extracts trivalent lanthanide and actinide ions via a neutral solvation mechanism, as shown in Equation 1.1;[72]

$$\mathrm{M^{n+}_{(aq)}} + \mathrm{m\ TODGA_{(org)}} + \mathrm{n\ NO_3^-} \rightleftarrows \mathrm{M(TODGA)_m(NO_3)_{n,(org)}} \quad (1.1)$$

HDEHP, which is an acidic extractant, on the other hand, proved to be a good extractant at higher acidities, with a separation factor greater than 10^7 at 0.01 mol.L^{-1} HNO_3.[71] Luo *et al.* describes the general extraction mechanism as a conventional complexation of metal ions via the extractant which is then paired to an ion-exchange process with an ionic liquid, where the high extraction efficiencies were related with the hydrophilicity of the selected ionic liquid cations.[71] The mechanism was described as follows:

$$\mathrm{M^{n+}_{(aq)}} + x\mathrm{HDEHP_{(IL)}} + y\mathrm{(NO_3^-)_{(aq)}} + z\mathrm{[C_4mim]^+_{(IL)}} + \mathrm{z[NTf_2]^-_{(IL)}} \rightleftarrows \mathrm{[M(DEHP)_x(NO_3)_y(NTf_2)_z]^{(n-x-y-z)+}_{(IL)}} + x\mathrm{H^+_{(aq)}} + z\mathrm{[C_4mim]^+_{(aq)}} \quad (1.2)$$

Another example is the purification of ^{99m}Tc, mainly based on two systems – cyclotron produced ^{100}Mo(p,2n)^{99m}Tc or low specific activity ^{99}Mo and ^{99m}Tc. In both, the solvent extraction is performed using methyl ethyl ketone (MEK) as the extractant. Highly pure methyl ethyl ketone was used to extract an alkaline solution of molybdenum as molybdate (MoO_4^{2-}). The ^{99m}Tc in the solution in the form of pertechnetate (TcO_4^-) was extracted into the methyl ethyl ketone

(MEK) phase while the molybdate stays in the basic aqueous solution. Narasimhan *et al.* explains the separation mechanism via solvation of pertechnetate ion, having Na^+ as the central ion and three water molecules composing the primary solvation sphere.[73] Six molecules of MEK attached to the water molecules via hydrogen bonding in the secondary solvation sphere. Thus, the positively charged species forms a neutral complex with pertechnetate resulting in extraction to the MEK phase.[73] However, additional washing steps are necessary to increase the recovery as well as the MEK phase is passed through a silica column to switch the solvent for further radiolabelling processes.[74–80] There are only a few examples[71,74–78,80–82] of this method used in medical radioisotope separation, since it consumes expensive special-grade solvents, and generates organic liquid radioactive waste.[82]

The most frequently applied purification method is column chromatography, due to its simplicity, speed, efficiency and the ease to be automated. Chromatography is a separation process utilizing exchange between a stationary phase and a mobile fluid phase. There are several various chromatographic techniques based on the exchange mechanism such as ion exchange, size exclusion or adsorption chromatography. There is already a well-established and commonly used technique regarding the radiolanthanide purification: the use of high performance liquid chromatography (HPLC) in combination with α-hydroxy isobutyric acid (α-HIBA) as complexing agent (**Figure 1.9**).[83]

Van de Voorde *et al.* describe the three equilibria of separation of lanthanides using α-HIBA.[16] Among the other complexing agents, to day separation using α-HIBA is the most often used one, due to its sensitivity towards the lanthanide cation radii. The separation is based on three equilibria: acid-base, complex formation and cation exchange. α-HIBA is a weak acid (pKa = 4.01), thus the pH of the aqueous phase has an importance in the separation process. The complex formation between α-HIBA and the lanthanide depends on the ionic radius and charge density of the lanthanide. The lanthanides with a higher charge density forms more stable complexes, therefore

due to the lanthanide contraction the heavier lanthanide will be the first one eluting from the column. The third equilibrium is between the functional groups of the ion exchanger and the lanthanide. As the interaction between the stationary phase and the lanthanide is more prominent, the elution will be slower. For the optimization of the separation process can be controlled via parameters like pH, concentration of cation, concentration of α-HIBA and selection of the ion exchanger. As a last step before the radiolabelling, the complexing agent should be removed. By acidification and using a cation exchanger, the separation can be achieved.[84]

For example, Lehenberger *et al.* performed purification of ^{161}Tb from the target material ^{160}Gd using a sulfonic type cation-exchange resin Aminex-A6 (NH_4^+-form) in a column chromatography setup and 0.13 mol.L^{-1} at pH = 4.5 α-HIBA as the eluent.[85] The first elution peak contains Dy, which is discarded, and the ^{161}Tb fractions collected are mixed with 1 mol.L^{-1} HCl solution adjusted the pH to ≈1. Then a purification step is done by loading the solution on a secondary column filled with a Bio-Rad AG 50 W-X8 cation exchanger in H^+ form. The isolation of up to 80-90% of the ^{161}Tb from the massive target with a decontamination factor larger than 10^5 is achieved.[85] Another example is the ^{166}Ho/^{166}Dy system separated by Aminex-A5 or Dowex-50W cation exchange columns with 0.085 mol.L^{-1} of α-HIBA at pH = 4.3. The Ho-α-HIBA complex is further treated with HCl for the removal of the complex. It is stated that the separation is achieved within 2 h with a radionuclidic purity of 99.9%.[86,87] In another example, ^{177}Lu has been separated from the Yb target with selective extraction by Na(Hg) amalgam followed by cation exchange chromatography.[88] With this method, selective extraction of Yb is performed by Na(Hg) amalgam from Cl^-/CH_3COO^- electrolyte where the quantity of Yb is reduced to around 0.01 - 0.02% of the starting mass, and about 85% of the nca ^{177}Lu remains in the solution. Further purification is done via eluting an Aminex-A6 column with 0.07 mol.L^{-1} α-HIBA at pH=4.7. It is reported that 75±5 % separation yield is achieved in 4-5h time with Yb contamination less than 1 ng Yb^{3+} per 100 mg target.[88]

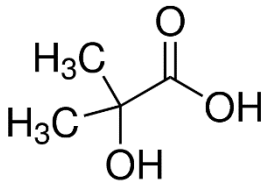

Figure 1.9. Structure of α-hydroxy isobutyric acid.

Another column chromatographic approach to radiolanthanide purification is extraction chromatography. It is a fast and efficient technique coupling the selectivity of solvent extraction and multistage feature of column chromatography.[89] Mostly, a stationary phase is chosen containing supported organic phosphorus compounds such as HDEHP, tri-*n*-butyl phosphate (TBP) or 2-ethylhexyl 2-ethylhexylphosphonic acid (HEH[EHP]). However, the best separation factors among the adjacent lanthanides (> 2.5) are achieved with HDEHP-supported stationary phases.

In a study by Monroy-Guzman *et al.*,[90] the separation of micro/macro systems ^{149}Pm/Nd, ^{161}Tb/Gd, ^{166}Ho/Dy and ^{177}Lu/Yb are investigated with extraction chromatography using HDEHP on a hydrophobic support eluted with nitric acid and compared with the previously reported distribution ratios D of Horwitz *et al.*[91] As can be seen in the equation 1.1, extractability is strongly dependent on the aqueous phase acidity with HDEHP, when the concentrations of both lanthanide salt and mineral acid are low.[92] In this report,[90] it is stated that as the atomic number of the lanthanide increases, the distribution coefficient also increases. Therefore, the elution order of adjacent lanthanides would depend on the atomic number. This is in favour of separation between macro- amounts of parent (which has a lower atomic number) and micro amounts of daughter radionuclides, resulting in the macro amount of target compound eluted first while micro amounts of radionuclide are retained in the column. Increase in nuclear charge and poor shielding of the 5s and 5p electrons by the 4f subshell lead to a smaller atomic radius throughout the lanthanide series when moving from lanthanum (1.16 Å with CN = 8) to lutetium

(0.977 Å with CN = 8). This phenomenon is often denoted as the 'lanthanide contraction'. Therefore, the charge density and the hydration energy increase with increasing atomic number for the trivalent lanthanides, also affecting the coordination number. The tendency of forming the cationic aqua complexes, i.e. $[Ln(H_2O)_x]^{3+}$ gradually increases with a decrease in atomic number. The coordination number of is assumed to be 9 for early lanthanides (La–Eu) and 8 for the later lanthanides (Dy–Lu), with the intermediate lanthanides exhibiting a mixture of 8-coordinate and 9-coordinate species. A change in coordination number leads to separation possibilities and might potentially lead to variations in biological behaviour when bioconjugates with the same chelator are labelled with a different lanthanide. The distribution ratios reported are in accordance with previous studies, and the most efficient separation processes are obtained with specified conditions regarding acid concentrations.[90]

$$\mathrm{Ln^{3+}} + \overline{3(\mathrm{HDEHP})_2} \leftrightarrow \overline{\mathrm{Ln[H(DEHP)_2]_3}} + 3\mathrm{H^+} \qquad (1.3)$$

Jelinek *et al.*, worked on the separation of Eu from other lanthanides again using an HDEHP impregnated resin, but with the strategy of reducing the Eu(III) first to Eu(II).[93] As the separation of the adjacent lanthanides is difficult due to their similar properties, and given that Eu(II) is stable in aqueous media, this drastic change in the chemical properties is expected to ease the process. Even though back-oxidation could interfere with the process, more than 99.8% purity yielded with achieving 70% recovery rate. Considering the conversion of Eu(III) to Eu(II) is 90%, this change is a result of back-oxidation. Van de Voorde *et al.* used a similar approach that can be used towards the purification of ^{153}Sm.[94] Eu(III) can be reduced to Eu(II) either electrochemically or chemically – by using zinc as a reducing agent in both aqueous and non-aqueous media.[95–99] In this study,[94] a mixture of nitrate salts of Sm and Eu in aqueous nitrate medium first undergo a reduction step in an inert atmosphere, followed by column separation using TEVA resin. Results show that more than 80% of the initial Eu(III) is collected in the very first fractions whereas the majority of Sm(III) is collected after changing the eluent from nitrate solution

to water. Chakravarty *et al.* also used an electrochemical approach to purify ^{153}Sm via electro-amalgamation.[100] Eu(III) is reduced to Eu(II) in an electrolysis cell with a mercury-pool cathode prior to the separation. These can provide new perspectives on traditional HPLC or chromatographic separations of radiolanthanides.

As can be derived from the described methods, the separation of micro amounts of daughter radionuclide from neighbouring macro amounts of target material is challenging due to the similar chemical properties of lanthanides. Despite achieving high purity, no complete separation can be achieved. This becomes a disadvantage towards the commercial radionuclide production, particularly at large scales. As a result, a strategy to change the chemical properties is expected to result in high separation factors and could provide a more selective separation of medical radiolanthanides, which can be introduced via the different valence states.

1.3. Redox chemistry of lanthanides

As discussed earlier, the main characteristic of lanthanide chemistry is the dominance of the trivalent oxidation state and thus similar chemical properties along the series. In the series, the cation radii decrease slightly with increasing atomic number. This is often referred to as the lanthanide contraction. As a result the charge density increases slightly as the atomic number of the lanthanide increases. As mentioned before, the chemical properties of lanthanides are quite similar, and it is challenging to separate the adjacent lanthanides.[101] In order to further improve the separation process, the chemical properties can be changed selectively for some lanthanides, which show some stability in unusual oxidation states other than (3+).

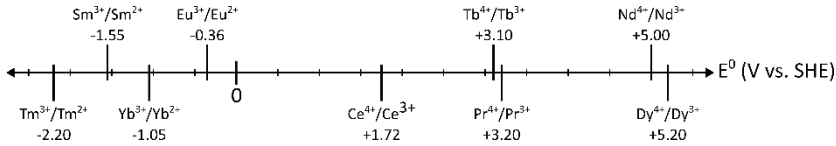

Figure 1.10. Standard reduction potentials of lanthanides.

1.3.1. Tetravalent oxidation state

Ce(IV) is the most well-established tetravalent lanthanide which is sufficiently stable in aqueous solution as well as in the solid state. The stability of the tetravalent oxidation state can be explained by the empty 4f shell with noble gas electronic configuration [Xe] $4f^0$. Ce(IV) compounds are commonly used as strong oxidizing agents. Ceric ammonium nitrate (CAN) is often used in oxidation reactions and many literature reports can be found on Ce(IV) reagents used in organic synthesis. Compared to the other tetravalent lanthanides Ce(IV) can exist in aqueous solutions; e.g. E(Ce(III)/Ce(IV)) = +1.70 V vs. SHE in 1 mol.L^{-1} $HClO_4$, +1.61 V vs. SHE in 1 mol.L^{-1} HNO_3, +1.44 V vs. SHE in 2 mol.L^{-1} H_2SO_4.[102–104] The different reduction potentials indicate that stable complexes in acidic media are formed as well as there exists a dependency on the anions of the various acids. According to the standard reduction potential (E^o (Ce(III)/Ce(IV)) = +1.72 V vs. SHE), it is expected to oxidize water whereas the system is kinetically stable.[104]

Solid-state compounds of terbium and praseodymium, like those of cerium, are well established, but Tb(IV) and Pr(IV) are unstable in aqueous solutions due to their very positive formal reduction potentials (+3.1 V vs. SHE and +3.2 V vs. SHE respectively), resulting in back reduction to their trivalent states by water as soon as they have been formed (**Figure 1.10**). However, there are multiple studies done to stabilize these compounds in solution.

The very first study of lanthanide stabilization was conducted by Hobart *et al.* where trivalent lanthanide chlorides of Tb, Ce and Pr

were dissolved in K_2CO_3 or $CsCO_3$ and the resulting colourless solutions containing 10^{-1} to 10^{-2} mol.L^{-1} of the lanthanide ion were placed in an electrochemical three electrode cell with a reticulated vitreous carbon (RVC) working electrode, Pt counter electrode and SCE reference electrode.[105] When +1.3 V vs. Ag/AgCl was applied, the working anode in this solution produced a golden colour at the surface of the electrode, which propagated in the bulk solution after 3h of electrolysis time. Adjusting the OH^-- ion concentration to ≈ 1 mol.L^{-1} stabilized Tb(IV), which could be observed by the colour change from a colourless to a dark, reddish-brown solution. Tb(IV) was characterized by its UV-Vis absorption spectra, having a broad-band absorption centred about 365 nm.[106] As a continuation of this study, Hobart *et al.* investigated the stabilization of actinides such as Am(IV), Cm(IV) and Cf(IV) with improved cell designs and new electrode materials.[107]

In another study, the electrochemical oxidation of Tb(III) on a conducting glass electrode (CGE) was reported using methods such as linear sweep voltammetry, and large amplitude pulse voltammetry.[108] The electrolyte was consisting of 2.5 mol.L^{-1} K_2CO_3 and 0.5 mol.L^{-1} KOH, and a brown colored layer was deposited on CGE. This deposit layer was characterized by UV-Vis spectroscopy, X-ray diffraction. The UV-Vis absorption peak with a maximum at 385 nm was comparable with the spectra of Tb_4O_7, whereas the deposit was found to be amorphous. After the deposition, the reduction of Tb(IV) was studied as well. It was concluded that the complex is a mix of Tb(III) and Tb(IV), and the chemistry is complex. As a part of it, radiotracer studies with ^{160}Tb were conducted as well. It was observed that more than 25% of the deposited material remained on the electrode after the reduction step. The duration of the deposition was kept between 1-5 minutes at +0.6 V vs. SCE, giving distinct linear scan voltammetry peaks.[108]

In the study of Varlashkin *et al.*, oxidation of Tb(III) in K_2CO_3–KOH solution was performed using two methods: electrochemical oxidation and chemical oxidation with ozone.[109] For the former one, various concentrations of OH^- ion between 0.1 to 1 mol.L^{-1} were explored and the emphasis was put on the applied voltage: i.e. when

+0.96 V was applied, it caused slight brown coloration in the solution, whereas at +1.06 V vs. SHE distinct brown colour was observed. However, when the applied potential was removed, the colour of the solution immediately faded. The absorption spectrum of the solution was similar to those observed in the previous works cited above, proving the stabilization of Tb(IV) in carbonate medium. However, the absorption spectra of the second solution could not be measured due to the interference of oxygen gas evolution. The yellow colour was correlated with formation of different terbium ion species consisting of carbonato and hydroxo complexes of mixed oxidation states of terbium.[109]

Another method used for oxidation is ozonolysis; chemical oxidation by bubbling ozone gas into the solution of Tb(III). Li *et al.*, obtained stable Tb(IV) in a more exotic electrolyte: aqueous tetrametaphosphate solution.[110] Again, the pH of the solution was kept at 12 by adding a NaOH solution, stressing the importance of the hydroxide concentration. However, the oxidation rate and stability was highly influenced by the temperature and pH, where it could be reached up to 60% at pH 12.6, 50 °C. The concentration ratio of Tb to electrolyte was also important, where Tb concentration was fixed to 2.26×10^{-4} mol.L^{-1}. It was stated that the reddish-brown Tb(IV) solution was stable up to 2 weeks in alkaline medium. The absorption peak in the 320-365 nm region was consistent with literature, indicating the oxidation to Tb(IV), despite the high redox potential of Tb(IV)/Tb(III) couple.[110]

1.3.2. Divalent oxidation state

The divalent oxidation state can be accessed in Eu, Yb and Sm, providing an unusual reductive chemistry among the lanthanide series. The stabilization of the divalent state originates from the half-filled shell ([Xe] $4f^7$) of Eu(II), the filled shell ([Xe] $4f^{14}$) of Yb(II) and nearly half-filled shell ([Xe] $4f^6$) of Sm(II). The reduction potentials for

the Ln(III)/Ln(II) couples are -0.43 V, -1.05 V and -1.55 V vs. SHE, respectively. The molecular divalent chemistry is well established for these lanthanides. Furthermore, solution chemistry is also studied via various methods. Among these lanthanides, the most stable one in aqueous solutions is Eu(II).

One of the methods used to reduce Eu(III) is using metal i.e. zinc amalgam, particles or powder in a weak acidic aqueous medium with the following reaction [98,111]:

$$2\mathrm{Eu}^{3+} + \mathrm{Zn} \rightarrow \mathrm{Zn}^{2+} + 2\mathrm{Eu}^{2+} \quad (1.2)$$

$$\mathrm{E}^{\circ}(\mathrm{Zn}^{2+}/\mathrm{Zn}) = -0.76\ \mathrm{V\ vs.\ SHE} \quad (1.3)$$

This process could be made into a continuous one via applying it to a column using zinc amalgam or zinc particles leading to a 98% reduction rate. As the reducibility of the zinc particles would be expected to decrease within time, diluted HCl could be used to reactivate the surface. However, the reduction of Sm or Yb using zinc could not be achieved.[89]

Another method for selective reduction is photochemical reduction of Eu(III), which is further followed by separation from other lanthanides in aqueous solutions. In the report of Donohue *et al.*, Eu(III) is reduced to Eu(II) by using several photolytic sources, precipitated in $EuSO_4$ form.[112] The separation of $SmCl_3$, $EuCl_3$ and $GdCl_3$ was carried out by photoreduction in an ethanol–isopropanol mixture, followed by precipitation. In this study, a high pressure mercury lamp is used and precipitation of $EuCl_2$ was achieved with 92% chemical purity.[113]

Reduction of lanthanides to the divalent state can also be achieved via electrochemistry. A variety of studies are conducted in different electrolyte systems to stabilize the divalent oxidation state in solutions. To start with, in the study of Myasoedov *et al.*, potential-controlled electrolysis and polarography were performed.[114] Dried acetonitrile was used as the solvent with 0.1 $mol.L^{-1}$ tetraethylammonium perchlorate (TEAP) as a supporting electrolyte to avoid back-oxidation of Eu(II) as happened in aqueous media. For the experimental set up, a standard calomel electrode (SCE) as the

reference electrode, mercury as the working electrode and platinum as the counter electrode were used. The reduction potential was lowered up to -0.6 V vs. SCE with accompanying bright yellow colour - giving a continuous absorption peak is at 320 nm indicating the conversion.[115]

In the works of Rabockai *et al.* and Steeman *et al.*, the reduction of Yb(III) ions in perchlorate solution was reported.[116,117] In addition to these, in a more recent paper the Eu(III) reduction was conducted in perchlorate media with the use of a boron-doped diamond (BDD) electrode.[118] This electrode offers lower capacitive current, wide potential window of 3 V with relatively low amounts of water decomposition and less surface redox activity leading to a significant improvement in electrochemical inertia. In the experiments, Ar is bubbled for elimination of oxygen and the solutions are transferred to the electrochemical cell via a peristaltic pump. The kinetic parameters were calculated and compared with previously reported literature data. A glassy carbon was used as a working electrode in 0.1 mol.L^{-1} KCl electrolyte. A significant increase of the kinetic reaction rate constant was observed for this electrode. Furthermore, investigation at different temperatures could not be conducted due to the reactivity of Eu(II) resulting in limiting information regarding the narrow range of experimental conditions.

There are several studies conducted on the reduction of Eu(III) in hydrochloric acid solution.[93,95,119] In the recent study of Jelinek *et al.*, Eu(III) was reduced at a glassy carbon electrode with the following steps explained as a two-step reduction of oxygen that is dissolved followed by the reduction of Eu(III):

$$O_2 + 2H^+ + 2e^- \rightarrow H_2O_2 \qquad E^0 = +0.68\ \text{V} \qquad (1.4)$$

$$H_2O_2 + 2H^+ + 2e^- \rightarrow 2H_2O \qquad E^0 = +1.77\ \text{V} \qquad (1.5)$$

$$Eu^{3+} + e^- \rightarrow Eu^{2+} \qquad E^0 = -0.43\ \text{V} \qquad (1.6)$$

$$2H^+ + 2e^- \rightarrow H_2 \qquad E^0 = 0.00\ \text{V} \qquad (1.7)$$

The hydrogen evolution reaction (HER) depends on the pH of the solution. It was also stated that the current efficiency is relatively low due to the initial amount of dissolved oxygen and re-oxidation to Eu(III).

As can be seen from the variety of methods for the redox chemistry of lanthanides in non-trivalent oxidation states in the literature, it can be concluded that stabilization can be achieved in various media, despite extremely high or low reduction potentials. Furthermore, due to its compatibility with subsequent separation processes and its high level of control, electrochemical reduction/oxidation is the most feasible method among them. Interference with radiolabelling reactions for future medical use can be avoided by removing harsh chemicals used in redox reactions. In addition, by varying parameters such as electrode material, electrolyte, solvent, cell design, pH, temperature, concentration, etc. it is possible to fine-tune the conditions for the separation process. There are examples of combining electrochemical or chemical reduction processes with a consecutive selective separation, especially for Eu(III) reduction, thanks to its high stability.[94,111,120,121] These can be expanded to medical radiolanthanide purification. In this PhD thesis, this is applied to Tb(III) oxidation for ^{161}Tb purification, as well as Eu(III) reduction for ^{153}Sm purification. Van de Voorde *et al.*, in their earlier study, investigated separation strategies combined with chemical and electrochemical reduction in nitrate media towards ^{153}Sm purification.[94,121] In these methods, when electrochemical reduction was compared to the chemical reduction, the reduction efficiency was higher via electrolysis as well as avoiding the impurities due to the reducing agent i.e. $Zn(OH)_2$ via Zn^{2+} hydrolysis. Therefore, in this thesis the electrochemical properties of the Eu(III)/Eu(II) redox couple was studied in detail, and complementary extraction chromatography methods are investigated for Sm/Eu separation. In parallel to that, Tb/Gd separation is studied via investigating electrochemical oxidation in various aqueous media, which then paired with column separation as well, towards ^{161}Tb purification.

Chapter 2.

Objectives

This PhD thesis focusses on the redox chemistry of the radiolanthanides and the development of a novel method for purification of medical radiolanthanides using a change in the oxidation state of one of the lanthanides in the mixture. By applying an electrochemical method, the use of chemicals for redox reactions can be avoided. Moreover, by avoiding complex chemical mixtures during the oxidation or reduction step, the likelihood increases that the system is compatible with a larger variety of separation strategies. In Chapter 1, a brief overview is given on the radiolanthanides, their redox chemistry and state-of-the-art separation processes, mainly focusing on ^{161}Tb and ^{153}Sm.

In Chapter 3, the electrochemical oxidation of Tb(III) to Tb(IV) in aqueous electrolytes is investigated. This in-depth analysis is done in order to achieve the oxidation in a relatively achievable potential window, with high Tb(IV) stability. The applied potential, stability and conversion rate are qualitatively determined to find the optimum conditions for the terbium oxidation. It was crucial to determine these parameters in order to obtain the highest yield as well as finding the electrolyte in which Tb(IV) is the most stable to proceed with the subsequent purification. In Chapter 4, the purification of ^{161}Tb is achieved by a column separation method compatible with the stable Tb(IV) carbonate complex. In addition, the complexation of Tb(III) and Tb(IV) in carbonate medium is studied, to elucidate the separation mechanism and provide insight to improve the overall separation efficiency. Complementary techniques are used in order to prove the change in the oxidation state, leading to a successful separation of Tb(IV) and Gd(III) based on the differences in oxidation state.

Another lanthanide of electrochemical interest is europium. This well-established redox chemistry of the reduction of Eu(III) to Eu(II) in

various aqueous and non-aqueous electrolytes is specifically investigated in aqueous nitrate medium. So far, only polarographic studies have been performed on the kinetics of this system. In Chapter 5, a kinetic study is carried out using a rotating disk electrode in various electrolytes to gain further insight into the redox chemistry of europium, particularly in nitrate medium.

As demonstrated by Van de Voorde *et al.*, Eu(III) can be electrochemically reduced to Eu(II) in highly concentrated nitrate medium.[98] Furthermore, to separate ^{153}Sm from long-lived ^{152}Eu, the strategy can again be based on the redox properties of these lanthanides. In addition to these preliminary studies, in Chapter 6, we demonstrate the separation of Sm and Eu using radioactive tracers, hereby replicate the conditions expected during the nuclear reactor production route to prove the applicability of these separation processes.

Overall, the research objectives of this PhD thesis are:

- to investigate the redox chemistry of Tb and Eu in aqueous media
- to identify compatible electrolytes where the oxidized/reduced species are sufficiently stable for further purification
- to study in depth the electrochemical kinetics of europium reduction reaction in aqueous nitrate medium as a case study for lanthanide redox chemistry
- to develop a suitable separation process for the Gd/Tb pair towards the medical ^{161}Tb purification based on changing redox properties
- to scale up the tracer studies to BR2 production conditions for the Sm/Eu pair towards medical ^{153}Sm purification

Chapter 3.

Electrochemical oxidation of terbium(III) in aqueous media: influence of supporting electrolyte on oxidation potential and stability

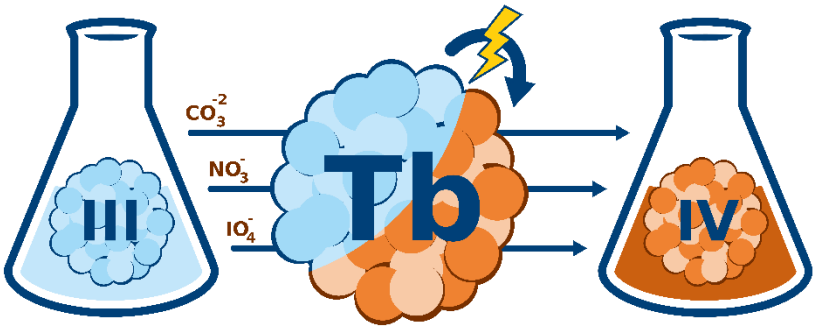

This chapter is based on the following paper:

M.O. Arman, B. Geboes, K. Van Hecke, K. Binnemans, T. Cardinaels

Journal of Applied Electrochemistry **52** (2022) 583–593.

DOI: 10.1007/s10800-021-01651-0

The text has been reproduced with permission from © Springer Nature B.V. 2021

The text might contain minor adjustments to the original publication.

All experimental work and compilation of the manuscript were performed by the author of this thesis. Co-authors contributed to the revision and design of the experiments.

3.1. Abstract

Apart from the generally dominant trivalent oxidation state, several lanthanides can occur in divalent or tetravalent states as well. Changing the valence state alters the chemical properties and therefore gives the opportunity to ease intragroup lanthanide separations. The hydrated terbium(III) ion has a highly positive reduction potential (E^0= +3.1 V vs. SHE), but it can be oxidized to its tetravalent state and via ozonolysis or electrolysis and stabilized in highly concentrated carbonate solutions. In this study, terbium(III) is electrochemically oxidized to terbium(IV) in aqueous carbonate, nitrate and periodate media. Spectroscopic and elemental analysis were done to characterize terbium(IV) and to gain insight in the stability of these complexes in the aqueous electrolytes of carbonate, nitrate and periodate. In all these electrolytes, oxidation and stabilization were achieved at different pH, terbium concentration, salt concentration and applied potentials. The most promising electrolyte was found to be carbonate, since it allowed to attain more concentrated and more stable terbium(IV) solutions.

3.2. Introduction

Lanthanides have various applications such as luminescent materials, magnets, catalysts, MRI contrast agents and (radio-)pharmaceuticals.[16,27,122,123] Across the lanthanide series, the 4f subshell is gradually filled with electrons that are shielded by the filled 5s and 5p subshells, resulting in 4f electrons not participating in ligand interactions and bond formation. As a consequence, the chemical properties of the lanthanides are quite similar. Lanthanide chemistry is dominated by the trivalent oxidation state.[101] However, a change in oxidation state leads to significant changes in chemical properties. This offers the opportunity to develop new separation processes of neighbouring lanthanides.[93,119,124–127] The availability of other valence states can therefore be advantageous in industrial processes such as

reprocessing of spent nuclear fuel, purification of medical radiolanthanides or recovery of lanthanides from ores.[16,124–126]

There are many studies on divalent lanthanides,[93,95,96,98,99,112–114,116,117,124,128] whereas tetravalent cerium is the most established tetravalent lanthanide both in solid state and in solution.[104,126,129–135] The stability of the tetravalent oxidation state for cerium and terbium can be explained by an empty ([Xe] $4f^0$) and a half-filled 4f subshell ([Xe]$4f^7$), respectively. Compared to the other tetravalent lanthanides Tb(IV) or Pr(IV) , Ce(IV) has a relatively high stability in aqueous solutions due to the slow kinetics of its reaction with water; e.g. E^0 (Ce(IV)/Ce(III)) = +1.70 V vs. SHE in 1 mol.L^{-1} $HClO_4$, +1.61 V vs. SHE in 1 mol.L^{-1} HNO_3 and +1.44 V vs. SHE in 1 mol.L^{-1} H_2SO_4.[102,136] Furthermore, the recovery of cerium from mixtures of rare earths can be done via oxidation of Ce(III) to Ce(IV), followed by separation from the other rare earths based on the significant change in the chemical properties.[126,137,138] Likewise, it has also been reported that europium can be separated from the neighbouring lanthanides samarium and gadolinium via selective reduction of Eu(III) to Eu(II).[139–141] Therefore the efficiency of separation and purification processes of lanthanides can be increased by taking advantage of their less-common oxidation states.

Similarly, tetravalent cerium, terbium and praseodymium are known in the solid-state, in the form of oxide or fluoride compounds.[142–145] However, Tb(IV) and Pr(IV) are unstable in aqueous solutions due to their very positive formal reduction potentials (+3.1 V and +3.2 V vs. SHE, respectively), resulting in their back reduction to the trivalent states by reaction with water. Only limited experimental information on stabilization of tetravalent terbium in aqueous solutions is available in the literature,[105,106,108–110,146,147] although recent studies showed the possibility of ligand design and chemical oxidation of these trivalent terbium complexes to their tetravalent state.[148–150] However, these solid-state molecular complexes are very sensitive to air and moisture and their solutions in organic solvents are stable only for a few days.[148–150]

So far, the methods used for oxidizing terbium(III) to terbium(IV) in aqueous solutions involve either ozonolysis or electrolysis in various alkaline media.[105,108–110,142,146] The major outcomes of these studies are that higher concentrations of hydroxide ions are essential for stabilizing tetravalent terbium, the efficiency of ozonolysis is higher than that of electrolysis, and the electrochemistry of terbium is complex. Nevertheless, an in-depth study of the electrochemical oxidation of terbium(III) is lacking. Electrochemical oxidation is a good alternative to chemical oxidation before no foreign ions are introduced, but the complexity of the system increases.

In this study, the electrochemical oxidation of Tb(III) in aqueous media is investigated by a combination of electrochemical, spectroscopic and complementary analytical techniques. The knowledge on oxidation of Tb(III) in the carbonate-hydroxide system is expanded by in depth analysis of varying electrolyte concentrations, terbium concentration, pH, applied potential and electrolysis time. The time needed to oxidize the maximum amount of Tb(III) to Tb(IV) is examined and the influence of terbium and carbonate salt concentrations are elucidated. Additionally, the effect of the formed terbium complex on the oxidation behaviour and the Tb(IV) stability is investigated by electrochemically oxidizing Tb(III) in nitrate and periodate electrolyte solutions as this has not been described previously in literature to the best of our knowledge.

3.3. Experimental

3.3.1. Materials

$Tb(NO_3)_3{\cdot}6H_2O$ (99.9%) and $TbCl_3{\cdot}6H_2O$ (99.9%) were purchased from Strem Chemicals, Inc. (Newburyport, USA). K_2CO_3 (anhydrous,≥ 98%), KOH pellets and C_2H_5OH (96 %) were purchased from VWR International B.V. (Leuven, Belgium). $Ca(NO_3)_2{\cdot}4H_2O$ (≥99%), $CaCl_2{\cdot}6H_2O$ (98%) and HNO_3 (65%) were purchased from Sigma-

Aldrich BVBA (Overijse, Belgium). KIO_4 (99.9%) and Nafion® N-117 membrane (0.180 mm thick, ≥0.90 meq/g exchange capacity) was purchased from Alfa Aesar (Karlsruhe, Germany). All chemicals were used as received without any further purification. All aqueous solutions were prepared with ultra-pure water (18.2 MΩ cm at 25 °C).

3.3.2. Bulk electrolysis

Electrochemical oxidation of terbium(III) was performed in an undivided three-electrode BASI QVMF1051 electrolysis cell. Two different set-ups were used depending on the total volume of the sample; 5 mL or 50 mL, respectively. In high volume experiments, solutions were purged with argon gas during the electrolysis for mixing purpose. A cylindrical platinum-gauze electrode (cylinder ø = 35 mm, height = 50 mm, 18 mesh) was used as working electrode, and a coiled platinum wire (ø = 1 mm) served as counter electrode. The reference electrode was BASi MF-2056 Ag/AgCl in a 3 $mol.L^{-1}$ KCl solution. A Metrohm Autolab PGSTAT302N potentiostat, operated by Nova 2.1.4 software, was used in potentiostatic mode to apply the electrolysis potential to the electrochemical cell. Various constant potentials in between +0.7 V to +2.1 V (vs Ag/AgCl) were applied, depending on the electrolyte media.

3.3.3. UV-Vis spectroscopy

The increase in Tb(IV) concentration and stability over time were measured by monitoring the change in absorbance during a wavelength scan. The Tb(III) solutions as well as the carbonate media and other electrolytes used in this study were colourless. Oxidation of Tb(III) led to a yellow-brown or dark reddish coloration depending, on the concentration of Tb(IV) and media. Depending on the intensity, quartz cuvettes with various path lengths (1 mm or 10 mm) were used. For some experiments, a flow cell with path length 0.1 mm was used

as well. Spectra were recorded in the 230–1000 nm range using a Shimadzu 1800 spectrophotometer, operated by UV Probe 2.5 software. The light source changeover occurred at 340.8 nm. A medium scan speed (accumulation time 0.2s) was used. The blank solutions containing all components besides terbium were used for baseline correction. In nitrate media, due to the broad band absorbance of nitrate between 260 to 340 nm, spectra were recorded in the range of 330 – 1000 nm.

3.3.4. Inductive coupled plasma mass spectrometry

Terbium concentrations of various solutions were determined via inductively coupled plasma mass spectrometry (ICP-MS) using an X2 Series II ICP-MS instrument (Thermo Fischer Scientific). The solutions were diluted with a matrix consisting of ultrapure water and HNO_3 (2% v/v). Different dilution factors were applied based on terbium concentrations in various media.

3.3.5. X-ray powder diffraction

To analyze the precipitations and depositions on the counter electrode at different media XRD analyses were done using a PANanalytical X'Pert Pro diffractometer. The device was applied in a Bragg-Brentano parafocusing geometry in a θ–θ configuration and a copper LFF X-ray tube ($K\alpha_1$ = 1.5405929 Å) was used as the radiation source. Lattice parameters were fitted by the software package HighScore Plus Version 4.8 by PANalaytical. The samples of the precipitates were collected via centrifugation. The sample from the deposits on the platinum electrode were collected via scratching. After collection, the samples were washed two times with ultra-pure water and one time with methanol.

3.4. Results and Discussion

3.4.1. Electrochemical oxidation of Tb(III) in various aqueous media

In the study of Hobart *et al.*, trivalent lanthanide chlorides were dissolved in K_2CO_3 or $CsCO_3$ and the resulting colourless solutions containing 10^{-1} to 10^{-2} mol.L^{-1} lanthanide ion were electrolysed for various time periods up to 3 hours.[105] It is reported that the standard reduction potentials for Ln(IV)/Ln(III) couples substantially shift towards less positive potentials when complexation occurs in this medium.[105,109] When +1.3 V vs. SHE was applied to a platinum screen, the working anode in this solution produces a golden colour at the surface of the electrode, which propagates in the bulk solution. Adjusting the hydroxide ion concentration to ≈ 1 mol.L^{-1} stabilizes Tb(IV), which can be observed by the colour change from colourless to a dark, reddish-brown solution. Tb(IV) is characterized by UV-Vis absorption spectra with a broad-band absorption centred about 365 nm.[105,106]

Apart from electrochemical oxidation, Tb(III) can be also oxidized via ozonolysis in tetrametaphosphate and periodate medium.[110,146] However, no detailed studies have been reported on the oxidation of Tb(III) via electrochemical methods. In present study, we investigated the electrochemical oxidation of Tb(III) in three different aqueous media: carbonate, nitrate and periodate media. The applied potentials were selected based on the previous literature mentioned above.

3.4.2. Carbonate medium

Tb(III) (0.04 – 0.2 mol.L^{-1}) was electrolysed at +1.3 V vs. Ag/AgCl in concentrated carbonate solutions (2 – 5.5 mol.L^{-1}) with ca. 0.06 mol.L^{-1} KOH added for stabilization of Tb(IV) depending on the carbonate concentration. The concentration range was selected based on the lowest concentration value where the oxidation could still be observed, and the highest concentration where the solubility limit of terbium salt in the carbonate media was not exceeded. Initially, a solution containing 0.1 mol.L^{-1} terbium(III) and 5.5 mol.L^{-1} potassium carbonate at pH = 14 was electrolysed at +1.3 V vs. Ag/AgCl and the current response was recorded (**Figure A.3.1**). The total charge calculated after 1h of electrolysis was 25.47 C. Since the applied potential was beyond the potential window of water, oxygen generation was more pronounced (Eqn. 3.1, 3.2). Therefore, the simultaneously occurring oxygen evolution reaction hinders any further electrochemical characterization of Tb(III) oxidation reaction.

$$2OH^- \rightarrow O_2 + 2H_2O + 2e^- \qquad (E^0 = +0.40\ \text{V vs. SHE}) \qquad (3.1)$$

$$Tb^{4+} + e^- \rightarrow Tb^{3+} \qquad (E^0 = +3.1\ \text{V vs. SHE}) \qquad (3.2)$$

A Tb(III) solution in carbonate media is colourless, whereas Tb(IV) has a colour ranging from yellow to brown, depending on the concentration of Tb(IV) and characterized by a broad charge transfer band with an absorption peak centred at 365 nm in UV-Vis absorption spectra (**Figure A.3.2**). With a constant potential of +1.3 V vs. Ag/AgCl applied, there is a yellow colour appearing on the working electrode, which dissipates into the bulk solution. Therefore, UV-Vis absorption spectra were measured to monitor the conversion of Tb(III) to Tb(IV). The measurements were done in triplicate, giving reliable and accurate results at high concentrations (**Figure A.3.3**).

In the same experimental conditions described above, electrolysis was performed in an undivided cell for 4.5 hours at different potentials, +1.15 V (**Figure 3.1**) and +1.3 V (**Figure 3.2**) vs. Ag/AgCl, respectively. Samples were taken every 30 minutes for off-line UV-Vis absorption

measurements. As can be seen in **Figure 3.3**, the absorbance is increasing as a function of electrolysis time and does not reach a plateau value after 4 hours. This is due to the contribution of both the competing oxygen formation reaction at the working electrode and back reduction of Tb(IV) at the counter electrode (Eqn. 3.1). The oxygen evolution reaction in the alkaline medium would result in a slow decrease in the hydroxide ion concentration and therefore this would influence the stability of Tb(IV) complex. Therefore, the complete conversion of Tb(III) to Tb(IV) could not be achieved. Electrolysis was achieved at +1.15 V vs Ag/AgCl and the Tb(IV) solutions were stable enough for further analysis. With decreasing applied potential, the conversion rate of Tb(III) to Tb(IV) decreases, but was still possible. When potentials applied lower than +1.15 V vs. Ag/AgCl, electrolysis was not successful.

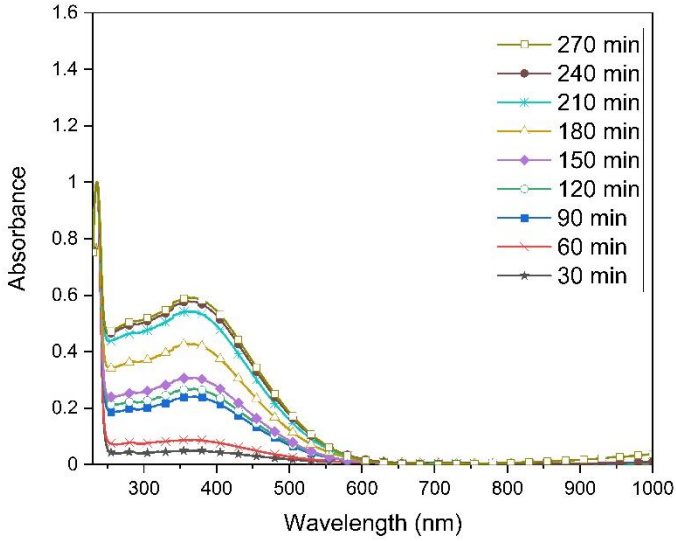

Figure 3.1. UV-Vis absorption spectra of 0.1 mol.L^{-1} Tb(III) in 5.5 mol.L^{-1} K_2CO_3 solution at pH = 14 at electrolysis times 0 min – 270 min. Tb(IV) formation was followed by the peak characterized with 365 nm. Electrolysis was at constant potential +1.15 V vs. Ag/AgCl, applied for 270 min. Blank solution was used as reference sample for baseline correction. The cell path length was 1 mm.

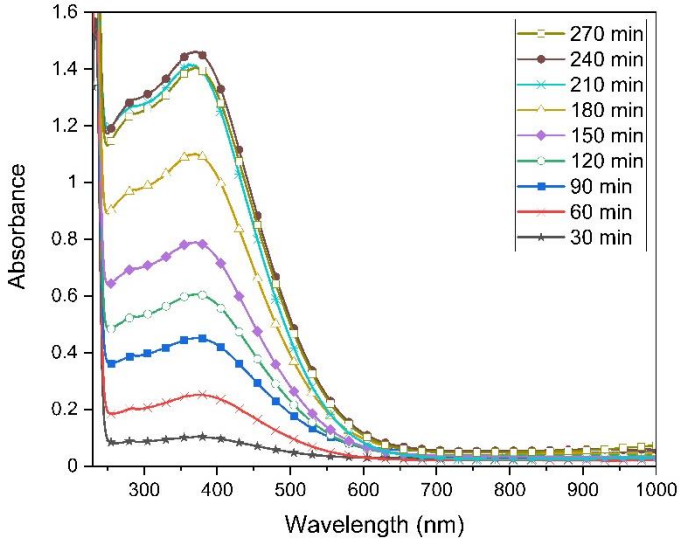

Figure 3.2. UV-Vis absorption spectra of 0.1 mol.L^{-1} Tb(III) in 5.5 mol.L^{-1} K_2CO_3 solution at pH = 14 at electrolysis times 0 min – 270 min. Tb(IV) formation was followed by the peak characterized with 365 nm. Electrolysis was constant potential +1.3 V vs. Ag/AgCl, applied for 270 min. Blank solution was used as reference sample for baseline correction. The cell path length was 1 mm.

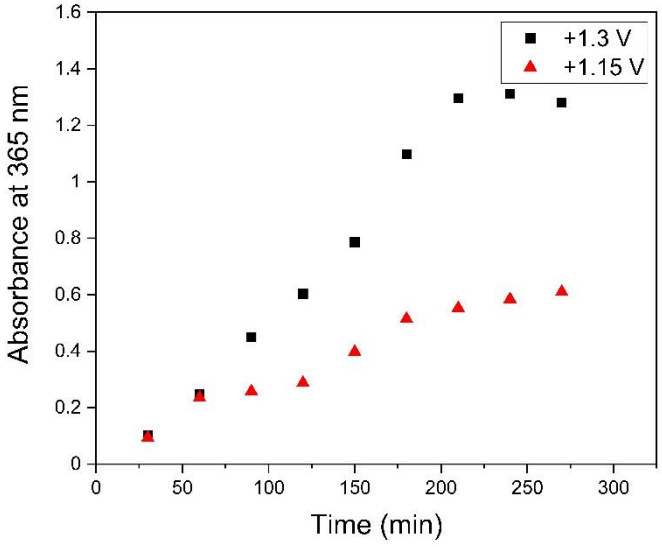

Figure 3.3. Correlation between the absorbance values at 365 nm and electrolysis times at potentials +1.15 V and +1.3 V vs. Ag/AgCl.

In addition to these, a divided cell was used in order to eliminate the possibility of the back reduction reaction of the Tb(IV) complex on the counter electrode. In this configuration, possible by-products could be avoided while achieving maximum conversion to the Tb(IV) state. A Nafion™ membrane was used giving minimal cell resistance and offering high stability in a wide pH range. Although initially a colour change to brown was observed, indicating Tb(IV) formation, it was not stable during further electrolysis. After 30 minutes of applying +1.3 V vs. Ag/AgCl, the solution was fading to colourless again. The pH values of anode and cathode compartments were measured afterwards and reported as ≈11.8 and 14.9 respectively.

This result shows that hydroxyl ions formed as the counter electrode product (Eqn. 3.3) are necessary to balance the pH in the electrolyte, given the fact that the stability of Tb(IV) is strongly pH dependent.

$$2H_2O + 2e^- \rightarrow H_2 + 2OH^- \qquad (E^0 = -0.83\ \text{V vs. SHE}) \qquad (3.3)$$

The effect of carbonate concentration was also investigated. When the same experimental conditions in an undivided cell were applied with lower carbonate concentrations of 2 or 3 mol.L^{-1}, coloration of the solution was observed on the electrode surface. However, this coloration disappeared immediately when switching off the applied potential. When the concentration of carbonate was increased to 4 or 5 mol.L^{-1}, both the oxidation rate and stability of the Tb(IV) complex increased, which was supported by the UV-Vis absorption spectra. On the other hand, when adding other lanthanides to the same solution e.g. 0.05 mol.$^{L-1}$ of Gd(III) , Tb(III) and Dy(III) mixture, it was observed that it did not inhibit the Tb(III) oxidation or stabilization in this medium.

Figure 3.4). However, the increase in carbonate concentration did not promote the oxidation of Tb(III) due to the solubility being limited at that high concentrations leading precipitation and pH change. Therefore, for all the measurements carbonate concentration was fixed to 4 mol.L^{-1} during further experimental studies.

In order to examine the maximum conversion point of Tb(III) to Tb(IV), a solution containing 0.07 mol.L^{-1} Tb(III) in 4 mol.L^{-1} carbonate salt was

electrolysed at a constant potential of +1.3 V vs. Ag/AgCl. During the electrolysis, every hour, a UV-Vis absorption spectrum was recorded and the maxima were plotted against the electrolysis time (**Figure 3.5**). It can be seen that a plateau value was reached after 10 hours of electrolysis. Considering that back reduction of Tb(IV) was concurrently happening with part of the anodic current being consumed by oxygen formation, this could result in slow kinetics and prevented achieving full conversion at early electrolysis times.

Figure 3.6 shows the UV-Vis absorption spectra of terbium in the concentration range, considering the solubility limit, between 0.04 and 0.2 mol.L^{-1} measured in 4 mol.L^{-1} carbonate solutions at fixed electrolysis time with an applied potential of +1.3 V vs Ag/AgCl. At terbium concentrations lower than 0.04 mol.L^{-1}, the oxidation was no longer observed. When the terbium concentration was increased, the absorbance values of Tb(IV) were also increasing at the fixed electrolysis time of 3 hours (**Figure 3.6**). Instead of a linear correlation, a logarithmic trend was observed with increasing Tb concentration. Two factors could explain this logarithmic behaviour; the maximum conversion is not achieved at 3 hours of electrolysis for higher concentrations of Tb(III) or with increasing carbonate concentrations, the minimum amount of Tb(III) concentration needed to oxidize increases due to strong complexation hindering the terbium oxidation reaction.[109] On the other hand, when adding other lanthanides to the same solution e.g. 0.05 mol.L^{-1} of Gd(III) , Tb(III) and Dy(III) mixture, it was observed that it did not inhibit the Tb(III) oxidation or stabilization in this medium.

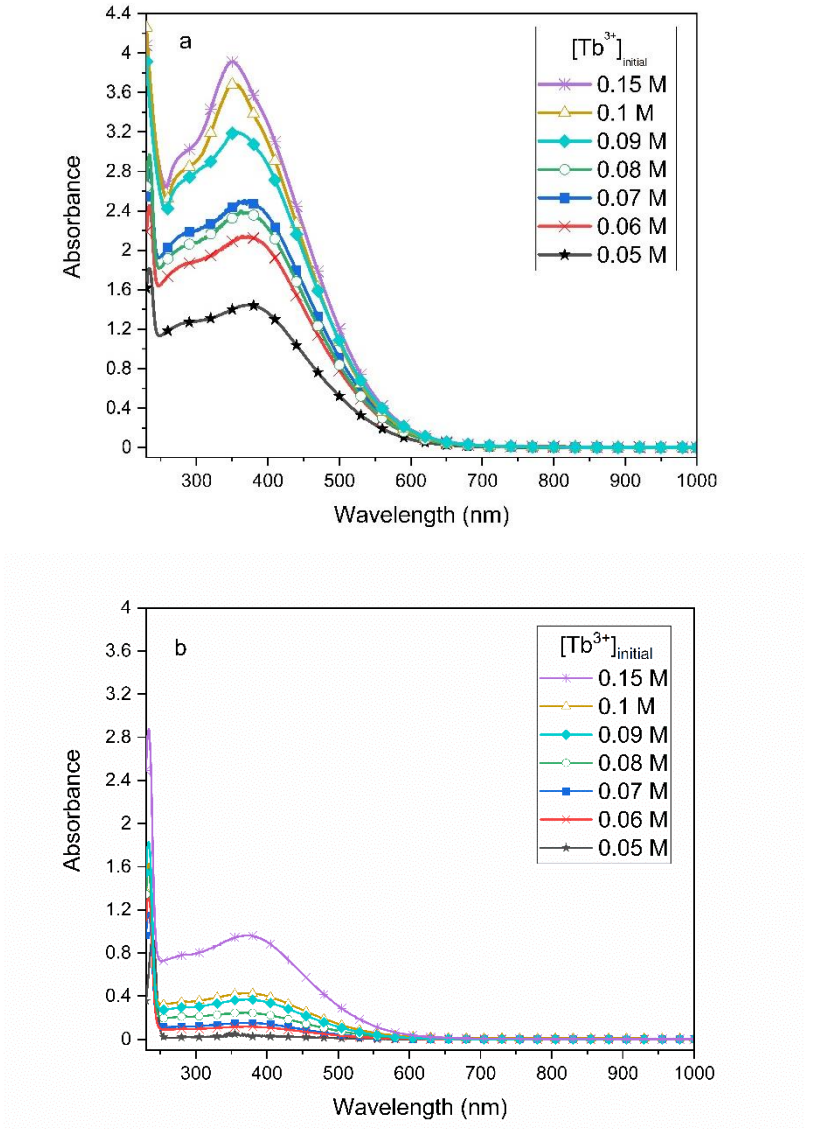

Figure 3.4. UV-Vis absorption spectra of solutions electrolyzed 2 h at +1.3 V vs Ag/AgCl containing 0.05 – 0.15 mol.L^{-1} Tb(III) in (a) 4 mol.L^{-1} (b) 5 mol.L^{-1} of K_2CO_3 at pH = 14. Tb(IV) formation was followed by the peak characterized with 365 nm. Blank solution was used as reference sample for baseline correction. The cell path length was 1 mm.

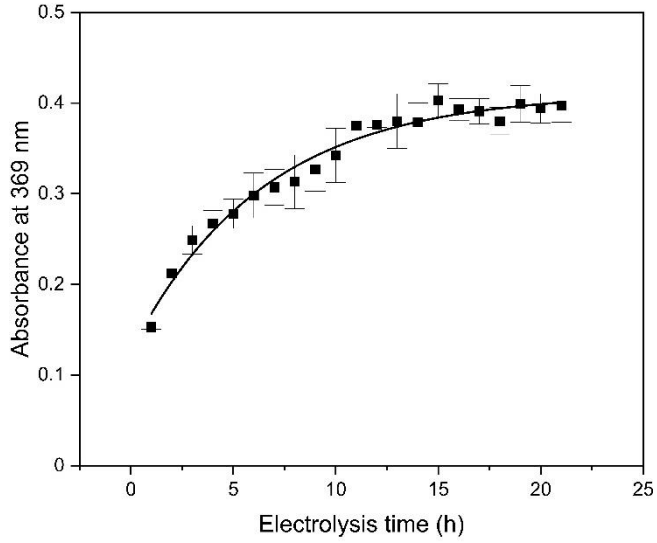

Figure 3.5. Correlation between absorbance values measured at 365 nm and electrolysis time. UV-Vis absorption spectra of 0.07 mol.L^{-1} Tb(III) in 4 mol.L^{-1} K_2CO_3 solution at pH = 14 is recorded in 1 h intervals. Blank solution was used as reference sample for baseline correction. The path length was 0.1 mm. The measurement was done triplicate. The uncertainty ranges from 0.001 – 0.04 a.u. At 11 hours of electrolysis, absorbance value is measured as 0.38 ± 0.04.

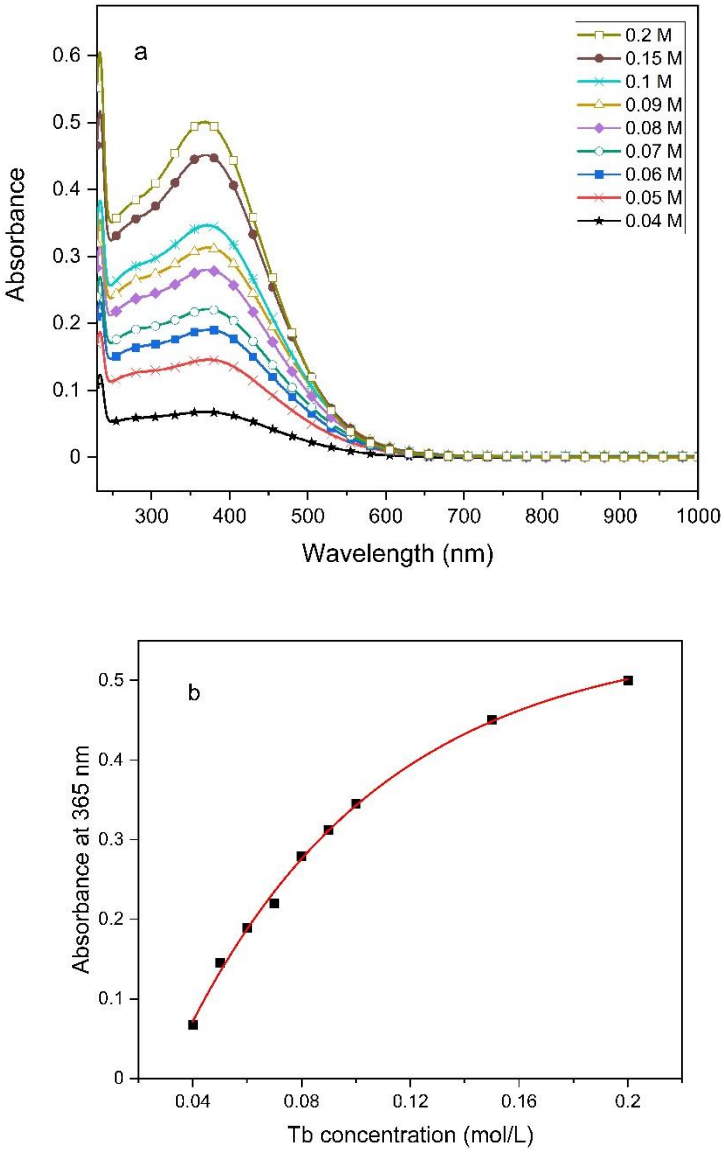

Figure 3.6. (a) UV-Vis absorption spectra of 0.04 – 0.2 mol.L^{-1} Tb(III) in 4 mol.L^{-1} K_2CO_3 solution at pH = 14. Blank solution was used as reference sample for baseline correction. The path length was 0.1 mm **(b)** Correlation between absorbance values measured at 365 nm and initial Tb(III) concentration.

3.4.3. Nitrate media

Recently, it was shown by our research group that europium(III) can be reduced to and stabilized in its divalent state via electrochemical reduction in highly concentrated nitrate media.[98] Although it is not a common electrolyte to be used, since it is not inert in the full aqueous potential window, it was investigated if a comparable lanthanide stabilization occurs in the oxidation of terbium at various concentration ratios. Different nitrate salts were used: ammonium nitrate, calcium nitrate, lithium nitrate and potassium nitrate. Due to the relatively high solubility and electrolysis only occurring at this solution, calcium nitrate was chosen as the electrolyte for the remainder of the experiments. In highly concentrated solutions of 6 and 9 $mol.L^{-1}$ nitrate, a slightly yellow coloration was observed when +2.1 V vs. Ag/AgCl in 3 $mol.L^{-1}$ KCl was applied. The charge calculated for the electrolysis was 113.72 C. At lower applied potentials than that or at lower concentrations of nitrate, only oxygen formation was observed on the working electrode, without any colour change.

After various parameter studies of terbium and nitrate concentrations, optimization was achieved in described conditions. A solution of 0.01 $mol.L^{-1}$ terbium(III) nitrate salt dissolved in 9 $mol.L^{-1}$ calcium nitrate was electrolysed for more than 3 hours. UV-Vis absorption spectra were recorded during the electrolysis. Spectra were recorded up to only 330 nm because of the strong absorption of nitrate ions at shorter wavelengths. As can be seen in **Figure 3.7**, a broad peak centred around 369 nm was observed, which is similar to spectra of Tb(IV) in carbonate media, although with relatively lower absorbance values. In contrast to carbonate media, considering that the initial terbium concentration was also lower, maximal conversion was observed after ca. 2 hours of electrolysis.

Additionally, nitrate itself causes a brown coloration in the solution, obscuring the absorbance of Tb(IV) (**Figure 3.8**). According to the previous research, when anodic potentials applied to $AgNO_3$ in acetonitrile, a brown coloration occurred as well.[151,152] This was

supported by Ag(II) reacting with N_2O_5 (Eqn. 3.4) resulting in the colour change.

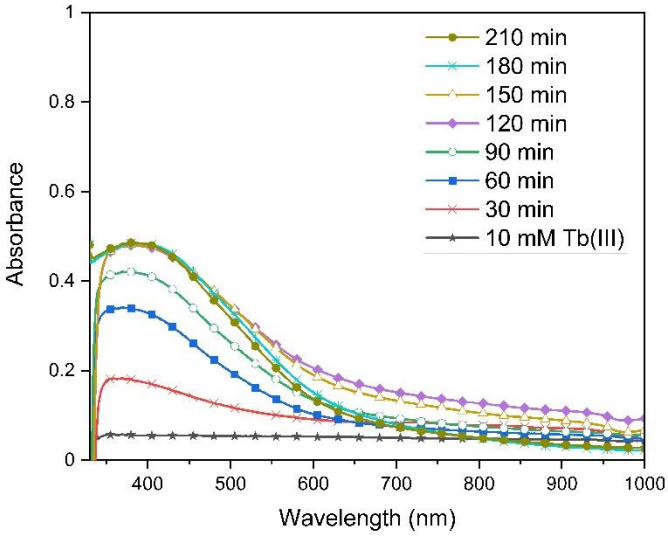

Figure 3.7. UV-Vis absorption spectra of 0.010 mol.L^{-1} Tb(III) in 4.5 mol.L^{-1} $Ca(NO_3)_2$ solution, followed up with increasing electrolysis time up to 210 min with samples taken in every 30 min, electrolyzed at constant potential of +2.1 V vs. Ag/AgCl. Tb(IV) formation was followed by the peak characterized with 369 nm. Blank solution was used as reference sample for baseline correction. The cell path length was 10 mm.

After 2 hours of electrolysis, UV-Vis absorption spectra of both blank and terbium solutions were recorded. The maxima of the broad peak differed only a few nanometres, and the distinction can be made by the shoulder appearing in the Tb solution. After blank correction of the UV-Vis spectra, the shoulder belonging to Tb(IV) became more pronounced, could be an indication of contribution of Tb oxidation as well as the blank. After electrolysis, the brown solution was centrifuged at 4000 rpm for 1 hour. While the coloration dissipated in the solution was precipitated and the remaining solution was colourless. This precipitate was obtained by filtration and both residue and filtrate were analysed. The XRD analysis of the residue was matching well with calcium nitrate salt (**Figure A.3.4**). Furthermore, by ICP-MS measurements on both the filtrate and precipitate, it was

shown that the solution contained all the Tb (1.47± 0.15 g/L), confirming that the precipitation was mainly coming from bulk calcium nitrate salt.

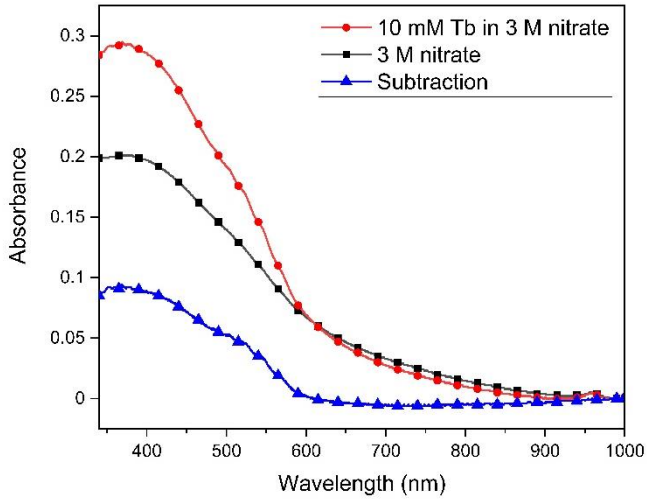

Figure 3.8. UV-Vis absorption spectra of blank in 3 mol.L^{-1} $Ca(NO_3)_2$ and 0.01 mol.L^{-1} Tb(III) in 3 mol.L^{-1} $Ca(NO_3)_2$ solution electrolyzed for 2 hours at +2.1 V vs. Ag/AgCl. Tb(IV) formation was followed by the peak characterized with 365 nm. Blank solution without terbium was used as reference sample for baseline correction. The cell path length was 10 mm.

Moreover, during the electrolysis, a deposition occurred at the counter electrode, resulting in a decreasing working electrode potential. The electrode was first rinsed with water in triplicate and then collected via scratching for further analysis. With XRD analysis (**Figure A.3.5**), the deposit was identified as $Ca(OH)_2$ when compared with the reference data from ISCD. Further ICP-MS analysis showed that there was only trace amounts of Tb present (1460 ± 150 μg/L) in the deposit. This would also explain the pH change of the solution after electrolysis, lowering from ca. pH = 4 to pH = 1. Although we could observe to some extent oxidation of terbium(III), supported by UV-Vis absorption spectroscopy, the results obtained in nitrate media showed that the system is quite complex with side reactions induced

by the electrolyte. Moreover, anodic reactions of nitrate ions could be a competing reaction in the electrochemical oxidation of Tb(III) (Eqn 3.4, 3.5).[151–153]

$$NO_3^- \rightarrow NO_2 + 0.5\ O_2 + e^- \quad (3.4)$$

$$2NO_3^- \rightarrow N_2O_5 + 0.5\ O_2 + 2e^- \quad (3.5)$$

3.4.4. Periodate medium

The periodate ion (IO_4^-) is a strong oxidizing agent and already well-established for stabilization of transition metals with high oxidation states.[154] In alkaline periodate medium, terbium is oxidized via ozonolysis and a relatively stable tetravalent complex formation occurred. It is stated that in the KIO_4–KOH system the redox potential of terbium can be lowered to +0.68 V vs. SHE.[147]

In this medium, relatively lower concentrations were used due to the limitations on solubility of potassium periodate (4.2 g/L at 20 °C). Therefore, optimum concentrations were defined to be solutions containing 0.006 mol.L^{-1} terbium and 0.09 mol.L^{-1} periodate salt and brought to pH 12.9 by addition of potassium hydroxide. The addition of potassium hydroxide led to increased periodate salt solubility and therefore contributes to complex formation and stabilization of Tb(IV). Lower potentials, up to +0.9 vs. Ag/AgCl were applied and still a coloration of the solution could be observed. A possible reaction, apart from the oxygen evolution reaction, competing with the oxidation of terbium is:

$$IO_4^- + 4H_2O + 8e^- \rightarrow I^- + 8OH^- \quad (E^o = +0.39\ \text{V vs. SHE}) \quad (4.6)$$

When a potential of +1.3 V vs. Ag/AgCl was applied for 1 hour (calculated charge was 25.02 C), the solution coloured yellow. The absorbance spectra is similar with the previous results, showing a broad absorption band with a maximum around 362 nm (**Figure 3.9**). As a result, oxidation of Tb(III) could be achieved at relatively lower pH compared to carbonate medium.

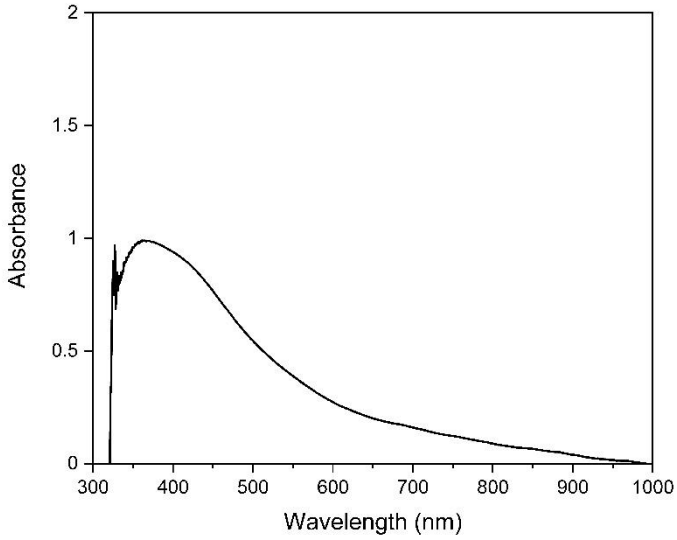

Figure 3.9. UV-Vis absorption spectra of 0.004 mol.L^{-1} Tb(III) in 0.09 mol.L^{-1} KIO_4 solution at pH 12.9, electrolyzed for 1 h at constant potential of +1.3 V vs. Ag/AgCl. Tb(IV) formation was followed by the absorbance peak at 369 nm. Blank solution without terbium was used as reference sample for baseline correction. The cell path length was 10 mm.

3.4.5. Stability studies

The oxidation of Tb(III) to Tb(IV) was achieved in various experimental conditions and media. Although Hobart *et al.* indicated that the coloration of the oxidized solution in carbonate medium remained for weeks,[105] no detailed study was performed regarding the stability of Tb(IV) in carbonate medium as a function of time. Therefore, the oxidized samples were stored up to 30 days and UV-Vis absorption spectra were recorded at fixed time intervals relative to the moment of electrolysis depending on the medium.

For carbonate media, the evolution of the absorbance values over time were plotted in **Figure 3.10**. The samples were stored in closed vessels in dark and at a controlled temperature environment. Since

the samples were stored in a closed vessel, at dark and in a controlled temperature environment, the CO_2 impact on the carbonate content is expected to be negligible. After only 1 day of electrolysis, the absorbance of all electrolysis times decreased with the same trend indicating a limited stability. The back-reduction of Tb(IV) to Tb(III) could explain the decrease in the absorbance values. After 20 days, precipitation was observed in all the solutions that were electrolysed for more than 90 minutes. This could be triggered by water evaporation over time although no substantial amount of loss was observed. The precipitation was analysed via XRD, however no crystalline structure could be detected. When ICP-MS analysis is done on the precipitate and the solution, it was found that the bulk amount of Tb (>99%) remains in solution. It can also be seen in the absorption spectra that there was a cut-off at 120 minutes, which could be related to the back-reduction. Furthermore, after 30 days of measurement, in all solutions with an electrolysis time of 30 minutes or more, a brown precipitate was formed. Although precipitation was occurring, as can be supported by the absorbance spectra as well, the intense dark-reddish colour remained visible for months, indicating Tb(IV) was still present in the solution. As can be seen in **Figure 3.10**, initially there is a steep decrease in the absorbance after one day of storage, whereas the decrease is less abrupt within increasing storage time. This trend is consistent at all the samples collected at different electrolysis times.

In both the works of Hobart *et al.*[106] and Varlashkin *et al.*[109] with electrochemical deposition and co-precipitation, terbium-containing solids were obtained. However, since the obtained material was non-crystalline, no XRD data was presented. IR and Raman spectroscopy indicated a mixture of different stoichiometry in these complexes, but no structure was proposed so far.[109] Moreover, Varlashkin *et al.* suggested a cluster formation as well.[109] The system is quite complicated and further reactions can be occurring as well at higher pH indeed influencing the oxidation mechanism:

$$C_2O_6^{2-} + 2e^- \rightarrow 2CO_3^{2-}$$

$$(E^0 = +0.21 \text{ V vs SCE at } 25\,^0\text{C pH} = 10.75) \quad (4.7)$$

In nitrate media, the stabilization was less compared to the carbonate media. The stability of the electrolysed solution was monitored by UV-Vis absorption at 369 nm over the course of 72 hours and is shown in **Figure 3.11**. The absorbance values decrease over time and the colour of the solution completely vanished after 3 days of incubation, indicating the limited Tb(IV) stability in this medium.

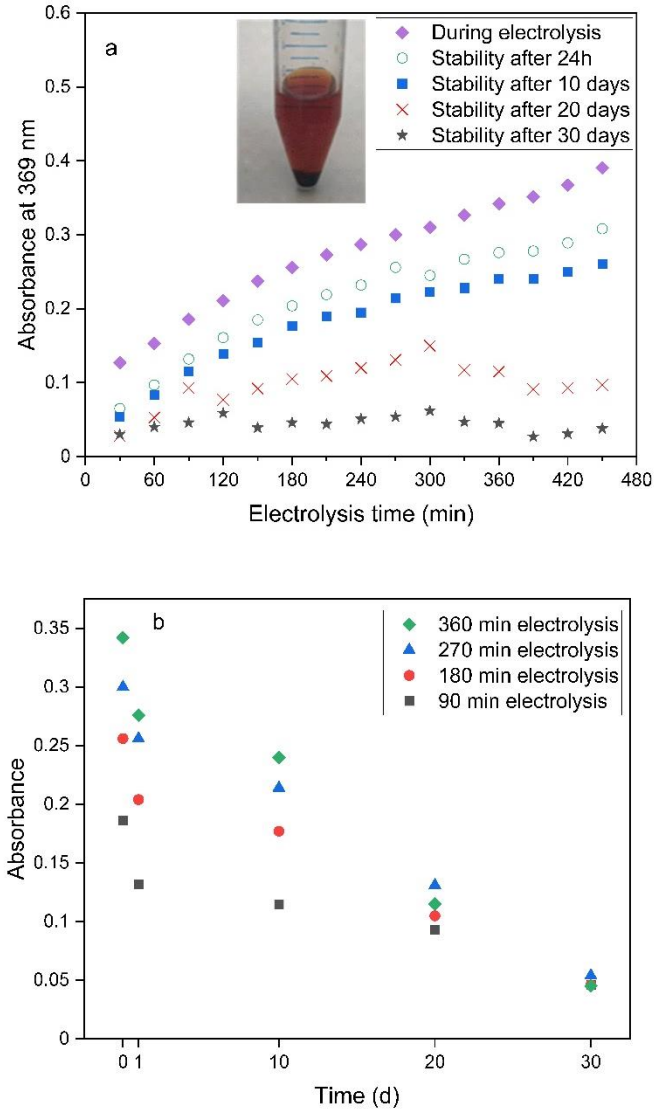

Figure 3.10. (a) Stability measurement of Tb(IV). UV-Vis absorbance values at 365 nm of 0.07 mol.L^{-1} Tb(III) in 4 mol.L^{-1} K_2CO_3 solution at pH 14 at varying electrolysis times (90 min – 360 min) during and certain time frames after the electrolysis at constant potential of +1.3 V vs. Ag/AgCl. **(b)** Correlation of data sets at various electrolysis times with absorbance measured during (0 day) and after the electrolysis (1 day, 10 days, 20 days and 30 days).

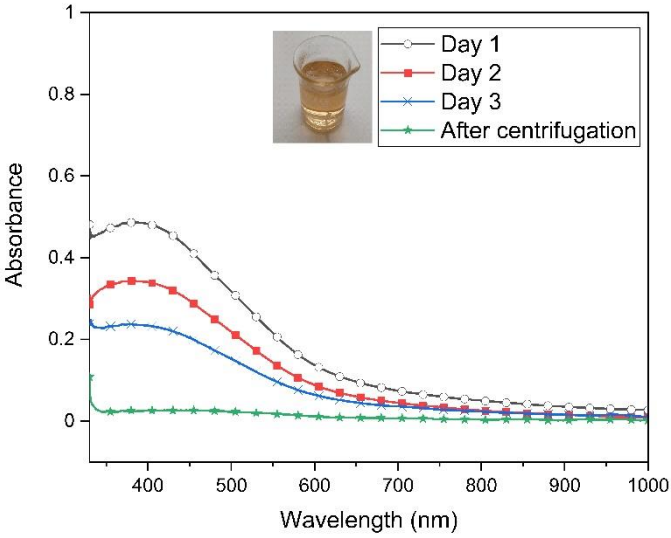

Figure 3.11. UV-Vis absorption spectra of 0.01 mol.L^{-1} Tb(III) in 4.5 mol.L^{-1} $Ca(NO_3)_2$ solution at different times after electrolysis at constant potential of +1.3 V vs. Ag/AgCl and centrifugation. Tb(IV) formation was followed by the absorbance peak at 369 nm. Blank solution without terbium was used as reference sample for baseline correction. The cell path length was 10 mm.

The advantages of periodate media are the possibility for the potential to be lowered up to +0.9 V vs Ag/AgCl and being able to work at a lower pH value of 12.9 compared to carbonate media. On the other hand, the fact that the solubility of the potassium peroxide salt and terbium chloride salt was relatively low, results in use of very low concentration values of terbium and peroxide, also causing precipitation to occur during the electrolysis process. Increasing the pH would increase the solubility of potassium peroxide; however, it might also trigger terbium hydroxide precipitation, which would decrease the efficiency. Furthermore, the stability was relatively lower compared to both nitrate and carbonate media, given that the brown solution changes to colourless after 24h. The stability of Tb(IV) in carbonate medium was relatively longer compared to nitrate and

periodate media, also giving the opportunity to reach to comparably higher terbium concentrations.

3.5. Conclusions

Electrochemical oxidation of terbium(III) to terbium(IV) was investigated in various electrolytes: carbonate, nitrate and periodate. It was shown that terbium(III) is oxidized and stabilized as Tb(IV) most efficiently in carbonate solutions. In this medium, the reaction rate is slow since maximum conversion only occurs after 9 hours of electrolysis at a constant potential of +1.3 V vs. Ag/AgCl.

To the best of our knowledge, this is the first time that electrochemical oxidation of Tb(III) has been investigated in nitrate media. Although the electrolyte itself is prone to oxidation and side reactions induced by the electrolyte interfering with the oxidation of terbium, the presence of Tb(IV) could still be observed via UV-Vis absorption spectroscopy. The oxidation of terbium was also achieved electrochemically in periodate medium for the first time at significantly lower applied potential and pH. However, solubility limitations made this oxidation reaction less favourable.

When these three media are compared, nitrate and periodate allow for oxidation at lower pH values than carbonate medium. Regarding the applied reduction potentials, the least positive potential value to oxidize Tb(III) is in periodate media at +0.9 V vs. Ag/AgCl. Nitrate and periodate media are poorly stabilizing Tb(IV) and require working with relatively lower terbium concentrations. After all, the most efficient stabilization of Tb(IV) is achieved in carbonate media with the advantage of allowing relatively high terbium concentrations and providing the highest long-term stability of all investigated electrolytes. Therefore, for developing a separation process based on oxidation state change of terbium, aqueous carbonate media seem to be the most promising electrolyte.

Chapter 4.

Separation of terbium as a first step towards high purity terbium-161 for medical applications

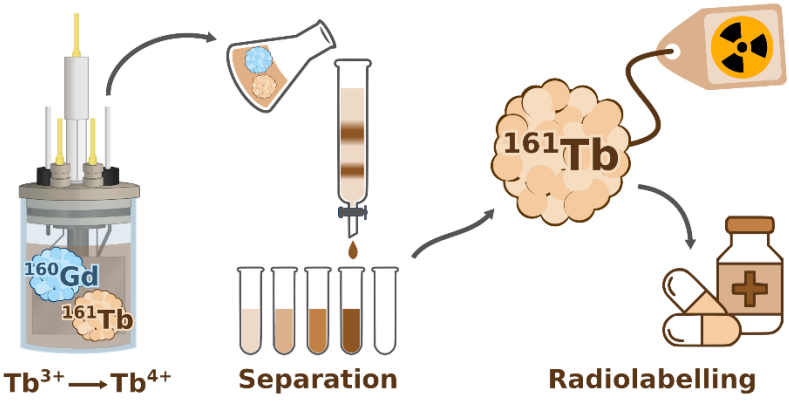

M.O. Arman, A. Mullaliu, B. Geboes, K. Van Hecke, G. Das, G. Aquilanti, K. Binnemans, T. Cardinaels

All experimental work and compilation of the manuscript were performed by the author of this thesis. G.D. and G.A. provided the opportunity and technical support for performing the XAS experiments in Elettra Sincrotrone Trieste. A.M. contributed to the analysis of XANES experiments. Co-authors contributed to the revision and design of the experiments.

4.1. Abstract

Terbium-161 is a medical radiolanthanide that has a beta decay energy and half-life similar to that of lutetium-177. Due to this similarity in radioactive properties and its additional therapeutic effect thanks to Auger/conversion electrons, it is considered as a promising alternative to lutetium-177. Terbium-161 can be produced via high-flux thermal neutron irradiation of an enriched gadolinium-160 target. Then, the separation of terbium-161, from the target material as well as the stable decay product, dysprosium-161, should be achieved. All lanthanides have the trivalent oxidation state as the most stable one, but some lanthanides can also occur in a divalent or tetravalent oxidation state. Changes in oxidation state affect the chemical properties of the lanthanide, so that intragroup separations are easier to perform. In this study, a novel separation method is investigated, comprising anion exchange chromatography, subsequent to the electrochemical oxidation of terbium(III), to separate terbium(IV) from trivalent lanthanides. The electrolysis conditions are set to the highest achievable conversion rate, followed by a dilution step during which the pH and electrolyte concentration are slightly lowered to obtain conditions that are compatible with the separation method. XAS analysis is done to characterize the carbonato complex of both oxidation states and to further elucidate the separation mechanism.

4.2. Introduction

Terbium is called a `Swiss army knife` for nuclear medicine,[40] since it has four different radioisotopes that are of potential interest to medical applications: ^{149}Tb ($t_{1/2}$ = 4.12h, E_α =3.697 MeV (16.7%)), ^{152}Tb ($t_{1/2}$ = 17.5h, $E_{\beta^+,av}$ =1.080 MeV (17%)) , ^{155}Tb ($t_{1/2}$ = 5.32d, E_γ =86.55 keV (32%) and 105.3 keV (25%)) and ^{161}Tb ($t_{1/2}$ = 6.98d, $E_{\beta^-,av}$ =0.154 MeV (100%)). These isotopes have complementary decay characteristic. ^{161}Tb is suitable for therapeutic use due to the emission

of low-energy β^- particles, conversion and Auger electrons.[39] ^{161}Tb has a half-life of 6.98 days, and emits low-energy β^--particles with a maximum of 0.59 MeV, which is very similar to clinically used ^{177}Lu ($t_{1/2}$: 6.65 d, E_β^{max}: 0.49 MeV).[155] ^{161}Tb is produced indirectly by thermal neutron irradiation of enriched gadolinium oxide targets in the research reactors via ^{160}Gd(n,γ)^{161}Gd → ^{161}Tb.[156,157] There are many in-vitro and in-vivo studies, comparing the therapeutic properties with a well-established ^{177}Lu counterpart.[42,44,157,158] Recently imaging of cancer patients has been successfully performed after administration of ^{161}Tb-DOTATOC.[45] Due to the comparable results and the fact that it is well-tolerated by the patients, the ^{161}Tb-DOTATOC conjugate is considered to be a suitable alternative for ^{177}Lu-DOTATOC. The efficacy of ^{161}Tb in targeted therapy and its potential for personalized treatment approaches, make it a great candidate for medical applications.

Lanthanides typically exist in the trivalent oxidation state, which results in a similar coordination chemistry for all the lanthanides. This gives a flexibility to select the radiolanthanide with the most suitable half-life, decay mode and decay energy for either diagnosis or therapy, from a range of possible radiolanthanides, that are all compatible with the same carrier molecule.[5,10,16,26–28] On the other hand, separation of lanthanides is challenging, due to these similar chemical properties. The current method to obtain non-carrier-added (nca) ^{161}Tb is using cation exchange and extraction chromatography with α-hydroxy-isobutyric acid (α-HIBA) as the complexing agent.[156] However, these methods have only a limited efficiency since the process requires long separation times and multiple separation steps. Another strategy involves substantially altering one of the lanthanide ions' chemical characteristics by changing its oxidation state, which creates possibilities for more effective separation methods.[94,111,120]

Terbium (E^0 = +3.1 V vs. SHE) is, besides cerium, one of the lanthanides that can be oxidized to its tetravalent state, but there is only limited information available in the literature on the oxidation of Tb(III).[105,109,146] In our previous work, a detailed parametric study was performed on the electrochemical oxidation of Tb(III) in various

aqueous media.[159] Although the applied potential could be lowered to +0.9 V vs. Ag/AgCl in periodate medium, the most stable Tb(IV) complex was obtained in concentrated carbonate medium. Therefore, an aqueous carbonate medium seems to be the most promising compared to the other media for developing a separation process.

The extraction of lanthanides and transplutonium elements from alkaline and carbonate media can be achieved mainly via liquid-liquid extraction,[86,160–166] using various extractants such as quaternary ammonium salts,[167–169] primary amines,[170] or alkylpyrocatechols.[171] There are only a few examples of combining extraction chromatography in carbonate media.[172,173] Thanks to its simplicity, ease of operation, speed, efficiency and the ease to be automated, solid phase extraction is used for the separation process.

In this study, a strategy for the separation of terbium from gadolinium is investigated based on the change of the valence state of terbium. An electrochemical oxidation is performed in highly concentrated carbonate medium, followed by a column separation using Dowex 1-X8 anion exchange resin. Prior to the separation, a dilution step is applied to lower the carbonate concentration. It was established in the work of Sherry *et al.*[172] that at lower carbonate concentrations, higher distribution coefficients can be obtained. The terbium(IV) complex is found to remain stable after dilution, which is advantageous for an anion exchange separation process. X-ray absorption spectroscopy measurements were performed to validate the change in the oxidation state as well as to gain information on the structure of the complexes.

4.3. Experimental

4.3.1. Chemicals

$TbCl_3 \cdot 6H_2O$ (99.9%), $GdCl_3 \cdot xH_2O$ (99.9%) and $DyCl_3 \cdot 6H_2O$ (99.9%) were obtained from Strem Chemicals, Inc. (Newburyport, USA). K_2CO_3

(anhydrous, ≥98%) and KOH pellets (≥85%) were purchased from VWR International B.V. (Leuven, Belgium). Dowex 1-X8 (chloride form) 200-400 mesh ion exchange resin was obtained from Thermo Fisher Scientific (Merelbeke, Belgium). All chemicals were used as received without any further purification. All aqueous solutions were prepared with ultra-pure water (18.2 MΩ cm at 25 °C).

4.3.2. Production of ^{161}Tb

[^{161}Tb]$TbCl_3$ was produced by following an adapted literature procedure.[156] Highly enriched $^{160}Gd_2O_3$ (1.0 mg, 98.2%, Isoflex USA) was loaded as a nitrate salt into a quartz ampoule, sealed inside an aluminum capsule. The irradiation was performed in the BR2 reactor at the Belgian Nuclear Research Centre (SCK CEN) at a thermal neutron flux of 3.0 x 10^{14} n/cm^2/s. After 10 days of irradiation, the target was removed from the reactor and cooled for 5 days. The irradiated material was then dissolved in trace-metal grade water and the ^{161}Tb was purified using high-pressure ion chromatography (HPIC, Shimadzu), with a strong cation exchange column (ø: 6 mm, l: 50 mm, Shodex IC R-621 by elution with α-hydroxyisobutyric acid. The collected fractions containing [^{161}Tb] were further concentrated by loading them onto an LN3 column (ø: 2.1 mm, l: 30 mm, TrisKem International) and eluted with 0.05 mol.L^{-1} hydrochloric acid. The isolated solutions of [^{161}Tb]$TbCl_3$ had a radionuclidical purity of 99.998%. An activity of about 2.5 MBq ^{161}Tb was added to a solution containing 4 mol.L^{-1} K_2CO_3 an 0.07 mol.L^{-1} $TbCl_3 \cdot 6H_2O$. The pH was then increased to 14 by adding KOH. This step is crucial for the electrolysis to be successful as well as for the stability of the Tb(IV) complex in carbonate medium.[105,159] The final volume was set to 10 mL to ensure the compatibility with the electrolysis cell volume.

4.3.3. Electrochemical oxidation of terbium

The electrochemical oxidation of terbium was performed in an undivided three-electrode voltammetry cell (BASI MF-1052 VC-2). A platinum-mesh electrode was used as working electrode, and a platinum wire (ø = 0.5 mm, length = 65 mm) served as auxiliary electrode and BASi MF-2056 Ag/AgCl in a 3 mol.L^{-1} KCl solution as reference electrode. A Metrohm Autolab PGSTAT302N potentiostat, operated by Nova 2.1.5 software was used in potentiostatic mode to apply constant a potential of +1.3 V vs. Ag/AgCl for 3 hours.

4.3.4. UV-Vis Spectroscopy

During the electrolysis, a colour change was observed, starting from the electrode surface and dissipating into the solution, from colourless to dark brown, indicating the Tb(IV) complex formation. This change in the oxidation state was characterized with UV-Vis spectroscopy, by a broad charge transfer band with an absorption peak centred at 365 nm.[105,159]

Absorption spectra were recorded in the 230–1000 nm range using a Shimadzu 1900i spectrophotometer, operated by LabSolutions UV-Vis software. The light source changeover occurred at 340.8 nm. A quartz cuvette with 1 mm path length was used. Spectra were collected at a fast scanning rate of 300 nm.min^{-1} with with steps of 0.5 nm. Baseline correction was done with the blank solutions of carbonate solutions without terbium.

4.3.5. Extraction chromatography

Experiments were conducted in a column separation setup using Triskem 2 mL bed volume cartridges with 1 cm inner diameter and a total length of 2.5 cm. An ISMATEC IPC 8-channel peristaltic pump was used to control the flow rate of the mobile phase. The Dowex 1-X8

resin in chloride form was packed into the column/cartridge as a slurry to ensure uniform packing, and to avoid cracks or holes that might end up in channel formation, hence impact the separation capability and column performance. The packed column was preconditioned with 4 mol.L^{-1} K_2CO_3 solution, and thus converted to carbonate form. The feed solution was prepared by diluting the initial carbonate concentration from 4 mol.L^{-1} to 1 mol.L^{-1} (pH ≈ 12), and thus the Tb(III) concentration decreases to 0.018 mol.L^{-1}. 0.4 mL of the feed solution was loaded onto the column with a flow rate of 0.3 mL/min by use of a peristaltic pump. Afterwards, the column was first eluted with water for the elution of Tb(IV). The mobile phase was switched to 2 mol.L^{-1} K_2CO_3 after collecting 9 fractions of 0.5 mL. The fractions were measured by gamma spectrometry for ^{161}Tb. All experiments were performed at room temperature.

4.3.6. Gamma spectrometry

Gamma spectrometric analysis of ^{161}Tb was done using the 57.20 keV, 74.57 keV, 77.41 keV, 87.94 keV, 103.06 keV, 106.11 keV, 292.41 keV and 550.25 keV γ-peaks. This was performed using a HPGe detector (Canberra Semiconductors N. V., Olen, Belgium) with Genie2000 software.

4.3.7. X-Ray absorption spectroscopy

XAS spectra were collected at room temperature at the XAFS Beamline in Elettra Synchrotron Trieste (Italy). The storage ring was operating at 2 GeV with an optimal current around 300 mA. The energy of the beam was tuned by using a fixed exit monochromator equipped with a pair of Si (111) crystals. An internal reference of iron foil is used for the energy calibration. Data were recorded in ambient pressure at Tb L_3-edge in dual transmission and fluorescence mode due to the low absorption of the material. A sample holder with Kapton® windows and a Teflon™ spacer with a thickness of 0.1 mm

were used as sample holders. The spectra were recorded by scanning through the terbium L_3 absorption edge (ca. 7514 eV) in energy interval of 7305-7715 eV. XAS primary data analysis was performed with the Athena program. The *ab initio* simulation of the XANES spectra was performed using the FDMNES software.[174] The Tb L_3-edge was calculated in the photoelectron energy range -10 < E < 80 eV with respect to the Fermi energy level using the Muffin-Tin approximation. The Hedin-Lundqvist complex potential[175] was used to calculate the excited states. The absorption cross-section was calculated within the dipolar approximation. Clusters of 5Å built around each non-equivalent absorbing atom were considered.

4.4. Results and Discussion

4.4.1. Stability of Tb(IV) complex

Dowex 1-X8 strong anion exchange resin was used in its carbonate form. There are multiple examples of this resin being used with alkaline media, specifically carbonate/bicarbonate systems.[172,173,176–179] The resin shows good physical and chemical stability in the pH range of 0–14.[180] Based on the previous studies on the carbonate medium using the Dowex 1-X8 resin as well as it`s stability, the separation experiments were conducted with this resin. The resin was prepared with washing 4 M K_2CO_3 and 0.08 M KOH mixture before introducing the feed solution, as explained in the previous section. Thus, the resin was expected to convert from Cl^- form to CO_3^{2-} form rather than OH^- form due to the high concentration of carbonato ions in the solution. The selectivity towards Tb(IV) complex rather than the Tb(III) complex, so that the former is retained on the column, could be explained by the difference in the total charge of these complexes. As the first eluent is water, the concentration of carbonate would drastically drop, and when it was switched back to the carbonate solution, where the carbonate ions might be exchanging with the Tb(IV) anionic complex.

Although the stability of Tb(IV) in carbonate medium was found to be high enough to follow up with a separation process, the possibility of back-reduction due to the resin itself can result in lower separation factors. To investigate this effect, UV-Vis absorbance spectra were collected after elution of different volumes of feed solution with water, and measuring the related Tb(IV) fractions. The UV-Vis spectra shown in **Figure 4.1** are for the feed solution after the electrolysis, and for the first fractions collected after 0.5 mL and 6 mL feed solution were introduced to the column respectively. In **Figure 4.1**, it can be observed that the absorbance value only changes by 0.01 at 365 nm for the feed and fraction collected from 6 mL of feed, showing that the back reduction due to the column material can be considered as negligible. When a small volume of feed solution (0.5 mL) was introduced, due to the dilution effect by the eluent, the absorbance obviously decreased.

In the studies of Sherry *et al.*, carbonato and bicarbonato complexes of lanthanides were investigated in a K_2CO_3 concentration range of 0.3 to 3 mol.L^{-1}.[172,173] These authors also showed that distribution coefficients of the rare earth carbonate complexes were drastically dropping with increasing carbonate concentration.[172,173] Therefore, to optimize the separation process, a dilution step was added after the electrolysis. The electrolysed solution was diluted from 4 mol.L^{-1} to 2 mol.L^{-1} and 1.3 mol.L^{-1} K_2CO_3. To check the stability of Tb(IV) complex after the dilution step, UV-Vis spectra were recorded at various time intervals (**Figure A.4.1** and Figure A.4.2). Absorbance was measured immediately after the electrolysis and any necessary dilutions are prepared swiftly in order to measure both diluted and undiluted samples in the same time frame. As can be seen in **Figure 4.2**, the absorbance values, for the undiluted, 1:1 and 1:2 diluted solutions are 0.127, 0.061 and 0.038 at 365 nm respectively. These values agree well with the dilution factors and these results show that the Tb(IV) complex remains stable under dilution, and the influence of back-reduction is negligible (**Figure A.4.1** and Figure A.4.2).

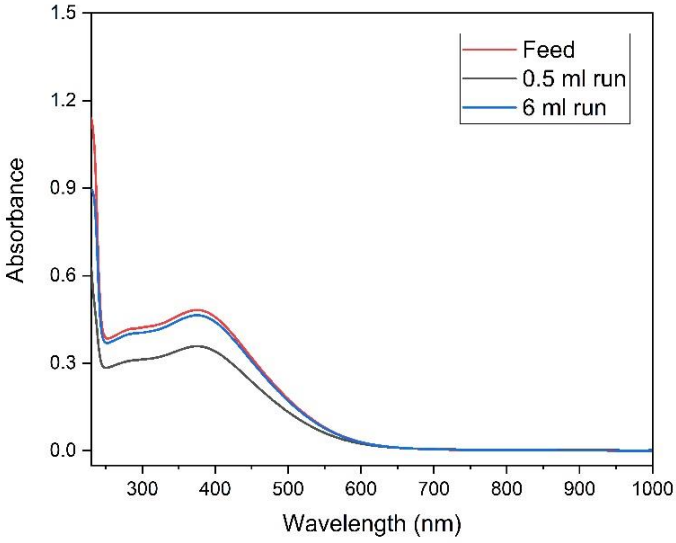

Figure 4.1. UV–Vis absorption spectra of the fractions collected at different feed volumes of 0.07 mol.L^{-1} Tb(IV) in 4 mol.L^{-1} K_2CO_3 solution at pH = 14. Electrolysis is performed at constant potential +1.3 V vs. Ag/ AgCl for 3h. The formation of Tb(IV) was followed by the absorbance peak at 365 nm. Blank carbonate solution is used as the reference sample for baseline correction. The cell path length was 1 mm.

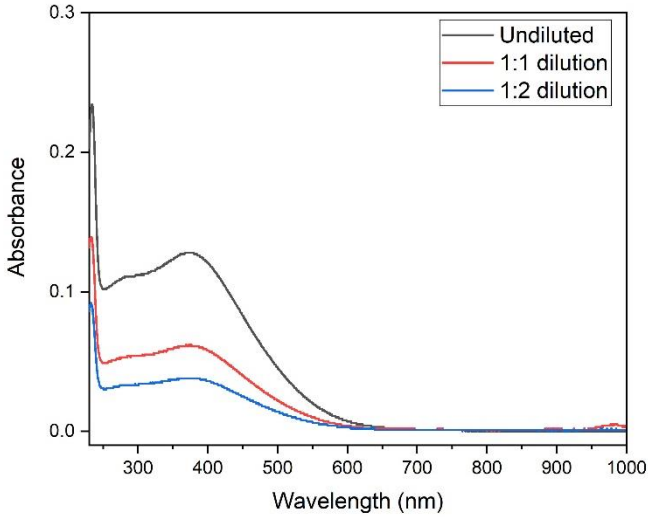

Figure 4.2. UV–Vis absorption spectra of undiluted 0.07 mol.L^{-1} Tb(IV) in 4 mol.L^{-1} K_2CO_3 solution at pH = 14, 1:1 (v:v) dilution and 1:2 (v:v) dilution. Electrolysis was performed on the undiluted sample at constant potential +1.3 V vs. Ag/ AgCl during 30 min. The formation of Tb(IV) was followed by the absorbance peak at 365 nm. Blank carbonate solution is used as the reference sample for baseline correction. The path length of the quartz cuvette is 1 mm.

In the proposed separation method (

Figure 4.3), Tb(III) and Tb(IV) complexes show different affinities to the column, based on the difference in the charge of these complexes. Because of this, a selective separation can be achieved. Misumi *et al.* described the separation mechanism for tetravalent metal ion complexes in 0.2 – 0.6 mol.L^{-1} carbonate medium as follows:[177]

$$M^{(IV)} + xCO_3^{2-} \leftrightarrow (MCO_3)_x^{4-2x} \quad (4.1)$$

$$(MCO_3)_x^{4-2x} + (y/2)R_2CO_3 \leftrightarrow R_yM(CO_3)_x + (y/2)CO_3^{2-} \quad (4.2)$$

Based on these equations, y was equal to 2x-4 to maintain the electrical neutrality of the resin.This was based on the assumption that the tetravalent metal ion forms a single complex with the carbonate ion, neglecting the presence of hydroxide ions, especially at higher concentrations of carbonate. In the study of Varlashkin *et al.*, [109] several stoichiometries of solid state Tb(IV) carbonato - hydroxo complexes were determined based on IR spectra, and it was assumed that the Tb(IV) solutions could contain complexes similar to these containing a mixture of carbonate and hydroxide groups. Similarly, in the works of Sherry *et al.*[172,173] rare earth carbonate systems are investigated by anion exchange column chromatography where the slope of plotted logarithmic functions of molality of the ligand and distribution coefficients, the ligand number of these complexes was predicted at lower carbonate concentrations. With increasing carbonate concentrations, the presence of hydroxide groups in the complex was assumed here as well. However, to the best of our knowledge, no further studies on Tb(III) and Tb(IV) complexes in highly concentrated carbonate solutions have been reported.

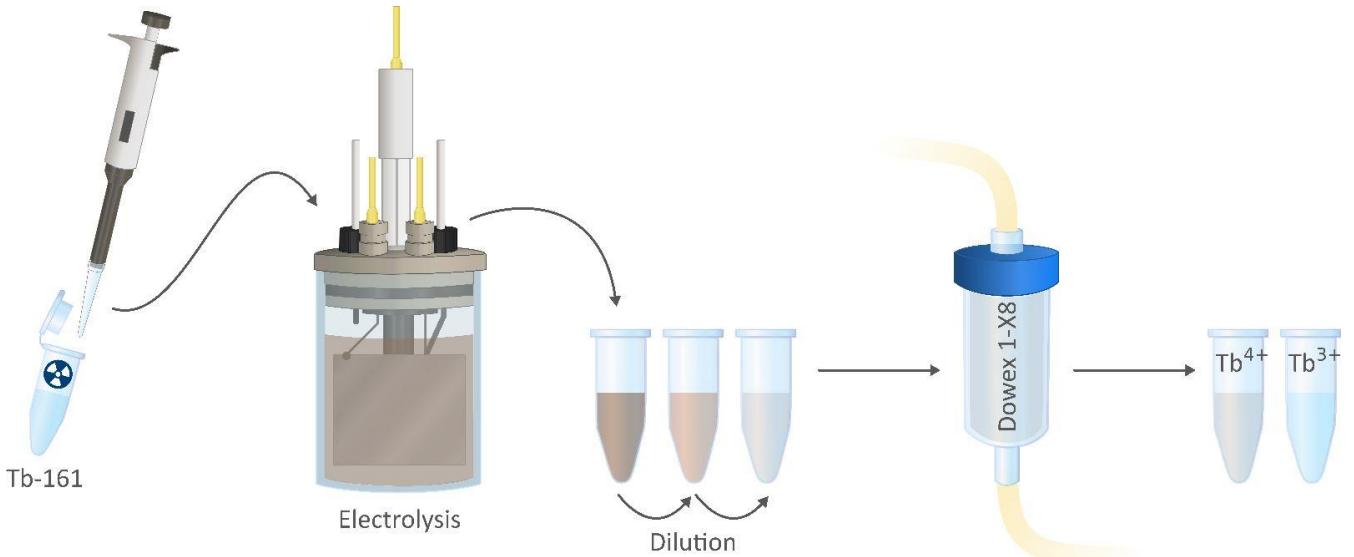

Figure 4.3. Schematic representation of the proposed purification method using Dowex 1-X8 resin packed column.

4.4.2. Column separation using Dowex 1X-8 resin

In **Figure 4.4**, the elution curve of a Tb(III) solution spiked with ^{161}Tb that was not treated by electrolysis is shown. With water as the mobile phase, the Tb(III) carbonate complex was completely retained on the column. After the mobile phase was switched to 2 mol.L^{-1} K_2CO_3, Tb(III) is completely eluted in the collected fractions. The radioactivity of the column material was checked after all fractions were collected, showing no presence of Tb^{161} tracers. In addition, when the activity of 0.4 mL of the feed solution (178.73±2.54 kBq) is compared to the total activity collected in the fractions (175.46±2.47 kBq), values are in good agreement. When the remainder of the feed solution was electrolysed during 3h, at constant potential of +1.3 V vs. Ag/AgCl, an immediate colour change was observed. In a second experiment, the same volume (0.4 mL) of feed solution was introduced onto the column.

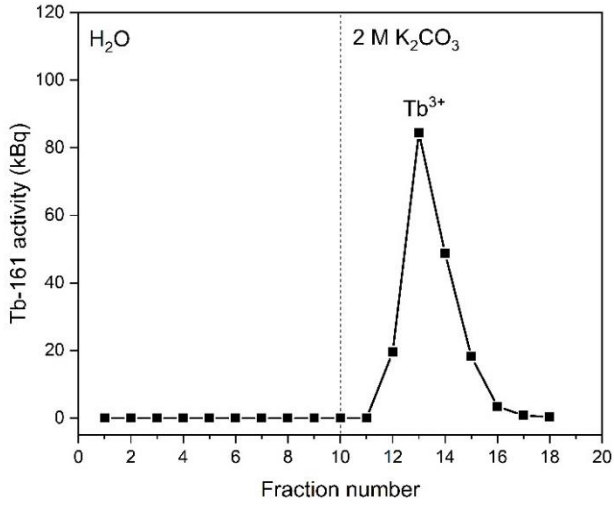

Figure 4.4. Elution curve of tracer spiked Tb(III) solution using a Dowex 1-X8 resin filled cartridge (ø: 1 cm, h: 2.5 cm, BV: 2 mL). Feed: 0.4 mL of a solution containing 0.018 mol.L^{-1} Tb(III) in 1 mol.L^{-1} K_2CO_3 solution (pH ≈ 12). The vertical dashed line denotes the change of mobile phase from water to 2 mol.L^{-1} K_2CO_3 . Flow rate: 0.3 mL min^{-1}.

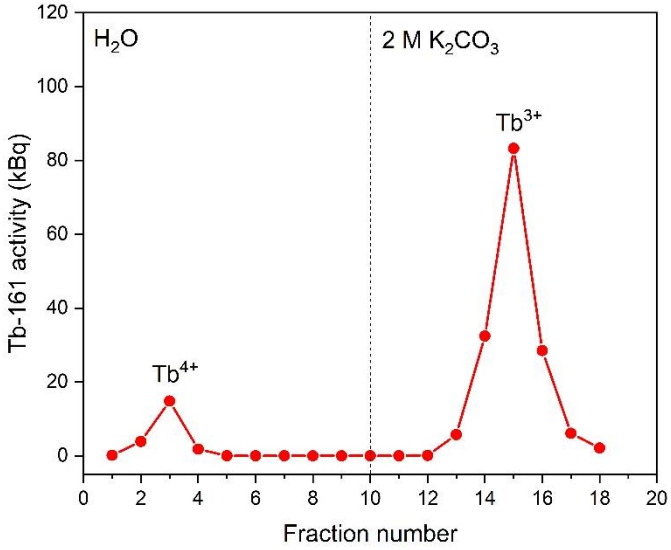

Figure 4.5. Elution curve of tracer spiked and electrolysed Tb(IV) solution using a Dowex 1-X8 resin filled cartridge (ø: 1 cm, h: 2.5 cm, BV: 2 mL). Feed: 0.4 mL of a solution containing 0.018 mol.L^{-1} Tb(III)/Tb(IV) in 1 mol.L^{-1} K_2CO_3 solution (pH≈12). The vertical dashed line denotes the change of mobile phase from water to 2 mol.L^{-1} K_2CO_3. Flow rate: 0.3 mL min^{-1}.

The elution curve of Tb(IV) solution can be seen in **Figure 4.5**. In this elution curve, it is observed that the Tb(IV) carbonato complex is not retained by the anion exchange resin, in contrast to the Tb(III) carbonato complex. In our previous study,[159] an in-depth qualitative analysis was performed on the electrochemical oxidation of Tb(III) to Tb(IV), but a quantitative electrochemical analysis could not be performed due to the limitation of the high formal reduction potential (E^o = +3.1 V vs. Ag/AgCl). In the current study, with the column chromatography experiments, full separation of Tb(IV) and Tb(III) is achieved. An estimation of the conversion of Tb(III) to Tb(IV) by electrochemical reduction can be done based on the assumption that back-oxidation is negligible during the dilution and separation, which was shown by the UV-Vis absorption spectroscopy results. Based on this, only ca. 11.2% of the mixture consisted of Tb(IV) whereas majority (88.8%) was still Tb(III) after 2 hours of electrolysis.

As a next step, electrolysis was performed in a mixture of lanthanides gadolinium, terbium and dysprosium, with a concentration of each of 0.05 mol.L^{-1} in 4 mol.L^{-1} K_2CO_3 at pH = 14. After 2 hours of electrolysis at +1.3 V vs. Ag/AgCl, UV-Vis absorption spectra were recorded, as can be seen in **Figure 4.6**. The spectra - recorded before and after the electrolysis - showed that, Tb(III) can be successfully oxidized in presence of other lanthanides without any inhibition. The concentration was chosen based on the solubility limit of the lanthanides in the carbonate solution, in which increasing the lanthanide concentration to more than 0.15 mol.L^{-1} resulted in precipitation. In the previous work, it was established that when terbium concentrations lower than 0.04 mol.L^{-1} were used, oxidation was no longer observed.[159] Furthermore, maximum Tb(III) to Tb(IV) conversion was not achieved at 3 hours of electrolysis for terbium concentrations higher than 0.15 mol.L^{-1}. This was explained by the strong complexation hindering the oxidation reaction at these high concentrations.[159] Thus, in these tests equimolar lanthanide mixtures were used with the total concentration of 0.15 mol.L^{-1}. After the electrolysis, the same protocol was followed for the separation process, except the feed volume was decreased to 0.2 mL instead of 0.4 mL due to the higher lanthanide concentration. In addition to ^{161}Tb, ≈ 200 ± 18.2 kBq ^{175}Yb was also added to the mixture to follow up the other trivalent lanthanides in the mixture. The elution curves for ^{175}Yb and ^{161}Tb is shown in **Figure 4.7**. The trivalent lanthanides, Gd, Dy and Tb were retained on the column as can be seen with ^{175}Yb and ^{161}Tb elution curves, which is similar to the results containing only Tb. There were no trivalent lanthanides detected in the first elutions with water as mobile phase, whereas a brown coloured solution was collected in the first fractions, corresponding to Tb(IV). When calculating the ratios of Tb(III) to Tb(IV) in the feed solution, the integration of the peak areas of the elution curves are used, assuming that there is no back-reduction occurring during the separation process and the contribution of first elution peak is purely originating from Tb(IV) complex whereas the second elution peak is only composed of Tb(III) complex.

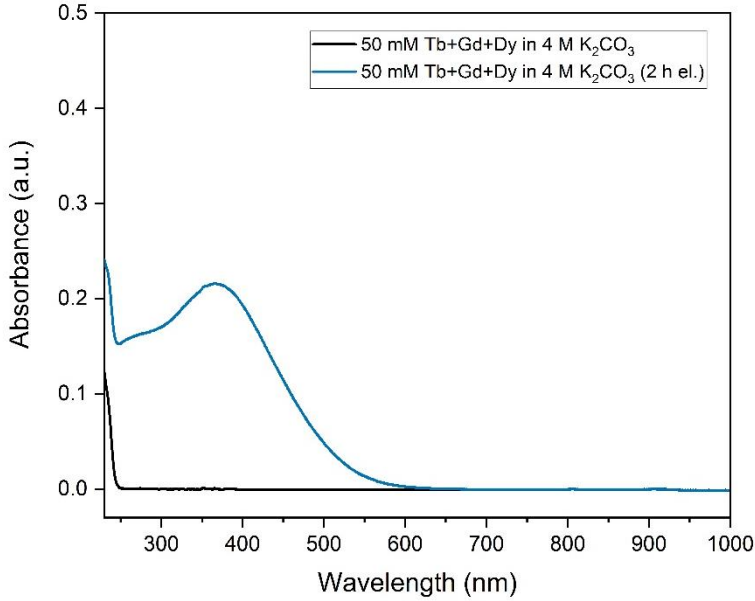

Figure 4.6. UV–Vis absorption spectra of 0.05 mol.L^{-1} Tb(III) , 0.05 mol.L^{-1} Gd(III) and 0.05 mol.L^{-1} Dy(III) in 4 mol.L^{-1} K_2CO_3 at pH = 14, before and after the electrolysis. Electrolysis is performed at constant potential +1.3 V vs. Ag/ AgCl for 2h. The formation of Tb(IV) was followed by the absorbance peak at 365 nm. Blank carbonate solution is used as the reference sample for baseline correction. The path length is 1 mm.

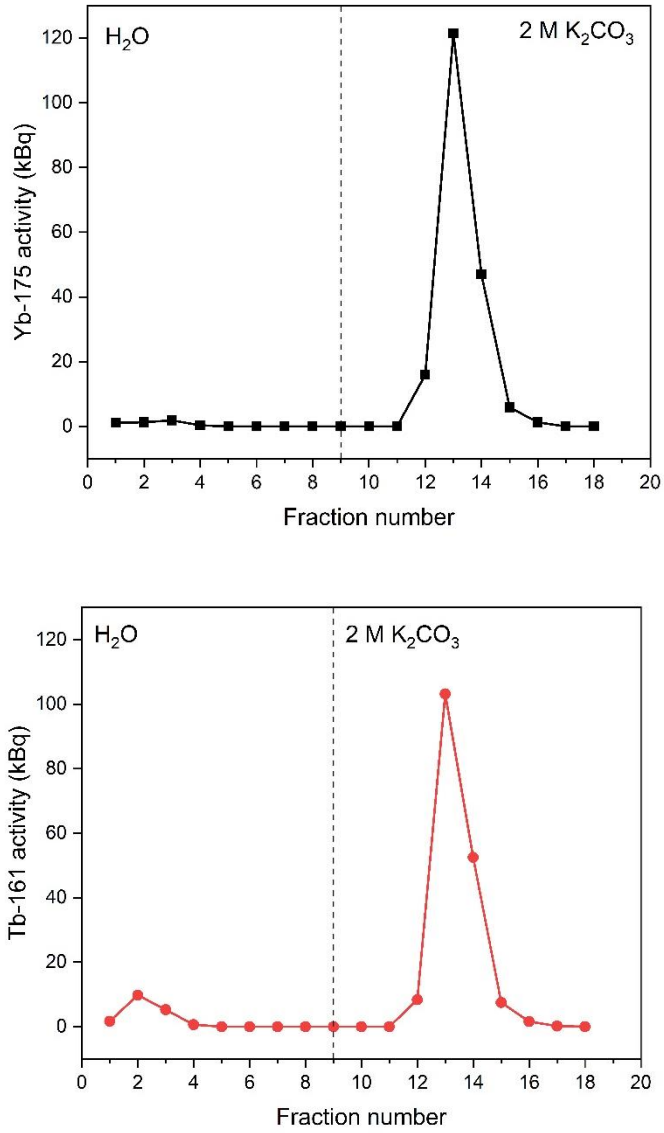

Figure 4.7. Elution curve of tracer spiked electrolyzed lanthanide mixture solution (0.05 mol.L^{-1} Tb(III) , 0.05 mol.L^{-1} Gd(III) and 0.05 mol.L^{-1} Dy(III) in 4 mol.L^{-1}) solution using a Dowex 1-X8 resin filled cartridge (ø: 1 cm, h: 2.5 cm, BV: 2 mL). Feed: 0.2 mL of a solution containing 0.018 mol.L^{-1} Ln(III) in 1 mol.L^{-1} K_2CO_3 solution (pH ≈ 12). The vertical dashed line denotes the change of mobile phase from water to 2 mol.L^{-1} K_2CO_3. Flow rate: 0.3 mL min^{-1}.

The amount of Tb(IV) in the mixture was calculated via the integration of the elution curve, found to be ca. 8.6%, after 2 hours of electrolysis. This difference in the amount of Tb(IV) can be explained by the difference in the electrolysis time. Therefore, Tb(III) was successfully oxidized to Tb(IV) and stabilized in the aforementioned experimental conditions, as well as Tb(IV) was separated from the other trivalent lanthanides. Based on this, a process flowsheet can be proposed (**Figure 4.8**), where 82% yield could be achieved after 5 runs. The steps can be defined as; (1) electrolysis of 70 $mmol.L^{-1}$ of Tb(III) and Gd(III) in 4 $mol.L^{-1}$ K_2CO_3, (2) dilution of the solution by 1:4 (v:v), (3) separation using K_2CO_3 conditioned Dowex I-X8 column, (4) collection of fractions with Ln(III) in 4 $mol.L^{-1}$ K_2CO_3 and Tb(IV) in water, (5) combining Ln(III) in 4 $mol.L^{-1}$ K_2CO_3 with the initial electrolysis solution, (6) introducing the Tb(IV) in water fraction to LN3 column in order to prepare for radiolabelling. However, considering the short half-life of Tb-161, long electrolysis or separation times are not feasible and thus further optimization is necessary.

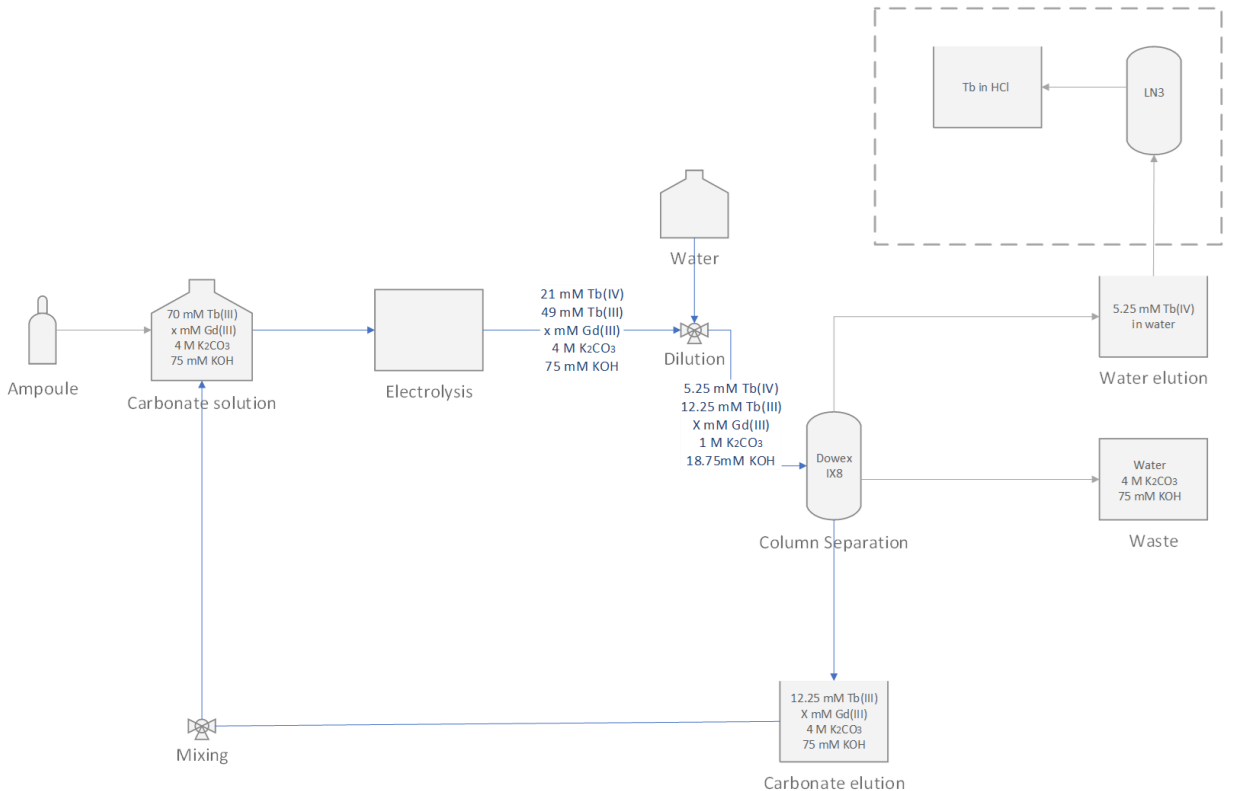

Figure 4.8. Suggested process flowsheet for terbium-161 purification.

4.4.3. XANES measurements

To explore the oxidation state of terbium ions during the course of electrolysis, XANES experiments have been carried out at the Tb L_3-edge. With the starting solution of 0.07 mol.L^{-1} Tb(III) in 4 mol.L^{-1} K_2CO_3 at pH = 14, electrolysis is performed and recorded every 30 minutes. The normalized spectra at various electrolysis times can be seen in **Figure 4.9**.

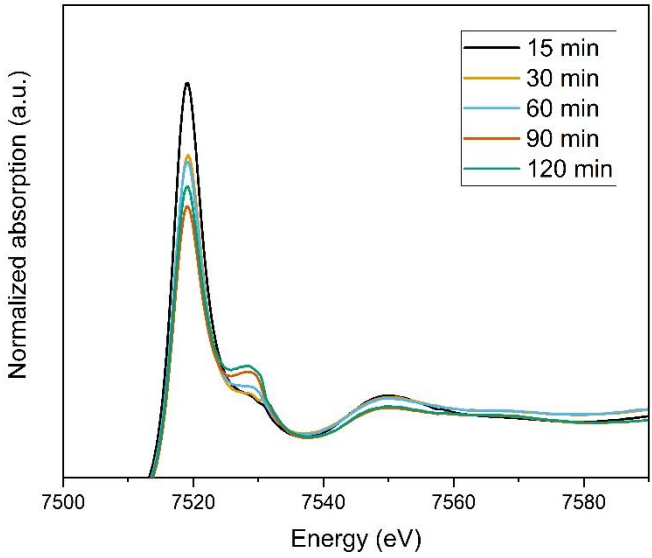

Figure 4.9. Normalized XANES spectra of the oxidation of Tb(III) (0.07 mol.L^{-1}) in a 4 mol.L^{-1} K_2CO_3 solution as a function of time (15 min – 120 min). White line of terbium was observed with a maximum at 7519 eV.

The white lines of terbium were observed with a maximum at 7519 eV, whereas a shoulder appeared at between 7525 – 7530 eV, which is an indication of Tb(IV) (**Figure A.4.3**). As the electrolysis time increases, the decrease in the white line could explain the conversion of Tb(III) to Tb(IV), and the final spectrum containing a mixture of both valence states. In order to quantify the conversion, linear combination

fitting was performed, using initial Tb(III) solution without electrolysis performed and Tb_4O_7 as the reference materials (**Figure A.4.4**). The final fitting using these references resembles the shape of the spectrum recorded after 24 hours of electrolysis. However, it was not possible to perform a quantitative analysis due to the partial oxidation of Tb(III) as well as the low concentration of terbium being a limitation. The conversion was calculated as 15% based on the poor fitting, which was in line with the results from the extraction chromatography experiments.

Ab initio simulation of L_3 XANES spectra was carried out by considering the structures reported by Michiba *et al.*[181] (ICSD 422736) and Dixey and Saines[182] (ICSD 7183) to gain more insight into the electronic and local structural features of Tb (**Figure 4.10**). As can be seen in **Figure 4.11**, there are five carbonato and two hydroxo ligands coordinated to Tb in the structure reported by Dixey and Saines,[182] (ICSD 7183) where only one carbonato is a bidentate ligand and the others are monodentate. Similarly, in the structure that was reported by Michiba *et al.*,[181] the lanthanides were coordinated with five carbonato ligands (one bidentate and four monodentate), whereas the only difference was a third hydroxo ligand present in the structure. Although both structures contain Tb(III) surrounded by carbonates and hydroxides, the different local environment around terbium determines differences in the simulated L-edge. For ICSD 7183, terbium has an overall coordination number of 8, with bond valence sum of 2.85 (considering a bond search factor of 0.87).

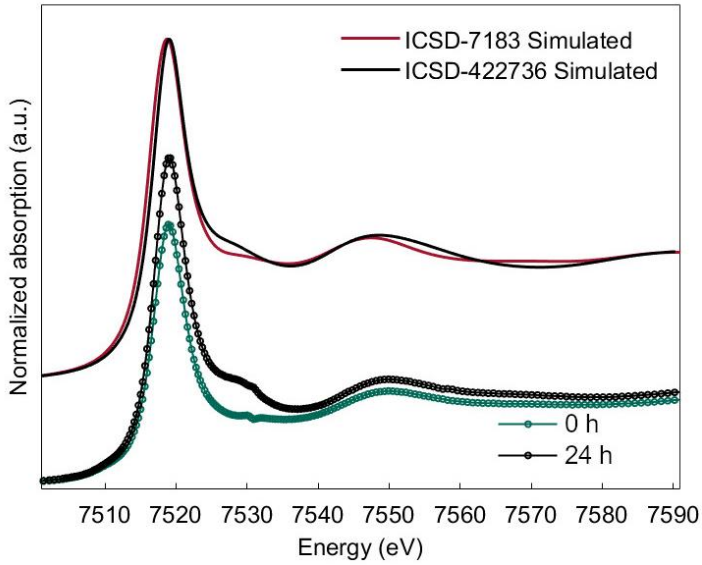

Figure 4.10. Simulated L3-edge spectra for reference structures ICSD-7183 and ICSD-422736 and comparison with experimental XANES traces of 0h and 24h electrolysis.

At the same time, the ICSD 422736 structure features Tb in a nine-fold coordination environment with average bond valence sum of 3.06 (bond search factor 0.87). Thus, the electronic distribution for the two structures is different to a small extent, with Tb in ICSD 422736 having a slightly higher effective charge. This can also be verified in the small shift of the edge toward higher energy in the simulated ICSD 422736 spectrum when compared to the respective one for ICSD 7183 (**Figure 4.10**).

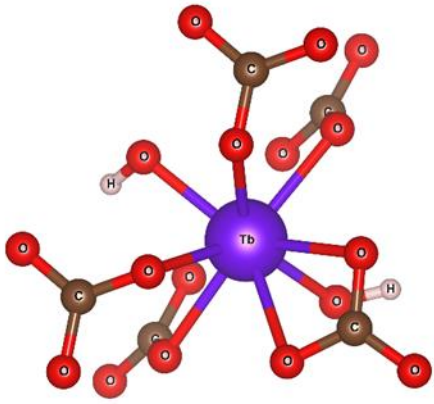

Figure 4.11. Molecular structure (ISCD 7183) adapted from Dixey and Saines *et al.*[182]

Interestingly, the experimental XANES trace recorded after 24h of electrolysis displays more similarities with ICSD 422736, while the experimental spectrum at time zero (0h) is closer to ICSD 7183. This might be related to a partially higher oxidation state of Tb at 24h, as discussed above, as well as a different coordination environment, possibly a nine-fold coordination for the Tb(IV)/Tb(III) complex after 24 hours of electrolysis, vs. an eight-fold coordination for the Tb(III) complex.

4.5. Conclusions

^{161}Tb tracer spiked solutions were successfully electrolysed, and further diluted without affecting the stability of Tb(IV). The separation of trivalent and tetravalent terbium was achieved by using Dowex 1-X8 anion exchange resin for the first time to our knowledge. Tb(IV) had no interaction with the column and eluted in the initial fractions, whereas the anionic carbonate complex of Tb(III) was retained on the column until the eluent is switched from water to concentrated

carbonate solution. Full separation is achieved without any back-reduction of Tb(IV) to Tb(III), proven by UV-Vis results. Based on these results, an estimation of the electrolysis yield was done, which was calculated as ≈11.2% after 3 h of electrolysis at a constant potential at +1.3 V vs. Ag/AgCl. The separation method was proven also successfully in the presence of other lanthanides in the feed solution. Similar results were obtained when the same protocol was applied with an equimolar mixture of Gd(III), Tb(III) and Dy(III). Therefore, this separation method was found to be applicable for intergroup lanthanide separation, and a process flowsheet was proposed to illustrate a future approach following the methods described in this study. Finally, X-ray absorption spectroscopy results show some minor differences in the structure of the Tb(III) and Tb(IV) carbonate complexes, where different coordination numbers were obtained based on the simulations. As a result, the separation method looks promising towards the purification of ^{161}Tb for medical use. The main focus of future work should rely in achieving a higher conversion yield of the Tb(III) to Tb(IV) oxidation.

Chapter 5.

Kinetics of electrochemical Eu(III) to Eu(II) reduction in aqueous media

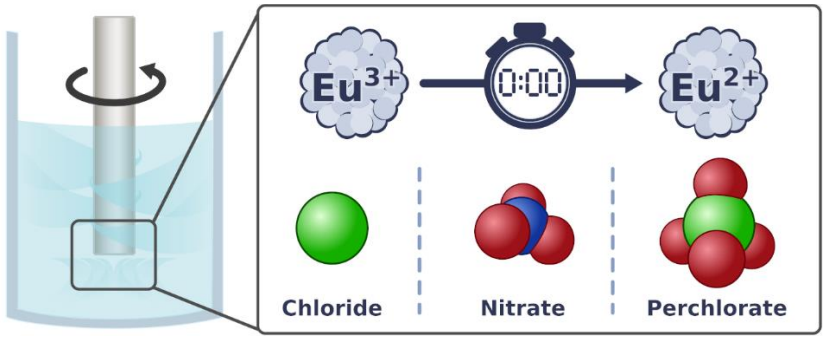

M.O. Arman, B. Geboes, K. Van Hecke, K. Binnemans, T. Cardinaels

All experimental work and compilation of the manuscript were performed by the author of this thesis. Co-authors contributed to the revision and design of the experiments.

5.1. Abstract

All lanthanides have a stable trivalent oxidation state, but some of them can also occur in the divalent or tetravalent state. Europium is well-known for its divalent oxidation state, which has been investigated in aqueous, organic, and molten salt media. In contrast to other lanthanides, Eu(III) can be easily reduced (E^0= -0.34 V vs. SHE), via chemical, electrochemical or photochemical routes, and Eu(II) is quite stable in a variety of electrolytes, including nitrate salts. To date, the kinetics of the Eu(III)/Eu(II) reduction reaction have been investigated only by polarography and chronopotentiometry, most often in perchlorate medium. In this study, the kinetics of the Eu(III)/Eu(II) couple were analysed in nitrate, chloride and perchlorate media by cyclic voltammetry and linear sweep voltammetry with a rotating disk electrode (RDE). The diffusion coefficient, charge transfer coefficient and rate constants were calculated based on the Levich and Koutecký-Levich analysis and Tafel plot to gain insight in the electrochemical process and the influence of the electrolyte type on it. Given the pre-existing characterization of this redox couple in perchlorate medium, it is selected as a reference system to both compare the kinetic parameters and to validate whether the methodology can be applied to other electrolytes. The Eu(III) reduction reaction was found to be quasi-reversible in these electrolytes and the calculated kinetic parameters are in line with the previously reported values.

5.2. Introduction

Lanthanide chemistry is dominated by the trivalent oxidation state and by the gradual filling of the 4f shell across the lanthanide series. However, some lanthanides display unusual oxidation states in the series such as cerium(IV), praseodymium(IV), terbium(IV), samarium(II), europium(II) and ytterbium(II). The divalent europium ion is well characterized, thanks to the facts that the reduction

potential of the Eu(III)/Eu(II) couple is readily accessible (E°(Eu(III)/Eu(II))= −0.34 V), and that the divalent oxidation state is relatively stable due to a half-filled 4f subshell. The electrochemical behaviour of lanthanide elements has been extensively studied as model systems in various electrolyte conditions, such as molten salts, ionic liquids, and aqueous/non-aqueous solutions.[99,149,159,183–193]

The reduction of Eu(III) has been investigated using chemical, photochemical and electrochemical approaches.[98,112,113,159,192,194–197] The kinetics of the electrochemical reduction reaction have also been investigated using several methods such as polarography, chronoamperometry or voltammetry.[95,96,198–205] In earlier works, the kinetics of Eu(III) reduction were investigated in aqueous formamide and perchlorate media using a dropping mercury electrode to understand the electrochemical behaviour of the system and the influence of viscosity and temperature.[96,116,204–206] In these media, the kinetic parameters transfer coefficient (α) and rate constant (k) of the reaction as well as the diffusion coefficient (D) have been calculated. The influence of the formamide concentration on the reversibility was discussed as well as that of the viscosity and pH. In these media, inner-sphere complexation is not very pronounced and Eu(III) ions are present mainly in hydrated form. However, with increasing concentration of the electrolyte, a negative shift of the peak potential occurs, which can be explained by the decrease of the solvent activity and lowering the hydration of the europium ions in solution, increasing the entropy. This results in a higher stability of Eu(II) complexes.[96,98] Furthermore, the reduction of Eu(III) has also been investigated in chloride and nitrate media, with the aim to develop efficient separation processes by change of oxidation state of europium.[94,112,113,124,140,196,197,207] Van de Voorde *et al.* reported that at high aqueous nitrate concentrations, Eu(III) can efficiently be electrochemically reduced to Eu(II) and that the Eu(II) ion is very stable in this system.[98] The Eu(III) reduction kinetics and mechanism were also investigated in hydrochloric acid solutions by Atanasyants *et al.* and these authors concluded that the process occurs in the mixed kinetics region.[95] In both studies of Van de Voorde *et al.* and Atanasyants *et al.*, a graphite electrode was used instead of a mercury

electrode, and the reactions were found to be quasi-reversible to irreversible based on the electrolyte and the concentrations.[95,98] The effect of non-aqueous solvents such as propylene carbonate and ethylene glycol on the reduction kinetics of Eu(III) were also investigated. The kinetic parameters were obtained via chronopotentiometry using a mercury electrode. The Eu(II) complexes were found to be stable, but water impurities decreased the stability.[99,208,209] The aim to gain further insight in the electron transfer reaction of Eu(III) reduction led to the use of room-temperature ionic liquids[210] and mixed solvents.[211] Based on this knowledge new electrode materials such as bismuth single-crystal or boron-doped-diamond thin film electrode were tested for the Eu(III)/Eu(II) redox couple to gain fundamental insight in the electron-transfer kinetics on solid-state electrodes.[198,200]

Present work is a fundamental study on the reduction kinetics of europium(III) with a conventional solid-state electrode, by cyclic voltammetry and linear sweep voltammetry with a rotating disk electrode (RDE). This work is the first study using a controlled convection method for europium reduction kinetics. Multiple electrolytes such as perchlorate, chloride and nitrate were tested and the results were compared with the existing literature data for perchlorate media. Given the extensive use of these media in literature, which were investigated by various techniques, nitrate, chloride and perchlorate media were chosen for this fundamental study to validate the applicability of the technique used in the present work. As discussed earlier, the Eu(III)/Eu(II) redox couple has been studied extensively in various electrolytes and has been used to explore new electrode materials. However the kinetic study has not been explored for nitrate media yet, and most often a mercury electrode was applied. To gain a better insight in the system, the electrochemical reduction of Eu(III) is investigated in three different media: perchlorate, chloride, and nitrate. Cyclic voltammetry and linear sweep voltammetry are performed using a glassy carbon rotating disk electrode under stationary or rotating conditions.

5.3. Experimental

5.3.1. Materials

$Eu(NO_3)_3 \cdot 6H_2O$ (99.9%), $EuCl_3.6H_2O$ (99.9%) and $Eu(ClO_4)_3$ in aqueous solution (50%) were purchased from Strem Chemicals, Inc. (Newburyport, USA). $Ca(NO_3) \cdot 4H_2O$ (≥ 99%) and $CaCl_2 \cdot 6H_2O$ (98%) and $NaClO_4$ (≥ 98%) are purchased from Sigma-Aldrich (Overijse, Belgium). All products were used as received, without any further purification. Aqueous samples are prepared with Milli Q water (18.2 MΩ·cm at 25 °C).

5.3.2. Instruments and electrodes

A three-electrode electrochemical cell was used for the electrochemical reduction of europium. The potential was controlled using a Metrohm Autolab PGSTAT302N potentiostat in potentiostatic mode, controlled by Nova 2.1.5 software. The rotating disk electrode (RDE) experiments were conducted with an AUTOLAB RDE2 rotator with the rotation speed (100 to 10000 rpm), remotely controlled by the Nova software. A custom-made glass electrochemical cell with 50 mL inner capacity was used for the voltammetry tests. Prior to the measurements, the solution was purged with argon gas. Experiments were conducted while an inert gas blanket was created by maintaining a continuous argon flow over the solution. The working electrode was a glassy carbon disk (Ø = 3 mm), the counter electrode was a coiled platinum wire (Ø = 1 mm) and the reference electrode was Ag/AgCl in 3 $mol.L^{-1}$ KCl. Prior to the measurements, the electrodes were cleaned first with 3 $mol.L^{-1}$ HNO_3, and then methanol. Solutions containing 10 mM Eu(III) in 0.1 $mol.L^{-1}$ nitrate and chloride media or 1 $mol.L^{-1}$ perchlorate media were used as electrolytes. Higher concentrations of the electrolytes were avoided due to inhibition occurring on the working electrode.

5.4. Results and discussion

5.4.1. Cyclic voltammetry

Cyclic voltammetry (CV) was used to investigate the redox behaviour of Eu(III) / Eu(II) in aqueous nitrate, chloride and perchlorate solutions, as well as to determine the reduction potentials as a function of the electrolyte composition. These experiments were performed using 10 $mmol.L^{-1}$ of Eu(III) salt containing the same anion as the electrolytes. The electrolyte concentrations were 0.1 $mol.L^{-1}$ for nitrate and chloride, and 1 $mol.L^{-1}$ for perchlorate media. The voltammograms were recorded in various scan rates in range 10 – 1000 $mV.s^{-1}$. The blank electrolytes were measured as well to validate that the electrochemical activity was originating uniquely from Eu(III) complexes (**Figure A.5.1**, **Figure A.5.2** and **Figure A.5.3**).

The influence of complexation in these electrolytes can be mainly explained by the change in hydration number and the inner/outer sphere coordination environment resulting in different reduction potentials. The formal reduction potential of a redox compound is affected by the interaction with ligands, i.e. the coordination of Eu(III) and Eu(II), and is a function of the ligand dissociation constants.[127] In addition, changing the electrolyte concentration leads to a considerable difference in activity, ionic strength and hydration of the ions in solution, thus changing their inner coordination sphere. Europium ions are strongly hydrated in aqueous media because of their high charge densities, with the highest charge density for trivalent europium, which is known to be coordinated by 8 to 9 water molecules, whereas divalent europium is coordinated by 7 to 8 water molecules. Chloride and nitrate show only modest levels of association with lanthanide ions in aqueous solutions, mostly in the form of double-solvent-separated ion pairs. Therefore, they are found to predominantly form outer-sphere complexes, even at high salt concentrations. Thus, Eu(III) and Eu(II) ions in aqueous media can be considered fully hydrated ions.

Figure 5.1, **Figure 5.2**, and **Figure 5.3** show the cyclic voltammograms of Eu(III) in perchlorate, nitrate and chloride media as a function of the potential sweep rate at a glassy carbon disk electrode. In all three media, a linear relationship between the cathodic peak currents and scan rate was observed, indicating a diffusion-controlled charge transfer. When the peak separation potentials are plotted as a function of potential sweep rate in logarithmic scale, as can be seen in **Figure 5.4**, a linear relationship (with $0.991 \leq R^2 \leq 0.996$) is found for all electrolytes.

Only minor differences in the peak potentials at different electrolyte solutions were observed, as can be seen in **Figure 5.1**, **Figure 5.2**, and **Figure 5.3**. At a sweep rate of 50 $mV.s^{-1}$, the cathodic peak potentials (E_p^c) are: -0.65, -0.68 and -0.68 V vs. Ag/AgCl, whereas the anodic peak potentials (E_p^a) are -0.40, -0.44 and -0.38 V vs. Ag/AgCl for perchlorate, nitrate and chloride media, respectively. The differences between the cathodic and anodic peak potentials are given in **Table 5.1**. Since these differences are larger than 59 mV in all media, and the E_p values change as a function of the scan rate, the reduction reaction in these electrolytes can be considered as being quasi-reversible.

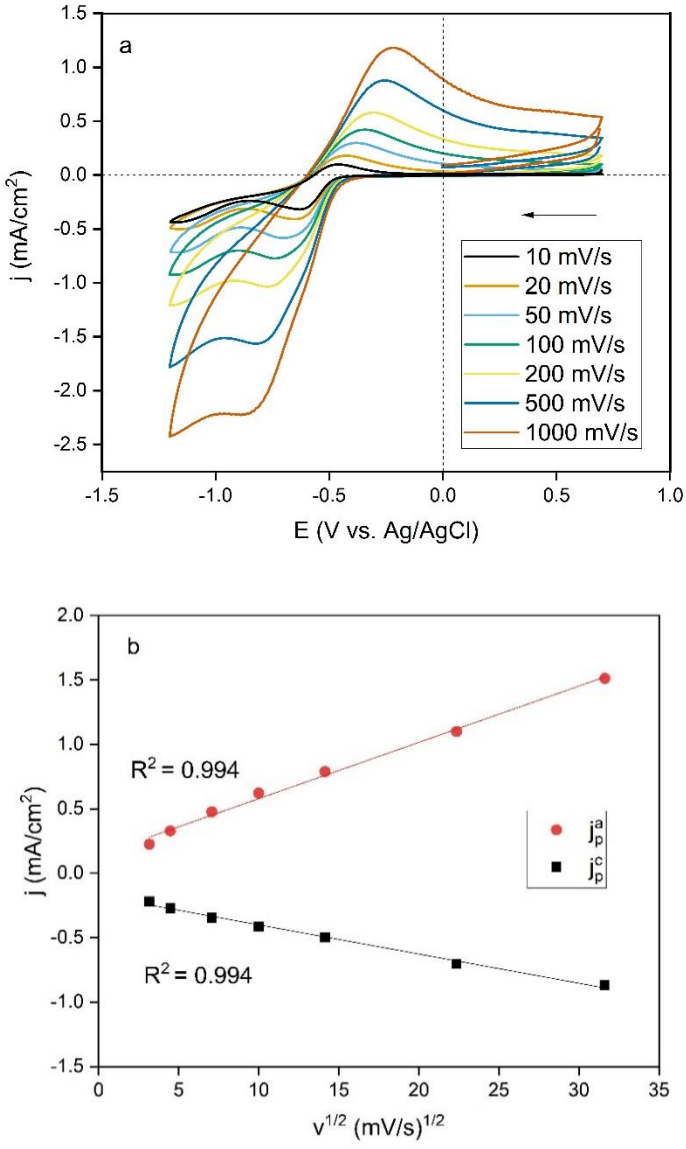

Figure 5.1. a) Cyclic voltammograms (second cycles) of 10 mmol.L^{-1} Eu(III) in 1 mol.L^{-1} $NaClO_4$ at various scan rates between 10 – 1000 mV/s b) Linear correlation of anodic and cathodic peak densities with respect to the square root at these scan rates.

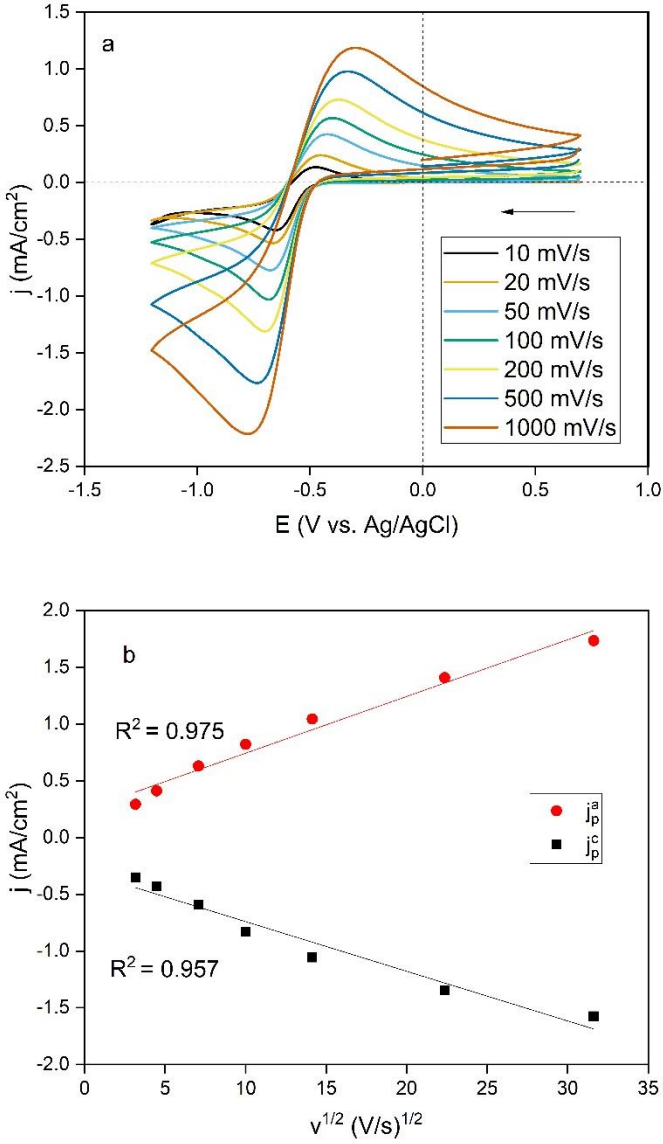

Figure 5.2. a) Cyclic voltammograms (second cycles) of 10 mmol.L^{-1} Eu(III) in 0.1 mol.L^{-1} $Ca(NO_3)_2$ at various scan rates between 10 – 1000 mV/s b) Linear correlation of anodic and cathodic peak densities with respect to the square root at these scan rates.

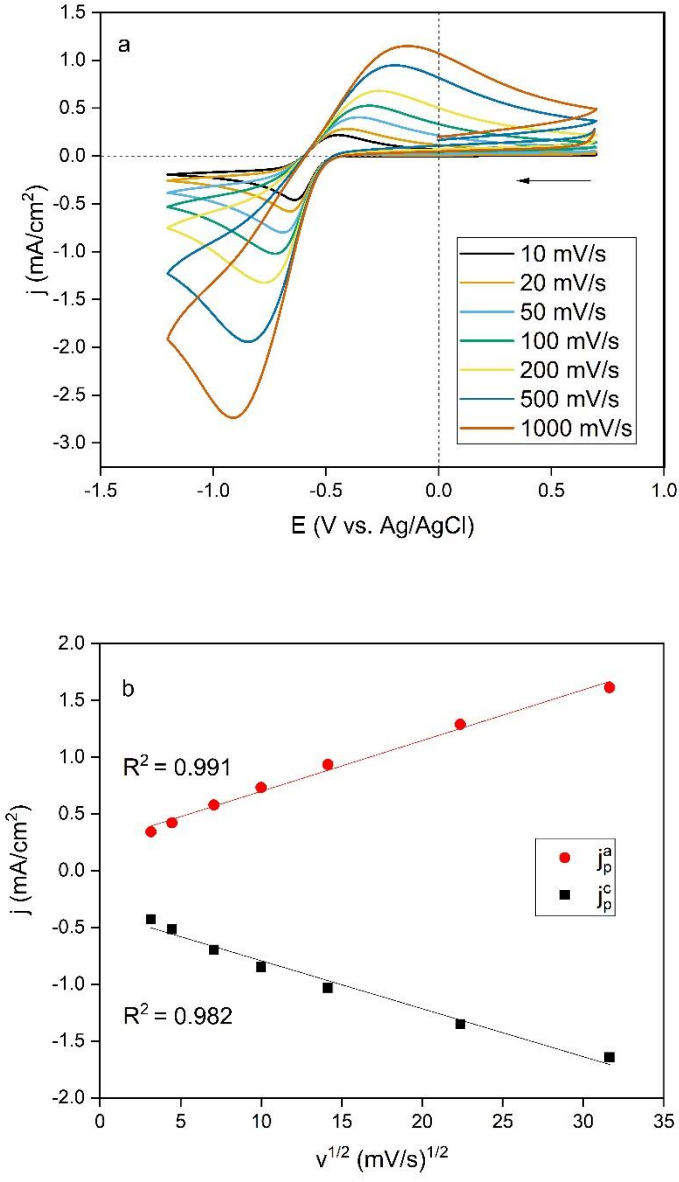

Figure 5.3. a) Cyclic voltammograms (second cycles) of 10 mmol.L^{-1} Eu(III) in 0.1 mol.L^{-1} $CaCl_2$ at various scan rates between 10 – 1000 mV/s b) Linear correlation of anodic and cathodic peak densities with respect to the square root at these scan rates.

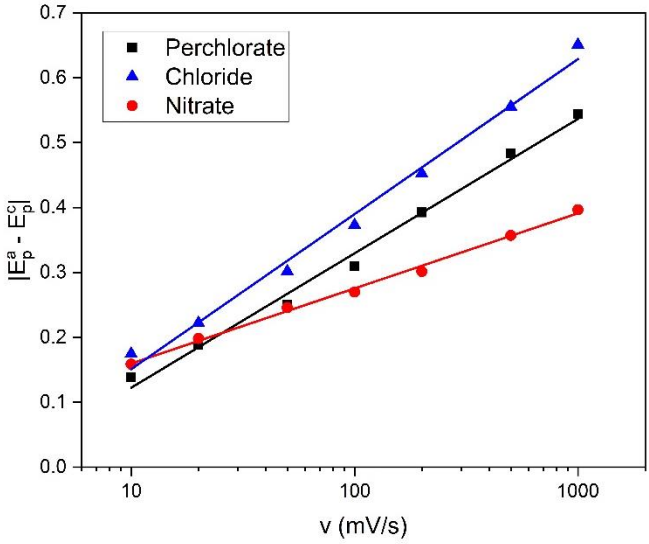

Figure 5.4. Peak separation potentials of 10 mmol.L^{-1} Eu(III) in 1 mol.L^{-1} perchlorate, 0.1 mol.L^{-1} chloride and 0.1 mol.L^{-1} nitrate media as a function of scan rate in logarithmic scale.

Table 5.1. Difference in anodic and cathodic potentials at 50 mV/s and diffusion coefficients of Eu(III)/Eu(II) reaction at different electrolytes.

Medium	**ΔE_p (V vs. Ag/AgCl)**	**D x 10^6 (cm^2/s)**	**Reported D values x 10^6 (cm^2/s)**
1 mol.L^{-1} $NaClO_4$	0.25	6.42	4.8 [208] 5.7 [205] 10 [206]
0.1 mol.L^{-1} $Ca(NO_3)_2$	0.25	25.3	-
0.1 mol.L^{-1} $CaCl_2$	0.30	23.2	-

In aqueous chloride and nitrate media, it was observed that varying the salt concentration resulted in a shift of the reduction potential, and the reduction reaction was found to be more favourable at higher electrolyte concentrations.[98] Although the electrolyte concentration was higher in perchlorate medium, the peak potentials differed only ± 20 mV from the other electrolytes. Among these, the reduction potential was the lowest in nitrate medium, similar to the observations made by Van de Voorde *et al.*, where the oxidation and reduction of europium in nitrate aqueous media, consistently have the lowest values at all concentrations.[98] Furthermore, chloride and perchlorate anions do only weakly interact with Eu(III) ions in aqueous media, so that only outer-sphere complexes are formed. However, Eu(III) nitrate solutions exhibit properties that lie between the behaviour of those of weakly complexing chloride and perchlorate ions and the more strongly complexing sulphate ion.[212–215] Therefore, Eu(III) and Eu(II) ions are hydrated in these electrolytes and they form dominantly outer-sphere complexes, resulting in similar reduction potentials (E_p^c of -0.65 V vs. Ag/AgCl in perchlorate, -0.68 V vs. Ag/AgCl in nitrate and -0.68 V vs. Ag/AgCl in chloride media) independently of the electrolyte.

The relationship between the peak current and the scan rate for reversible reactions, which is also valid for quasi-reversible reactions, is given by the Randles–Sevcik equation:

$$i_p^c = 0.496nFCAD^{1/2}\left(\frac{(\alpha n_\alpha)Fv}{RT}\right)^{1/2} \quad (5.1)$$

where i_p^c is the cathodic peak current (in amperes), n is the number of exchanged electrons, F is the Faraday constant (96485 C. mol^{-1}), C is the europium concentration (in mol.cm^{-3}), A is the electrode surface area (in cm^2), D is the diffusion coefficient (in cm^{2}s^{-1}), v is the potential sweep rate (in V.s^{-1}), α is the charge-transfer coefficient, n_α is the number of electrons transferred in the rate-determining step, R

is the universal gas constant and T is the absolute temperature (in K). In all electrolytes, the linear dependence of cathodic peak current to the square root of the scan rate , shows that the reduction of Eu(III) in these solvents is diffusion-controlled (**Figure 5.1**, **Figure 5.2** and **Figure 5.3**). In order to calculate the diffusion coefficients in these electrolytes, the αn_α value was estimated by using the half-peak potential relationship equation for irreversible systems:

$$\left|E_p^c - E_{\frac{p}{2}}^c\right| = \frac{1.857\ RT}{\alpha n_\alpha F} \qquad (5.2)$$

where $E_{\frac{p}{2}}^c$ is the cathodic half-peak potential. The calculated and reported D values can be found in **Table 5.1**. The experimental values for the diffusion coefficient in perchlorate medium are in close agreement with values reported in the literature, which were derived from chronoamperometric techniques or polarography. [205,209] To the best of our knowledge, there have been no studies reported in chloride or nitrate media yet, apart from the kinetic study in 2 mol.L^{-1} HCl by Atanasyants *et al.* who reported mixed kinetics.[95] The diffusion coefficients in all media are of the same order of magnitude, slightly higher in nitrate and chloride media. The difference in the concentrations would impact the viscosity of these solutions. Thus, the increase in the diffusion coefficient can be attributed to the decreasing viscosity in nitrate and chloride media.[216]

5.4.2. Linear sweep voltammetry at rotating disk electrode

Cyclic voltammetry is a valuable technique to qualitatively study the reactivity of compounds and to learn about the potential at which redox processes occur, the oxidation states, the number of electrons involved in the process, any possible chemical processes involved with the electron transfer etc. However, due to its non-stationary

behaviour and capacitive contributions involved, quantitative determination of kinetic parameters cannot be determined. Therefore, to further evaluate the kinetic parameters of the Eu(III) reduction reaction in perchlorate, nitrate and chloride media, linear sweep voltammetry at a rotating disk electrode (RDE) was used. Compared to polarography or chronoamperometry, rotating disk electrode experiments have advantages such as supplying more reliable mass transport conditions, quickly achieving steady-state electrode currents, a well-defined electrode surface for quantitative analysis and, as a result, higher sensitivity.[217,218] For these experiments, an in-house made water-jacketed three electrode glass cell with 100 mL inner volume was used. The solutions were purged with argon gas, at least for 30 minutes, before the experiment, and during the experiment an argon blanket was supplied to avoid oxidation of Eu(II) by air. In order to check the electrochemical activity of Eu(III)/Eu(II), voltammograms were recorded at different rotation speeds.

In previous work of Van de Voorde *et al.*, a detailed parameter study was performed on the stability of Eu(II) as a function of the electrolyte composition, and it was found that the stability of Eu(II) increased at higher nitrate and chloride concentrations.[98] Based on this results, the initial experiments were conducted at 3 mol.L^{-1} electrolyte solutions (**Figure A.5.4** and **Figure A.5.5**). However, at these high electrolyte concentrations, the voltammograms were not reproducible, and inhibition of the glassy carbon electrode was observed at higher rotation speeds. There are issues related with the use of nitrate salts as supporting electrolyte, due to the possible interactions with the electrode surface, anodic reactions of nitrate ions and complex formation with the ion of interest.[151,152,219] The inhibition of the electrode could also be explained by the selective adsorption of nitrate ions on the electrode which prevents the charge transfer reaction of europium. Therefore, the electrolyte concentrations was kept at 0.1 mol.L^{-1} or 1 mol.L^{-1} to obtain reliable results and to enable comparison of calculated kinetic parameters with literature data.

The dependence of current density on the electrode potential is presented in the linear sweep voltammograms in **Figure 5.5.a.**, **Figure 5.6.a.** and **Figure 5.7.a.** in chloride, nitrate and perchlorate media, respectively. These curves can be separated into three regions: the charge-transfer-limited region with initial exponential increase in current density, the mixed kinetics region where diffusion and charge transfer both contribute to the kinetics, and the mass-transfer limited plateaus.

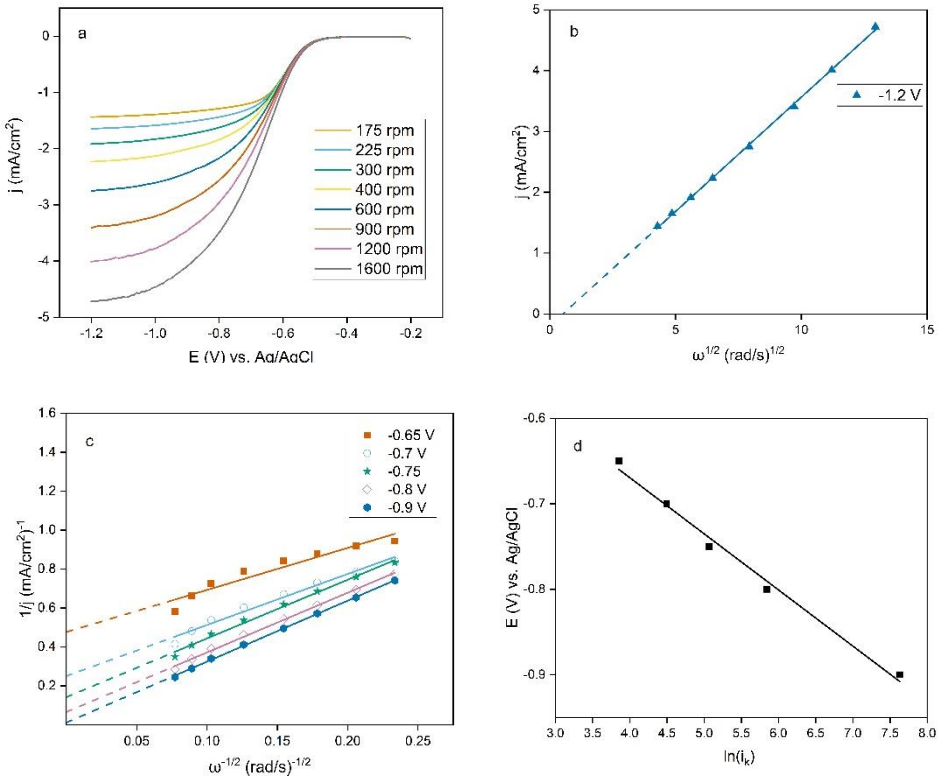

Figure 5.5. a) Linear sweep voltammogram on a glassy carbon rotating disk electrode in 0.01 mol.L^{-1} Eu(III) in 0.1 mol.L^{-1} $CaCl_2$ solution at a scan rate of 50 mV s^{-1} for rotation speeds 175 – 1600 rpm b) Levich plot at -1.2 V vs. Ag/AgCl and c) Koutecký – Levich plot at various potentials (-0.65 V to -0.9 V vs. Ag/AgCl) d) Tafel plot deducted from the Koutecký–Levich analysis.

The kinetic analysis using a rotating disk electrode can be performed using two correlations in the respective regions: Levich and Koutecký-Levich analysis. The equations to calculate the kinetic parameters via these methods are given as:

$$\frac{1}{i} = \frac{1}{i_k} + \frac{1}{i_l} = \frac{1}{i_k} + \frac{1}{B\omega^{1/2}} \quad (5.3)$$

$$B = 0.62AnFD^{2/3}v^{-1/6}C \quad (5.4)$$

$$i_k = nFAkC \quad (5.5)$$

$$i_l = 0.62AnFD^{2/3}v^{-1/6}C\sqrt{\omega} \quad (5.6)$$

The variables for these equations are; n is the number of exchanged electrons, F is the Faraday constant (96485 C. mol^{-1}), C is the europium concentration (in mol.cm^{-3}), A is the electrode surface area (in cm^2), k is the rate constant for electron transfer (in cm.s^{-1}), D is the diffusion coefficient (in cm^{2}s^{-1}), v is the potential sweep rate (in V.s^{-1}) α is the charge-transfer coefficient, n_α is the number of electrons transferred in the rate-determining step, R is the universal gas constant (8.314 J mol^{-1} K^{-1}), T is the absolute temperature (in K), ω is the angular frequency of rotation (rad/s), ν is the kinematic viscosity of the electrolyte (cm^2/s), i_k is the kinetic current and i_l is the limiting current (in A).

The Levich plots are presented in **Figure 5.5.b.**, **Figure 5.6.b.**, and **Figure 5.7.b.**, and were fitted by linear regression analysis, with the intercepts shown. Based on Eqn. 5.6, the slope of the Levich plot can be used to calculate the diffusion coefficients. These calculated values are given in **Table 5.2**. There is no deviation from the linearity in these plots, with linear fitting R^2 values ($R^2 \geq 0.99$), proving the mass transport regime at the limiting current. The kinematic viscosities for the electrolyte solutions were estimated by the literature values reported as 0.00899 cm^{2}s^{-1} for 0.1 mol.L^{-1} $Ca(NO_3)_2$, 0.00896 cm^{2}s^{-1} for 0.1 mol.L^{-1} $CaCl_2$, and 0.00917 cm^{2}s^{-1} for 1 mol.L^{-1} $NaClO_4$.[98,217] By using the Levich equation, the diffusion coefficients were calculated with

the assumption that the reaction is a one-electron process. For perchlorate medium, the diffusion coefficient values are in the same order of magnitude compared to the earlier calculations from cyclic voltammetry, where the values are slightly higher in less concentrated nitrate (10.7×10^6 $cm^2.s^{-1}$) and chloride (11.71×10^6 $cm^2.s^{-1}$) solutions compared to the perchlorate media (7.28×10^6 $cm^2.s^{-1}$). Koutecký-Levich analysis was performed to calculate the rate constant for the charge transfer in these media, and the results are summarized in **Table 5.2**. The rate constants were calculated by using equations 5.3, 5.4 and 5.5, where the intercept of the Koutecký-Levich plot equals to the inverse of the kinetic current. The value for the reference perchlorate medium was calculated as 1.13×10^{-4} $cm.s^{-1}$, which is very similar to the literature values.[204,208]

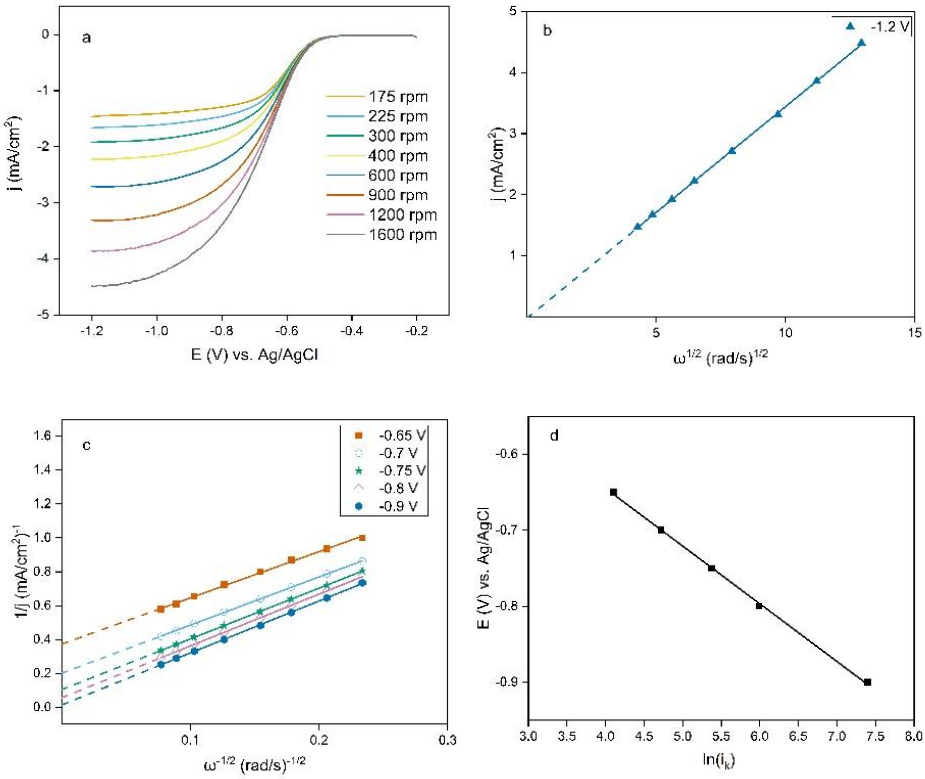

Figure 5.6. a) Linear sweep voltammogram on a glassy carbon rotating disk electrode in 0.01 mol.L^{-1} Eu(III) in 0.1 mol.L^{-1} $Ca(NO_3)_2$ solution at a scan rate of 50 mV s^{-1} for rotation speeds 175 – 1600 rpm b) Levich plot at -1.2 V vs. Ag/AgCl and c) Koutecký – Levich plot at various potentials (-0.65 V to -0.9 V vs. Ag/AgCl) d) Tafel plot deducted from the Koutecký–Levich analysis.

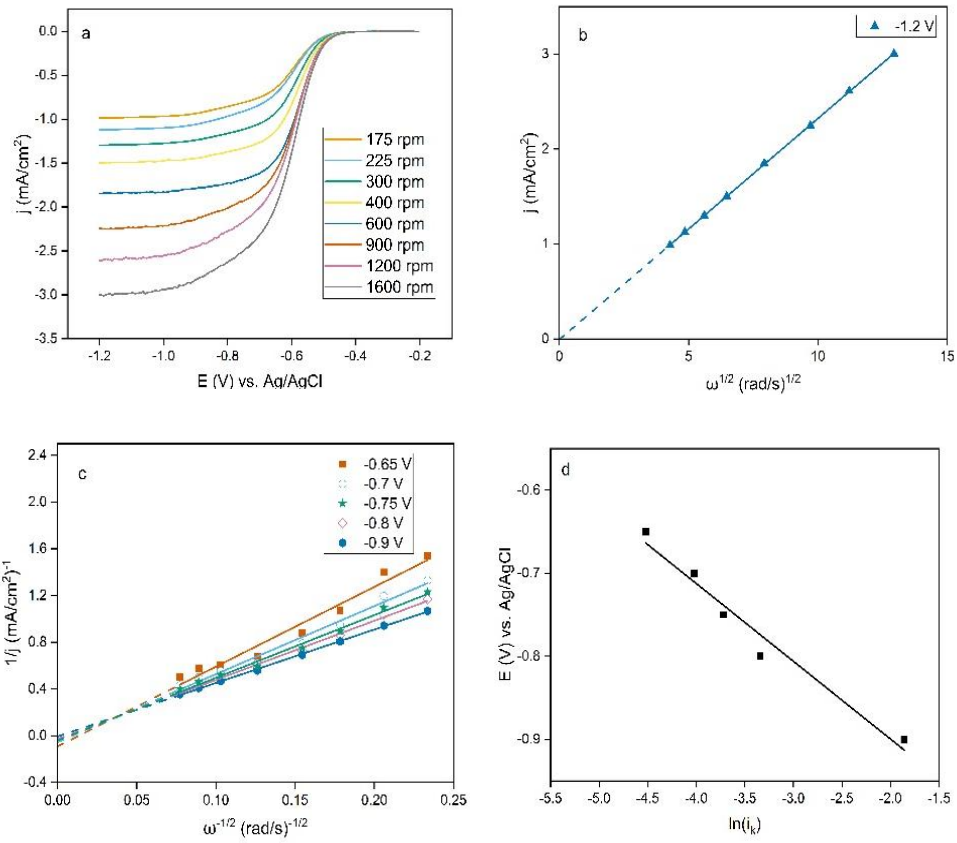

Figure 5.7. a) Linear sweep voltammogram on a glassy carbon rotating disk electrode in 0.01 mol.L^{-1} Eu in 1 mol.L^{-1} $NaClO_4$ solution at a scan rate of 50 mV s^{-1} for rotation speeds 175 – 1600 rpm b) Levich plot at -1.2 V vs. Ag/AgCl and c) Koutecký – Levich plot at various potentials (-0.65 V to -0.9 V vs. Ag/AgCl) d) Tafel plot deducted from the Koutecký–Levich analysis.

Table 5.2. D, α and k values calculated based on Levich and Koutecký-Levich analysis.

Medium	D x 10^6 (cm^2/s)	k (cm/s)	k (cm/s)*
1 mol.L^{-1} $NaClO_4$	7.28	1.13 x 10^{-4}	1.6 x 10^{-4} 2.4 x 10^{-4}
0.1 mol.L^{-1} $Ca(NO_3)_2$	10.7	2.88 x 10^{-3}	-
0.1 mol.L^{-1} $CaCl_2$	11.71	2.18 x 10^{-3}	-

*The values are based on the literature.[96,203]

The calculated value being similar to the literature value validates that this method is applicable to the aqueous electrolytes that are studied. It was observed that in nitrate and chloride media, the rate constant was ten times larger than in perchlorate medium with 2.88 x 10^{-3} cm.s^{-1} in nitrate and 2.18 x 10^{-3} cm.s^{-1} in chloride solutions. These differences can be explained by the differences in hydration at different concentrations. In addition to the differences in hydration of the europium ions and viscosity of the solutions due to the electrolyte concentration, for nitrate medium, reduction products of nitrate might influence the electrode reactions.[98,219]

According to the literature data,[96,203] the rate of the electrode process in chloride and perchlorate solutions should be similar ($k \approx 10^{-4}$ cm.s^{-1}) since inner-sphere complexation and anion adsorption are not prominent, whereas in nitrate medium an opposite observation is made. Additionally, it was demonstrated that the first coordination sphere of Eu(III) in perchlorate and chloride solutions solely contains water molecules, even at very high salt concentrations, whereas $EuNO_3^{2+}$ can also form in nitrate medium.[212] Based on a study by Kinard *et al.*,[203] the reversibility as a function of supporting electrolytes shows the following trend: $ClO_4^- < Cl^- < NO_3^- < Br^- < I^- < SCN^-$ and the outer-sphere complexes give the same limiting current, indicating similarities in reduction mechanism within this series. Although the differences in complexation could impact the

kinetics at higher concentrations, based on these results, the differences in rate constants and diffusion coefficients can be attributed rather to the concentration of these electrolytes.

5.5. Conclusions

The kinetics of the Eu(III) to Eu(II) reduction reaction were studied in perchlorate, nitrate and chloride media using cyclic voltammetry and linear sweep voltammetry on a rotating disk electrode. The perchlorate medium was selected as a reference condition to explore the methodology, and the kinetics study in the nitrate and chloride electrolytes are explored, to the best of our knowledge, for the first time. The diffusion coefficients were calculated by both cyclic voltammetry and Levich analysis, and these values are in the same order of magnitude and in a good agreement with literature data based on polarographic methods. The reaction is quasi-reversible in all the electrolytes under these chosen experimental conditions, which is confirmed by the difference in peak separation potential. Koutecký-Levich analysis was performed to retrieve information on the kinetic parameters such as reaction rate constant and the slope of the Tafel plot. The reaction rates in the different solvents were calculated to be 1.13×10^{-4} $cm.s^{-1}$ for the perchlorate medium, 2.88×10^{-3} $cm.s^{-1}$ for the nitrate medium and 2.18×10^{-3} $cm.s^{-1}$ for the chloride medium. Hence, the values for nitrate and chloride differ one order of magnitude. These minor differences in the nitrate and chloride electrolytes can be attributed to differences in concentration and viscosity rather than to the complexation or sluggish kinetics, since the concentrations were low. The good agreement of kinetic parameters with literature data indicates that the methods used to perform the kinetic analysis are reliable and that it is not necessary to use a mercury electrode for this type of measurements.

Chapter 6.

Samarium-153 purification using electrochemistry and column separation techniques

M.O. Arman, B. Geboes, K. Van Hecke, K. Binnemans, T. Cardinaels

All experimental work and compilation of the manuscript were performed by the author of this thesis. Co-authors contributed to the revision and design of the experiments.

6.1. Abstract

^{153}Sm is a β^--emitting medical radionuclide that is used in nuclear medicine for palliating bone pain due to skeletal metastasis or imaging. ^{153}Sm is produced via the reactor route by irradiating an enriched ^{152}Sm target with a high flux of thermal neutrons. However, during this process, long-lived ^{154}Eu impurities are also formed. The presence of these impurities poses a limitation on the shelf life of this radiopharmaceutical. Eu(III) can be readily reduced to Eu(II) in aqueous nitrate media where it is sufficiently stable for further separation. In the current study, electrochemical reduction of Eu(III) was combined with subsequent extraction chromatography. ^{153}Sm and ^{152}Eu tracers were used and chromatograms are constructed by gamma spectrometry. TEVA and DGA resins were investigated; where Eu(II) was efficiently eluted thanks to the poor retention on the columns, whereas retained Sm(III) was removed by changing the eluent to water. The TEVA column resulted in a better separation performance compared to the DGA column when equimolar lanthanide solutions were used. Reactor production conditions were also replicated where macro amounts of ^{153}Sm must be separated from micro amounts of ^{154}Eu. For the stability of Eu(II), a certain amount of Eu must be present in the solution, and therefore carrier-added separation shows the most promising results to purify medical ^{153}Sm.

6.2. Introduction

^{153}Sm is a radiolanthanide with a 1.93d half-life, and it emits β^- particles with a mean energy of 233 keV, which makes it interesting for nuclear therapeutics. It also simultaneously emits γ photons with an energy of 103.2 keV allowing SPECT imaging, thus making it a good candidate for possible theranostic applications.[12,16,50,54,220,221] ^{153}Sm-EDTMP complex was authorized as a palliative agent with the tradename Quadramet® in clinical applications.[222] Many more

studies are conducted to use other ^{153}Sm-labeled compounds to treat other type of cancers as well.[47,48,51,53,220]

^{153}Sm is produced via carrier-added route with thermal neutron activation (n,γ) of highly enriched ^{152}Sm target material (98.7% enriched, σ_{th} = 206 barn) at SCK CEN.[223] Due to the very short half-life of ^{153}Sm compared to the irradiation time (nine days), it already decays to ^{153}Eu during the irradiation. The neutron capture of this radionuclide would lead to formation of long-lived ^{154}Eu ($t_{1/2}$: 8.593 y), which impacts the shelf-life of ^{153}Sm radiopharmaceuticals drastically. The current method to produce carrier-added ^{153}Sm concerns an HPLC method using complexing agent α-hydroxy isobutyric acid (α-HIBA) which is applicable for other lanthanides as well.[66,90,224] However, this method involves multiple stages with long durations and hence ending up with only limited efficiency. Therefore, an efficient separation method should be developed to separate Sm and Eu, which is very challenging due to the characteristics of the lanthanides. The electron configuration of lanthanide ions makes the trivalent oxidation state prominent, resulting in very similar chemistry, as explained in Chapter 1. However, some lanthanides display unusual oxidation states such as tetravalent cerium and terbium or divalent ytterbium and europium.[104,105,108,116,159,225–228] The stabilization of Eu(II) is due to the half-filled shell ([Xe] $4f^7$), and the standard reduction potential for Eu(III)/Eu(II) is -0.36 V vs. SHE. A separation strategy can make use of this stable oxidation state, which leads to a change in chemical properties of Eu. So far, chemical and photochemical reduction of europium are well established.[98,101,113,114,229,230] By using an electrochemical method, reduction can be achieved while avoiding introduction of reducing agents. In previous studies, such combination of electrochemical reduction followed by column chromatography or solvent extraction has been used mainly for hydrometallurgical purposes.[93,95,119] Van de Voorde *et al.* established a method that was promising for the purification of radiopharmaceutical ^{153}Sm from Eu impurities, first mainly performing chemical reduction of Eu with Zn, or electrolysis, in highly concentrated nitrate media followed by solvent extraction with the

ionic liquid Aliquat 336 in nitrate form.[94,124] Later on, this was further tested with supported ionic liquid phase (SILP) and commercial TEVA column, achieving more than 80% of the Eu recovered in the first fractions. In the current study, only the electrochemical method was used for reduction of Eu(III) in nitrate medium. The solutions were spiked with ^{153}Sm and ^{152}Eu tracers, and elution curves were constructed by their activity being measured via gamma spectrometry. The extraction chromatography experiments were performed using either TEVA or DGA resins, in accordance with the literature showing promising results with rare earths.[84,231] Eu(III) was successfully reduced and the stability was maintained for the separation process. As a next step, reactor production conditions were replicated to test the scalability of the current method to the real scale – where the separation is between macro amounts of ^{153}Sm and micro amounts of ^{154}Eu impurities.

6.3. Materials and methods

6.3.1. Chemicals

$Eu(NO_3)_3.6H_2O$ (99.9%) and $Sm(NO_3)_3.H_2O$ (99.9%) were supplied from Strem Chemicals Inc. (Newburyport, USA). $Ca(NO_3)_2.4H_2O$ (≥99%), NH_4NO_3 (≥99%), 67% HNO_3 and 25% NH_3(aq) were obtained from Sigma-Aldrich (Overijse, Belgium). ^{152}Eu tracer (>99% radionuclidic purity) was purchased from Eckert and Ziegler Nuclitec GmbH (Braunschweig, Germany). ^{153}Sm tracer was obtained by irradiation of a highly enriched $^{152}Sm_2O_3$ target (98.7% ± 0.1, Neonest AB) in the BR1 reactor (ϕ_0 = 3.67x10^{11} neutrons cm^{-2}.s^{-1}, 1 day irradiation) at SCK CEN , which was dissolved in 1 mol.L^{-1} HNO_3 solution after a cooling time of half a day. The 2 mL bed volume cartridges (PP, frits in PE, 20µm porosity) , TEVA (100–150 µm) and DGA resin (N,N,N',N'-tetrakis-2-ethylhexyldiglycolamide, branched, 50–100 µm) resins were purchased from TrisKem International (Bruz, France). MilliQ water (18.2 MΩ cm at 25 °C) was used to prepare the aqueous solutions.

6.3.2. Electrochemical reduction of Eu(III)

The electrochemical reduction of Eu(III) was performed in a 50 mL two compartment electrolysis cell purchased from redox.me. The counter electrode was separated from the working and reference electrode by a glass chamber having a ceramic frit. The working electrode material was reticulated vitreous glassy carbon (outer diameter 30 mm, inner diameter 20 mm, height 25 mm) with a platinum wire contact. The reference electrode was Ag/AgCl in 3 mol.L^{-1} KCl, and the counter electrode was a Pt coil (ø: 0.6 mm). Before starting the electrolysis, the solution was purged with argon (Ar) for 30 minutes to eliminate the dissolved oxygen, and an Ar blanket was applied during the electrolysis to avoid contact with air. A constant potential of -0.75 V vs. Ag/AgCl was applied for 120 minutes by using a Metrohm PGSTAT204 potentiostat with a compliance voltage of 20 V and a maximum current of 400 mA, operated with the NOVA 2.1.5 software.

6.3.3. Extraction chromatography

The TEVA and DGA resins were packed into the cartridge (ø: 1 cm, h: 2.5 cm, BV: 2 mL) as a slurry to provide uniform packing without channel formation. Mobile phases were consisting of 3 mol.L^{-1} $Ca(NO_3)_2$ or 6 mol.L^{-1} NH_4NO_3. The second eluent was water. All these eluents were purged with Ar to eliminate the dissolved oxygen. The packed columns were preconditioned with purged 3 mol.L^{-1} $Ca(NO_3)_2$ or 6 mol.L^{-1} NH_4NO_3. The column was connected to an ISMATEC IPC 8-channel peristaltic pump, to control the flow rate. Fractions of 1 mL volume were collected for analysis.

6.3.4. Gamma spectrometry

^{153}Sm and ^{152}Eu were analyzed by gamma spectrometry using an HPGe detector, a DSA-1000 Multi-Channel Analyzer, and Genie2000 software (Canberra Semiconductors N. V., Olen, Belgium). 121.8 keV, 344 keV, 778.9 keV, 964 keV, 1112 keV and 1408 keV γ-peaks were used for measurement of ^{152}Eu. 69.67 keV, 97.43 keV and 103.18 keV γ-peaks were used for measurement of ^{153}Sm.

6.4. Results and Discussion

6.4.1. Electrochemical reduction of Eu(III)

Eu(III) was reduced in an aqueous solution spiked with ^{152}Eu and ^{153}Sm tracers containing a high concentration of nitrate salts, where the nitrate ion concentration was kept constant, (3 mol.L^{-1} $Ca(NO_3)_2$ or 6 mol.L^{-1} NH_4NO_3), as the first step of the separation process. A constant potential of -0.76 V vs. Ag/AgCl was applied for 3 hours in a bulk electrolysis cell. The recorded chronoamperograms of both the blank and the Eu(III) solution are presented in **Figure 6.1**. Based on Faraday's law (Eqn. 6.1), where Q is the charge in Coulombs, I is the current in amperes, t is the time in seconds, m is the number of moles of the reactant, n is the number of electrons transferred and F is the Faraday`s constant, the charges are estimated by integrating the current vs. time graphs.

$$Q = \int I \,.\, \mathrm{d}t = mnF \qquad (6.1)$$

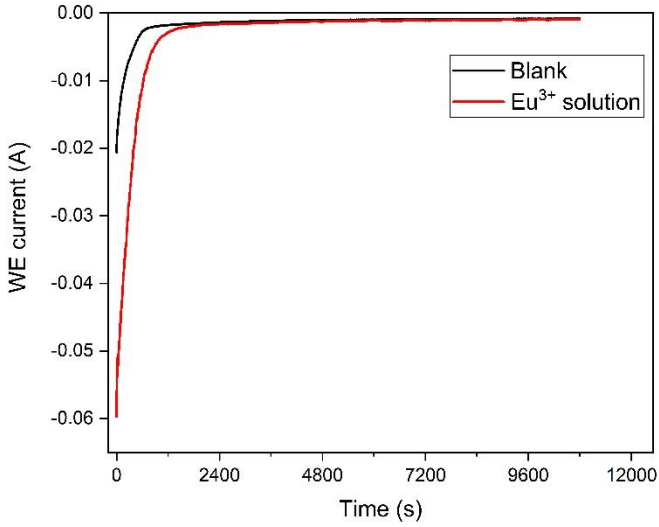

Figure 6.1. Chronoamperograms of blank (6.6 mmol.L^{-1} Sm(III) in 3 mol.L^{-1} $Ca(NO_3)_2$) and Eu(III) solution (6.6 mmol.L^{-1} Eu(III) and Sm(III) in 3 mol.L^{-1} $Ca(NO_3)_2$) recorded during 3h of electrolysis.

As the reactant is Eu(III) reducing with an one electron process (Eqn 6.2), the yield can be calculated via the charge corrected with the blank. The charges are calculated as -16.19 C for the blank and -33.06 C for the solution containing 6.6 mmol.L^{-1} Eu(III) and Sm(III) in 3 mol.L^{-1} $Ca(NO_3)_2$. From **Figure 6.1**, the conversion of Eu(III) to Eu(II) is calculated as ca. 24.2% after 3h of electrolysis.

$$Eu^{3+} + e^- \rightarrow Eu^{2+} \qquad E^o = -0.36\,V\ vs.SHE \qquad (6.2)$$

$$NO_3^- + 3H^+ + 2e^- \rightarrow HNO_2 + H_2O \quad E^o = 0.934\,V\ vs.SHE \qquad (6.3)$$

$$2H^+ + 2e^- \rightarrow H_2 \qquad E^o = 0\,V\ vs.SHE \qquad (6.4)$$

$$O_2 + 2H^+ + 2e^- \rightarrow H_2O_2 \qquad E^o = -0.695\,V\ vs.SHE \qquad (6.5)$$

$$H_2O_2 + 2H^+ + 2e^- \rightarrow 2H_2O \qquad E^o = 1.776\,V\ vs.SHE \qquad (6.6)$$

In the study of Van de Voorde *et al.,*[98] a conversion rate of more than 95% is achieved after 2 hours of reduction, using 66 mmol.L^{-1} of Ln(III) in 6 mol.L^{-1} $LiNO_3$ or 3 mol.L^{-1} $Ca(NO_3)_2$ by both electrochemical and chemical reduction. It was also established that reduction of Eu(III) in ammonium nitrate differs slightly in behaviour, showing a more negative reduction potential ($E_{p,c}$ = −0.73 V vs. Ag/Ag^+) compared to the other nitrate salts ($E_{p,c}$ = −0.65 V and – 0.68 V vs. Ag/Ag^+ for Ca^+ and Li^+ salts, respectively) with a larger current density in reduction. Furthermore, it was also observed that due to the acidity of $NH_{(IV)}$, hydrogen generation (Eqn. 6.4) is more pronounced.[98]

In addition, in this study, the electrochemical cell had a smaller volume (50 mL) compared to the previous study (100 mL), as well as the lanthanide concentrations were different. As a result, since the effective surface area of the working electrodes substantially differs, the conversion yield was lower at the same electrolysis times.

6.4.2. UV-Vis absorption spectroscopy

During the electrolysis, a colour change was observed from colourless to yellow, indicating the formation of Eu(II). The colour of these solutions remained yellow as long as the inert atmosphere was maintained, whereas it is observed that it gradually turned back to colourless when in contact with air. The back-reduction was already observed in previous studies in other media as well,[97,98,119] due to either contact with oxygen (Eqn. 6.5 and 6.6) or increase in the acidity of the solution. Jelinek *et al.* have determined the Eu(II) formation by UV-Vis spectroscopy after the electrochemical reduction of Eu(III) to Eu(II) in a 10 mmol.L^{-1} HCl solution.[97] The two absorption peaks at 280 and 320 nm, characteristic for Eu(II), were observed. These absorption peaks are related to $4f^7$-$4f^6 5d^1$ transition, where the energy of the 5d states is reduced by crystal and ligand field effects.[232,233] The absorbance values decrease sharply with decreasing pH.[93,97] H^+ is reduced to H_2 during the electrolysis, and this results in

an increase in pH of the solution (Eqn. 6.4). However, increase in pH to a value of more than 6.5 will result in precipitation of Eu(III) with the hydrolysis.[98] Therefore, in order to achieve a high stability, maintaining an inert atmosphere and having a moderate pH is crucial. UV-Vis absorption spectra were recorded before and after the electrolysis of a solution containing 10 mmol.L^{-1} Sm and 10 mmol.L^{-1} Eu in 6 mol.L^{-1} NH_4NO_3 and 3 mol.L^{-1} $Ca(NO_3)_2$ electrolytes. Eu(II) showed comparable absorption spectra in both solutions (**Figure 6.2**).[98]

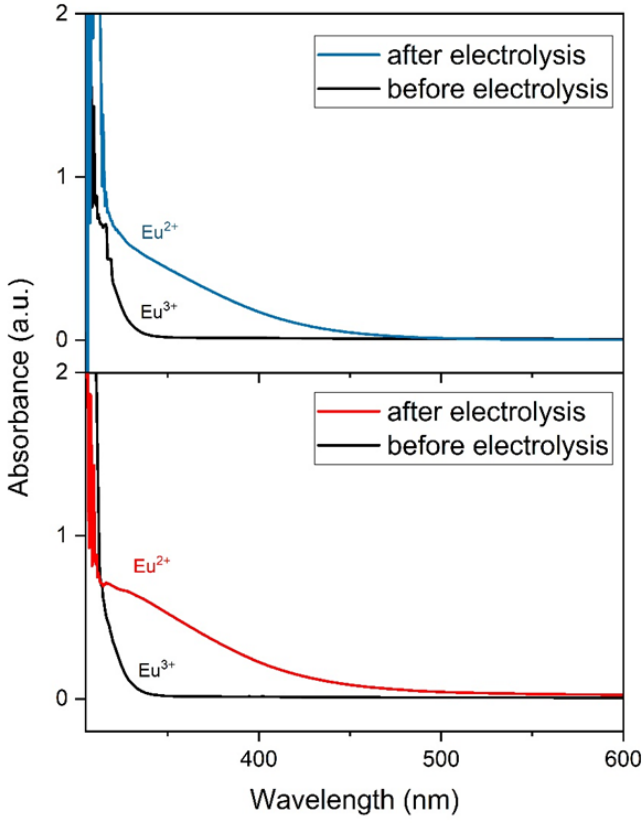

Figure 6.2. UV-Vis absorption spectra of 10 mmol.L^{-1} Sm(III) and 10 mmol.L^{-1} Eu(III) in 6 mol.L^{-1} NH_4NO_3 (top) and 3 mol.L^{-1} $Ca(NO_3)_2$ (bottom) measured before and after 2h of electrolysis at -0.75 V vs. Ag/AgCl. Blank solution of the electrolyte is used for background correction and 1 mm path length is used.

6.4.3. Extraction chromatography using radiotracers

6.4.3.1. TEVA resin

TEVA (tetravalent actinides) resin composes of a quaternary ammonium salt Aliquat 336®, mainly used for the separation of actinides. In previous studies of Van de Voorde et al. the successful separation of Sm(III) and Eu(II) was achieved using undiluted Aliquat 336® in nitrate form,[121] as well as immobilizing it on a solid support as a direct comparison to the commercially available TEVA.[94] Based on these studies, the separation mechanism of Sm(III) from Eu(II) relies on the coordination of Sm(III) to the column material and complete lack of affinity for Eu(II), and therefore complete lack of column retention. The coordination chemistry between Sm(III) and Aliquat 336® is described by Eqn 6.7.[94,121]

$$\mathrm{Sm}^{3+}_{(\mathrm{aq})} + 3\mathrm{NO}^{-}_{3(\mathrm{aq})} + 2[\mathrm{A336}][\mathrm{NO}^{-}_{3}]_{(\mathrm{org})} \rightleftarrows [\mathrm{A336}]_2[\mathrm{Sm(NO_3)_5}]_{(\mathrm{org})} \quad (6.7)$$

As described earlier, Eu(II) stability depends on the acidity of the solution as well as the dissolved oxygen. For this reason, in the extraction chromatography experiments the eluents were purged with Ar prior to the introduction onto the column as well. In the initial tests, to evaluate the stability of the Eu(II) solutions, UV-Vis absorption spectra of the feed solution containing 10 mmol.L^{-1} Eu(III) and 10 mmol.L^{-1} Sm(III) in 3 mol.L^{-1} $Ca(NO_3)_2$ and the first eluted fraction were recorded. As can be seen in **Figure 6.3**, the absorbance at 320 nm (peak of Eu(II)) is 0.0692 and 0.0625 for the feed and first fraction, respectively. Since the change in the absorbance is negligible, it is concluded that at the described experimental conditions, the amount of dissolved oxygen in the eluents can be held minimal as well as that TEVA particles do not cause back-oxidation of the Eu(II).

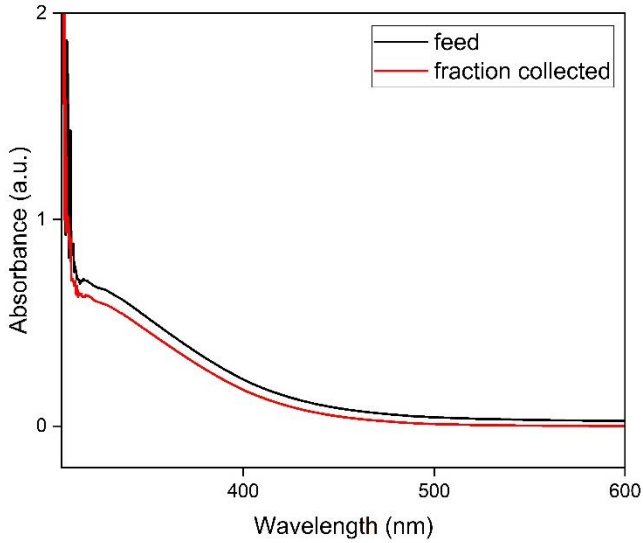

Figure 6.3. UV-Vis absorption spectra of the feed consist of 10 mmol.L^{-1} Eu(III) and 10 mmol.L^{-1} Sm(III) in 3 mol.L^{-1} $Ca(NO_3)_2$ and the first fraction collected from the column. Blank solution of the electrolyte is used for background correction and 1 mm path length is used.

After establishing the Eu(II) stability, in the first extraction chromatography experiments, a cartridge with 2 mL bed volume (ø: 1 cm, h: 5 cm) was packed with TEVA particles as described earlier, and conditioned with the Ar-purged 3 mol.L^{-1} $Ca(NO_3)_2$ or 6 mol.L^{-1} NH_4NO_3 mobile phase. After completion of the electrolysis, 1 mL of the electrolysed solution containing 6.6 mmol.L^{-1} Eu(III) and 6.6 mmol.L^{-1} Sm(III) in 3 mol.L^{-1} $Ca(NO_3)_2$ was loaded to the column with 1 mL.min^{-1} flow rate. The column was first eluted with a pure nitrate mobile phase (Ar-purged 3 mol.L^{-1} $Ca(NO_3)_2$ or 6 mol.L^{-1} NH_4NO_3) for collection of Eu(II). After collection of 6 fractions of 1 mL volume, water was used to elute Sm(III). The fractions were then measured in gamma spectrometer and the activities were calculated for ^{153}Sm and ^{152}Eu radiotracers. The resulting elution curve can be seen in **Figure 6.4**. 76.6% of Eu(II) was eluted in the first fractions whereas 89.7% Sm was collected in the stripping step with water. These results are in agreement with those of the previous study.[124] Since small amounts

of Sm were detected in the first fractions, the flow rate was decreased to 0.2 mL.min^{-1}. It can be seen in **Figure 6.5** that the majority of the europium was eluted in the later fractions together with Sm(III). It is assumed that the longer interaction time of the Eu(II) with the resin led to back-oxidation to Eu(III), resulting in separation co-elution of Eu(III) with Sm(III). Therefore, to avoid the exposure to the atmospheric or dissolved oxygen, the flow rate was held between 0.7 to 1 mL.min^{-1} for the remainder of the experiments.

Van de Voorde *et al.* performed a detailed study on electrochemical reduction using various nitrate salts, and observed that there were only minor differences in electrochemical reduction due to the counter ion.[98] While Ca^{2+} and Li^{+} ion salts resulted in similar reduction potentials for Eu(III) (E= − 0.65 V and -0.68 V vs. Ag/Ag^{+}, respectively), the $NH_{(IV)}$ ion salt showed more negative reduction potential (E= − 0.73 V vs. Ag/Ag^{+}) due to the acidity of the NH_4^{+} ion.[98] In this study, the electrochemical reduction and subsequent separation was tested using ammonium nitrate as the electrolyte as well. When using the ammonium nitrate electrolyte, the pH was increased to 5 to optimize the electrolysis by adding 1 mol.L^{-1} $NH_{3(aq)}$ solution. In **Figure 6.6**, the elution curves for Sm and Eu are represented. Although the majority of Sm(III) was collected in the later fractions after changing the eluent, only 50% of Eu(II) was present in the first fractions. It was already observed that pH plays an important role especially in ammonium nitrate solution, that eventually influences the stability of divalent complex.[98] Based on this, for the rest of the column experiments with TEVA, calcium nitrate was used as the electrolyte for a better reproducibility.

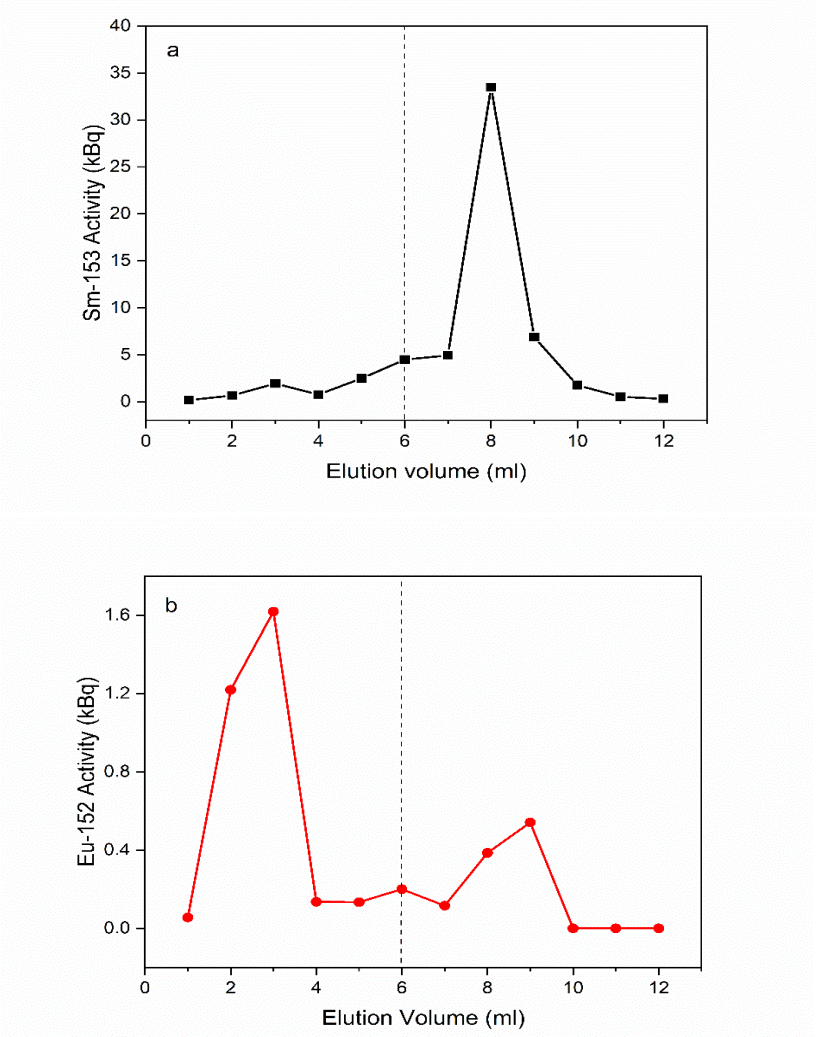

Figure 6.4. Elution curves of Sm(III) (a) and Eu(II) (b) using a TEVA resin filled cartridge (ø: 1 cm, h: 2.5 cm, BV: 2 mL) based on the radiotracer activities. Feed: 1 mL of a spiked solution containing 6.6 mmol.L^{-1} Eu(III) and 6.6 mmol.L^{-1} Sm(III) in 3 mol.L^{-1} $Ca(NO_3)_2$. The vertical dashed line indicates the switch of mobile phase from 3 mol.L^{-1} $Ca(NO_3)_2$ to water. Flow rate: 1 mL.min^{-1}.

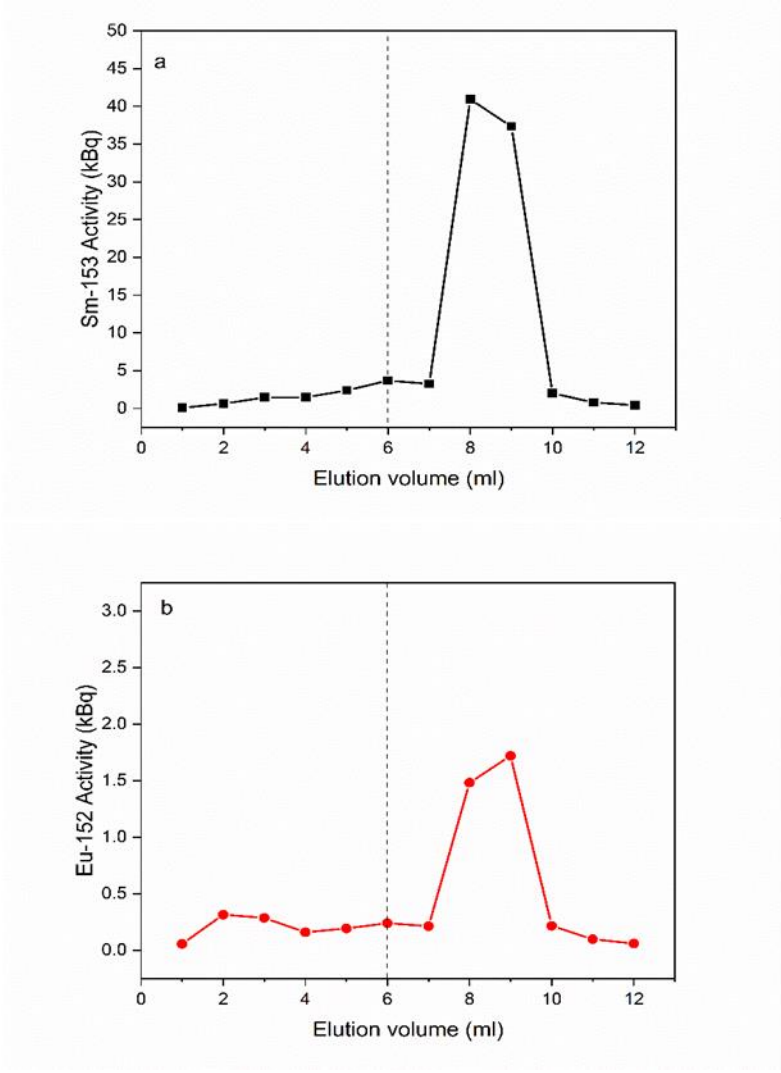

Figure 6.5. Elution curves of Sm(III) (a) and Eu(II) (b) using a TEVA resin filled cartridge (ø: 1 cm, h: 2.5 cm, BV: 2 mL) based on the radiotracer activities. Feed: 1 mL of a spiked solution containing 6.6 mmol.L^{-1} Eu(III) and 6.6 mmol.L^{-1} Sm(III) in 3 mol.L^{-1} $Ca(NO_3)_2$. The vertical dashed line indicates the switch of mobile phase from 3 mol.L^{-1} $Ca(NO_3)_2$ to water. Flow rate: 0.2 mL.min^{-1}

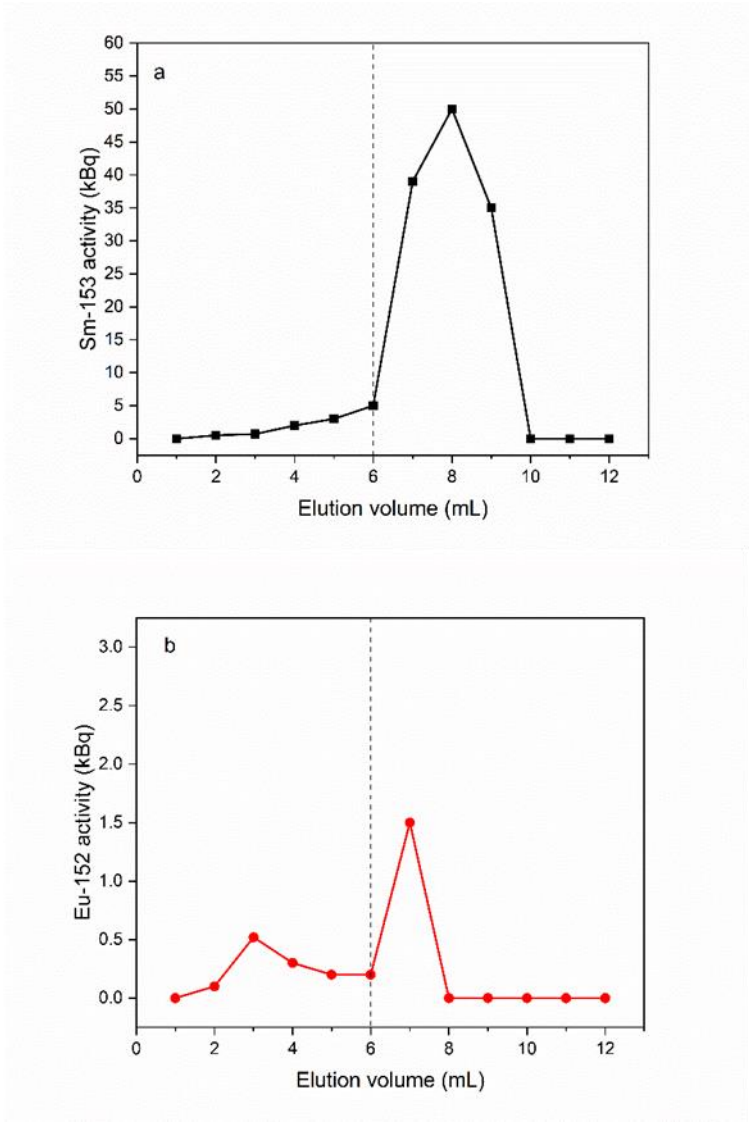

Figure 6.6. Elution curves of Sm(III) (a) and Eu(II) (b) using a TEVA resin filled cartridge (ø: 1 cm, h: 2.5 cm, BV: 2 mL) based on the radiotracer activities. Feed: 1 mL of a spiked solution containing 6.6 mmol.L^{-1} Eu(III) and 6.6 mmol.L^{-1} Sm(III) in 6 mol.L^{-1} NH_4NO_3. The vertical dashed line indicates the switch of mobile phase from 6 mol.L^{-1} NH_4NO_3 to water. Flow rate: 1 mL.min^{-1}.

6.4.3.2. DGA Resin

DGA resins have affinities for trivalent lanthanides in acidic media with the following extraction mechanism:

$$\mathrm{Ln^{3+} + 3X^{-} + 3\,\overline{DGA} \leftrightarrow \overline{LnX_3(DGA)_3}} \quad (6.7)$$

where X is NO_3^- or Cl^-.[234] Due to this high affinity, it is expected that Sm(III) efficiently retains on the column whereas Eu(II) would be eluted due to less affinity. A similar method is used for removal of Zn^{2+} from Sm(III) where a quantitative elution of ^{153}Sm was achieved.[54] Therefore, the same approach was used and a spiked solution containing 6.6 mmol.L^{-1} Eu(III) and 6.6 mmol.L^{-1} Sm(III) in 6 mol.L^{-1} NH_4NO_3 was electrochemically reduced prior to the separation of samarium and europium. The resulting elution curves can be seen in **Figure 6.7**. Sm(III) was retained on the column efficiently, with only 11% of loss in the first fractions, whereas all Eu(II) was eluted in the first fractions. This shows slightly better properties compared to TEVA resin, although in both methods, Sm(III) elution in the first fractions cannot be avoided. When the same experiment was conducted with 3 mol.L^{-1} $Ca(NO_3)_2$ as the electrolyte for the reduction, the extraction was not successful, since all Sm and Eu were eluted in the first fractions. Further tests should be performed to evaluate the role of the counter ion, and to elaborate the differences between extraction properties of TEVA and DGA columns.

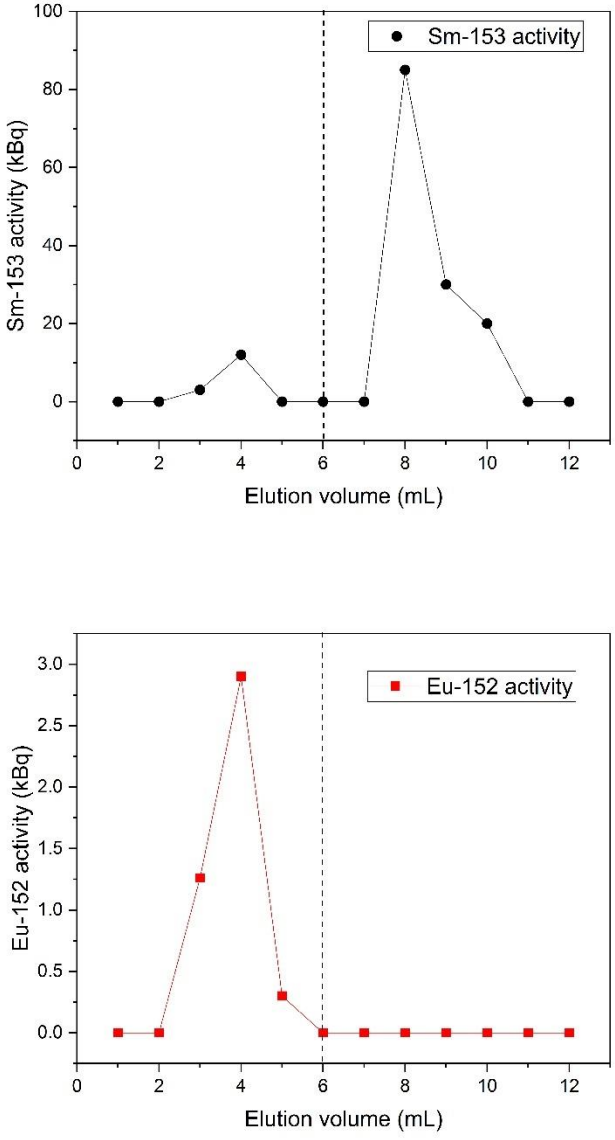

Figure 6.7. Elution curves of Sm(III) (a) and Eu(II) (b) using a DGA resin filled cartridge (ø: 1 cm, h: 2.5 cm, BV: 2 mL) based on the radiotracer activities. Feed: 1 mL of a spiked solution containing 6.6 mmol.L^{-1} Eu(III) and 6.6 mmol.L^{-1} Sm(III) in 6 mol.L^{-1} NH_4NO_3. The vertical dashed line indicates the switch of mobile phase from 6 mol.L^{-1} NH_4NO_3 to water. Flow rate: 1 mL.min^{-1}.

6.4.3.3. BR2 irradiation experimental conditions

The tracer studies showed that, by reducing Eu(III) to Eu(II) electrochemically, the separation can be achieved between Eu(II) and Sm(III) successfully when equimolar lanthanides are used. After the tracer studies, as a next step, reactor production conditions of BR2 were taken into account and calculations were performed based on the 9 days irradiation period. After dissolution of the irradiated and cooled targets, a concentration ratio of Sm:Eu of 25:1 would be obtained. In these experiments, the concentration ratios were maintained by adding stable Sm(III) and Eu(III) salts, and the feed volume had to be reduced to 0.7 mL due to the higher concentrations and the limited capacity of the column. The extraction experiment was performed in the same way as described in the previous sections. The resulting elution curve can be seen in **Figure 6.8**. Both Sm and Eu were retained on the column and eluted with water. This shows that at these low concentrations, the Eu(II) complex is not stable, and more prone to back-oxidation. The amount of Eu should therefore be increased prior to the electrolysis, to ensure the stability of Eu(II). Thus, the addition of stable Eu should be considered in the case this electrochemical reduction and separation method is used.

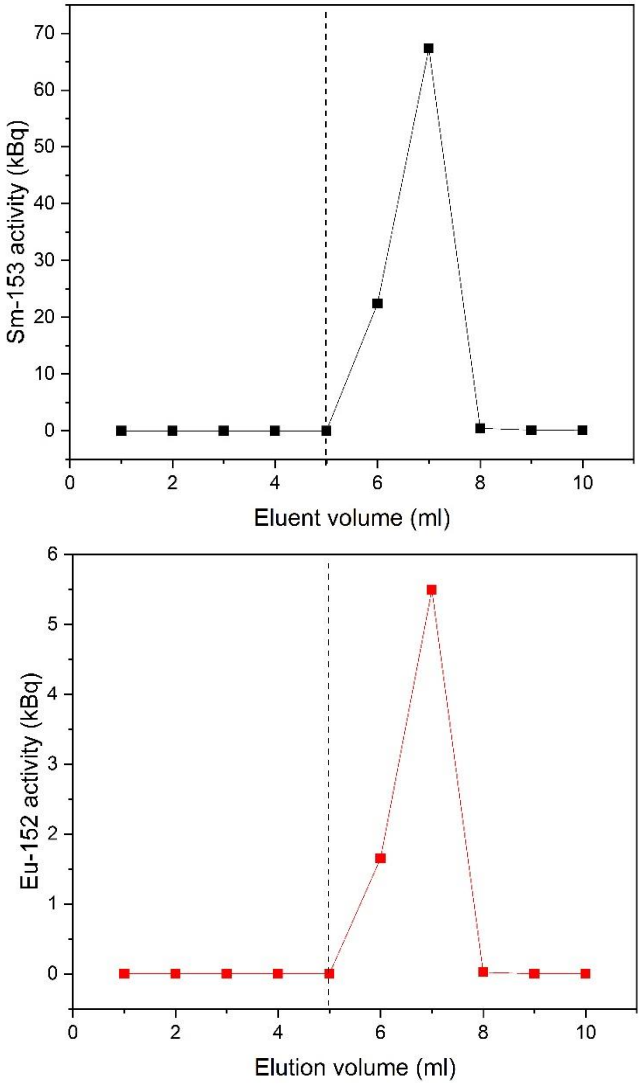

Figure 6.8. Elution curves of Sm(III) (a) and Eu(III) (b) using a DGA resin filled cartridge (ø: 1 cm, h: 2.5 cm, BV: 2 mL) based on the radiotracer activities. Feed: 0.7 mL of a spiked solution containing 0.86 mmol.L^{-1} Eu(III) and 21.5 mmol.L^{-1} Sm(III) in 3 mol.L^{-1} $Ca(NO_3)_2$. The vertical dashed line indicates the switch of mobile phase from in 3 mol.L^{-1} $Ca(NO_3)_2$ to water. Flow rate: 1 mL.min^{-1}

6.5. Conclusions

The electrochemical reduction of Eu(III) to Eu(II) was successfully conducted using ^{153}Sm and ^{152}Eu radiotracers in ammonium nitrate and calcium nitrate media. The conversion yield was calculated based on the charge. TEVA and DGA resins were used for the separation experiments. Almost 90% of Sm(III) was recovered from the column when equal amounts of Eu(III) and Sm(III) were present in the solution, using TEVA column. The Eu(II) nitrate complex was stable enough and 76% of Eu was recovered from the TEVA column by elution with 3 $mol.L^{-1}$ $Ca(NO_3)_2$. The flow rate should be maintained high enough to avoid long interaction times of Eu(II) with the column, which results in back-oxidation and therefore poor separation. DGA column was for the first time used for the extraction chromatography experiments, using tracers. When ammonium nitrate salt was used instead of calcium salt, separation using DGA column was comparable as those obtained with the TEVA column were achieved, which can be further investigated and optimized. Whereas DGA shows promising results which merits future exploration, its limitations with the use of calcium nitrate electrolyte might indicate that TEVA is a more suitable column material for the separation of radiolanthanides. Finally, reactor irradiation conditions were used in order to perform a more representative case for the total concentrations of lanthanides. The initial tests showed that to maintain the stability of Eu(II), the concentration should be high enough, which shows the necessity of using carrier added method for an efficient separation.

Chapter 7.

Conclusions and Outlook

A wide range of radiolanthanides can be used in nuclear medicine. Their use is based on the physical decay properties as well as the availability and achievable specific activity. Thanks to their very similar chemical properties and variety in half-life, particle emission and energies, they offer many possibilities in both diagnosis and therapy. Radiolanthanides can be produced in research reactors or cyclotrons, by means of carrier-added or non-carrier-added routes. The choice of the route affects the specific activity as well as the possible radionuclidic impurities. Prior to radiolabelling, the radiolanthanide should be effectively separated from the target material and any impurities, in order to maximize the specific activity of the radionuclide solution, prolong the shelf-life of the pharmaceutical and to ensure safe administration of the radiopharmaceutical to the patients. In addition, new production cycles can be started with the recovered target material. For these reasons, extensive research has been carried out into the selective separation of radiolanthanides.

The similar chemical properties of the lanthanides offer an advantage for radiolabelling strategies but complicate the separation of adjacent lanthanides. Apart from the dominant trivalent state of the lanthanides, there are lanthanides showing divalent and tetravalent oxidation states of some, such as terbium(IV) and europium(II). This difference in oxidation state changes the chemical properties, which could ease the purification of intragroup lanthanides. Therefore, a novel separation method can be developed for the separation of the Gd/Tb and the Sm/Eu couples for the purification of medical terbium-161 and samarium-153. This separation method consists of two steps: (i) electrochemical reduction/oxidation of the lanthanide and (ii) subsequent valence state selective column separation. For this purpose, a detailed parametric study of the electrochemical oxidation

of Tb(III) in aqueous nitrate, carbonate and periodate media was carried out in Chapter 3. It was shown that terbium(III) is most effectively oxidized and stabilized as terbium(IV) in carbonate solutions. The reaction rate in carbonate electrolyte is slow; the maximum conversion requires 9 hours of electrolysis time at a constant potential of +1.3 V vs. Ag/AgCl. In nitrate electrolyte, the formation of terbium(IV) was observed and identified via UV-Vis spectroscopy, however, the stability in this medium was found to be lower. In periodate medium, the lowest applied potential of +0.9 V vs, Ag/AgCl was achieved, but the solubility was the limiting factor. When compared on the basis of solubility, pH, applied potential and most importantly stability, the carbonate medium was found to be the optimal medium to proceed with the separation.

In Chapter 4, the separation of terbium(IV) from gadolinium(III) by extraction chromatography was studied using terbium-161 tracers. After the electrochemical oxidation, the solution was diluted to reach 1 mol.L^{-1} K_2CO_3 and to reduce the pH from 14 to about 12. A successful isolation of terbium(IV) was achieved on a Dowex 1-X8 anion exchange column. The electrolysis yield determined the amount of terbium(IV) recovered as well since quantitative separation of terbium(IV) was possible. The electrolysis yield was calculated to be ≈ 11.2% for 2 hours of electrolysis at a constant potential of +1.3 V vs. Ag/AgCl. Although the electrolysis yield was low, the quantitative separation of Tb(III) and Tb(IV) shows the potential of exploiting electrochemical methods towards lanthanide separation. Furthermore, X-ray absorption spectroscopy was performed on terbium(III) and terbium(IV) complexes in carbonate medium. The L_3 XANES spectra proved the formation of tetravalent terbium while the simulations of the XANES spectra based on the reported structures, suggested that not only carbonate but also hydroxide ions are present in the first shell. In addition to that, there was a difference observed in the coordination environment of these complexes.

The Eu(III)/Eu(II) redox couple has been studied extensively due to the easily achievable reduction potential and relatively stable europium(III) complexes. To increase the shelf-life of samarium-153,

long-lived europium-154 should be eliminated, and therefore an approach similar to Tb can be applied here. For this reason, a detailed kinetic study of the electrochemical reduction of europium(III) was performed in nitrate, chloride and perchlorate electrolytes, as described in Chapter 5. Hydrodynamic analysis was performed using a rotating disk electrode. The reaction rate constants and diffusion coefficients were similar to the literature values that are calculated from polarographic data. The viscosity and concentration of the electrolytes play an important role, which leads to the selection of the electrolytes for the best application. Moreover, the kinetics are, for the first time, determined in chloride and nitrate media and compared with perchlorate medium as a benchmark, marking the way for further improvement.

As a final step, the Sm/Eu separation experiments were conducted using samarium-153 and europium-152 tracers, as discussed in Chapter 6. The electrochemical reduction of europium(III) to europium(II) was carried out in ammonium nitrate and calcium nitrate media prior to the separation. TEVA and DGA resins were used for separation studies, When equal quantities of Eu and Sm were present in a solution, nearly 90 % of Sm was recovered from the TEVA column. The europium(II) complex was sufficiently stable, and 76% of the Eu was recovered . The DGA resin also gave comparable results when ammonium nitrate salt was used as the electrolyte. Finally, reactor irradiation conditions were employed to generate a more representative method for full- scale application. Initial tests revealed that the concentration of europium(II) must be high enough to maintain its stability, indicating that carrier-added methods are required for an efficient separation.

Looking at the objectives of this PhD thesis, it can be concluded that the majority of the goals have been met, although, there is an opportunity for further research. Firstly, the oxidation of terbium was only performed in aqueous solutions, where the electrochemical window is limited, resulting in oxygen evolution at the anode. This might be one of the reasons of limited conversion for the oxidation of Tb(III) to Tb(IV), as well as the electrochemical characterization. Non-

aqueous electrolytes may be an alternative, considering their wider electrochemical window. The efficiency of the electrolysis can be improved by exploring the other electrolytes or electrode materials towards future applications.

The separation of terbium(IV) from gadolinium(III) was achieved by column chromatography. Since the electrolyte solution was a highly concentrated carbonate, finding a compatible separation method was quite challenging. If new electrolytes are explored, a possibility for a higher yield and a more feasible separation might be found. However, the current separation method offers some advantages. Since the second eluent is a carbonate solution, it provides the opportunity to collect terbium(III) at higher carbonate concentrations as well as to regenerate the column. This can lead to a continuation of the electrolysis-column separation cycle and increase the overall yield of the multiple cycle separation, where a proposed process flowsheet is shown in **Figure 4.8**. Due to the short half-life of Tb-161, lengthy electrolysis or separation steps are impractical, necessitating additional optimization of current proposed process.

Changing the oxidation state of one of the lanthanides prior to a separation step proved to be an effective method for Sm/Eu separation as well. In the current study, the reduction was achieved in aqueous nitrate medium and subsequent separation was tested in TEVA and DGA resins. Although the TEVA column has been studied previously, the DGA resin was not tested. Preliminary tests with the DGA column showed promising results. As the DGA resin is known for its affinity towards Ln(III) , the Sm(III) loss occurring with TEVA column in the first fractions can be prevented by using this resin. Therefore, a detailed parametric study was performed to expand the knowledge on this resin for its application in samarium-153 purification. In addition, to check the scalability, the column capacity can be increased by simply using larger column dimensions. To avoid the possible back-oxidation of Eu(II) , the experiments can be performed in an inert gas glovebox rather than maintaining the inert atmosphere by purging. This would eliminate the dissolved oxygen and create a more controlled environment.

In order to investigate the applications of the developed methods, some initial tests were carried out using the mass ratios identical to the ones expected in a dissolved samarium-152 target from the reactor production route for samarium-153. This can be extended by the testing of other resins such as DGA or increasing the column capacity of the TEVA resin. Similar tests can be done for terbium-161 produced via irradiation of a gadolinium-160 target. The current methods usually involved lanthanide concentrations optimized for the electrochemical experiments, whereas in the real-life production of these radionuclides, the mass ratios of these elements are significantly different. Therefore, the scalability should be tested to ensure the applicability of these methods. Although the initial research idea involves the purification towards the medical applications, the evaluation of these methods for other applications can be carried out as well.

Chapter 8.

Health, Safety and Environment (HSE)

The experimental work in this dissertation was carried out in the laboratories of the SCK CEN in Mol (Belgium). As safety, health, and the environment are of the highest priority at SCK CEN, employees are required to comply with strict regulations. These rules cover the standard components of industrial safety and conventional laboratory procedures, as well as unique requirements based on the researcher's specific tasks. To this end, several introduction sessions and training courses were followed during the first year of the PhD, and repeated as necessary in subsequent years. A five-day radiation protection course, a fume hood and glove box course and training on working with radioactivity was followed throughout the PhD study

All experimental work carried out for the thesis work required the use of hazardous chemicals and/or radioactive substances. All sample manipulations were performed in a fume hood while wearing personal protective equipment (safety goggles, nitrile gloves, lab coat). When working in the controlled area, additional requirements were met such as the use of dedicated labcoats and goggles, safety shoes, and the use of dosimeters, two types of dosimeters should be used in the controlled area; an optically stimulated luminescence (OSL) dosimeter (InLight® body dosimeter) where the reading is done every month, and an electronic personal dosimeter (EPD), where a summary of the radiation exposure is given at the end of the laboratory activity on the same day. In addition, EPD gives an alarm if the dose rate and/or accumulated dose is higher than a preset value. In addition, a whole-body-count and lung measurements as well as medical check including blood and urine tests were done regularly to monitor any possible accumulation of radionuclides and/or damage due to radiation or hazardous substances.

A risk assessment form was required to evaluate the experimental setup, chemicals, and waste disposal before an experiment was carried out. In this form, the experiments were summarized in detail, taking into account all the possible risks and related preventive actions, which is then run through an approval process. Work involving the manipulation of radioactive materials is subject to the *as low as reasonably achievable* (ALARA) principle, to limit the accumulated dose to the workers. For this reason, it is essential to minimize the amount of the time spent in the vicinity of the source, to provide a good shielding and to plan the manipulations in detail in advance is crucial. In this research, an extensive study was done using stable lanthanide salts prior to the experiments with radiolanthanides. Only after the procedures were optimized in a normal chemical laboratory, were tests using radiotracers performed in the controlled area. Finally, for some manipulations in the controlled area required the transfer of the sources or samples to other laboratories in the controlled area. For such transfers, the radioactive source must be checked by the radiation protection officer to ensure that there is no contamination. To ensure that during the experimental work there is no contamination, when leaving the controlled area, measurement of α- and β^-- rays are done via hand-foot monitors.

Appendices

Supplementary information for Chapter 3

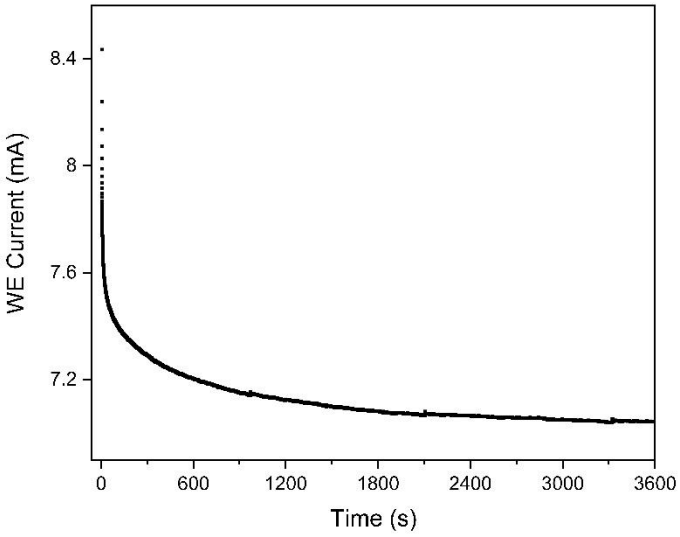

Figure A.3.1. Current response graph of electrolysis of 0.1 mol.L^{-1} terbium(III) and 5.5 mol.L^{-1} potassium carbonate at pH = 14. The applied potential was +1.3 V vs. Ag/AgCl.

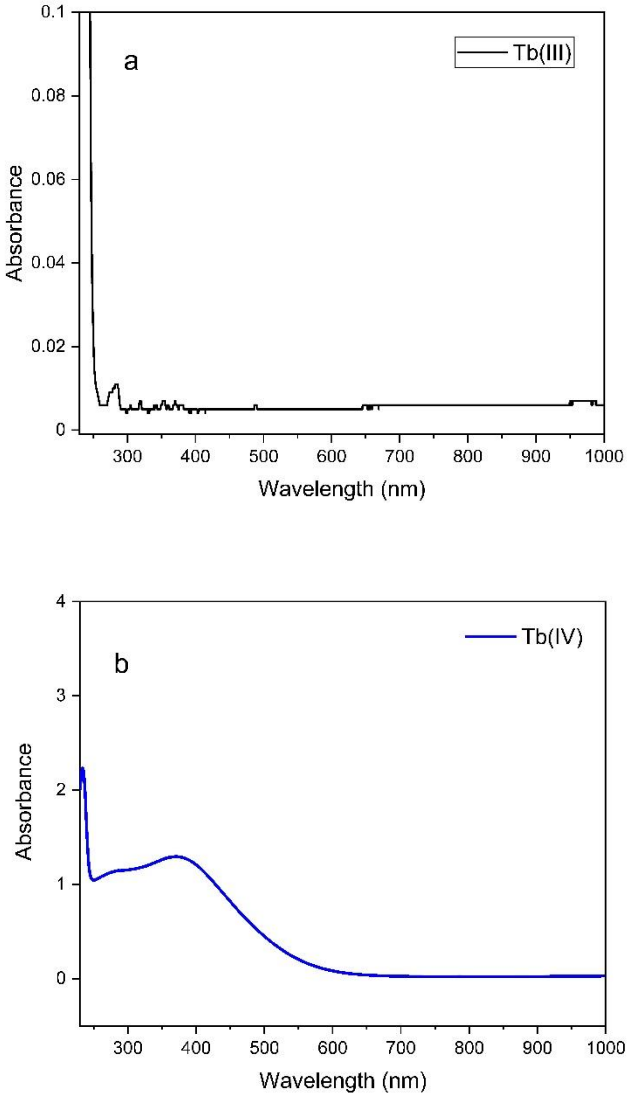

Figure A.3.2. (a) UV-Vis absorption spectra of 0.1 mol.L^{-1} Tb(III) in 5.5 mol.L^{-1} K_2CO_3 solution at pH=14. **(b)** UV-Vis absorption spectra of 0.1 mol.L^{-1} Tb(III) in 5.5 mol.L^{-1} K_2CO_3 solution at pH=14 after 2h of electrolysis at +1.3 V vs. Ag/AgCl. Blank solution without terbium was used as reference sample for baseline correction. A path length of 10 mm was used. Tb(IV) solution was 10-fold diluted for UV-Vis absorption measurement.

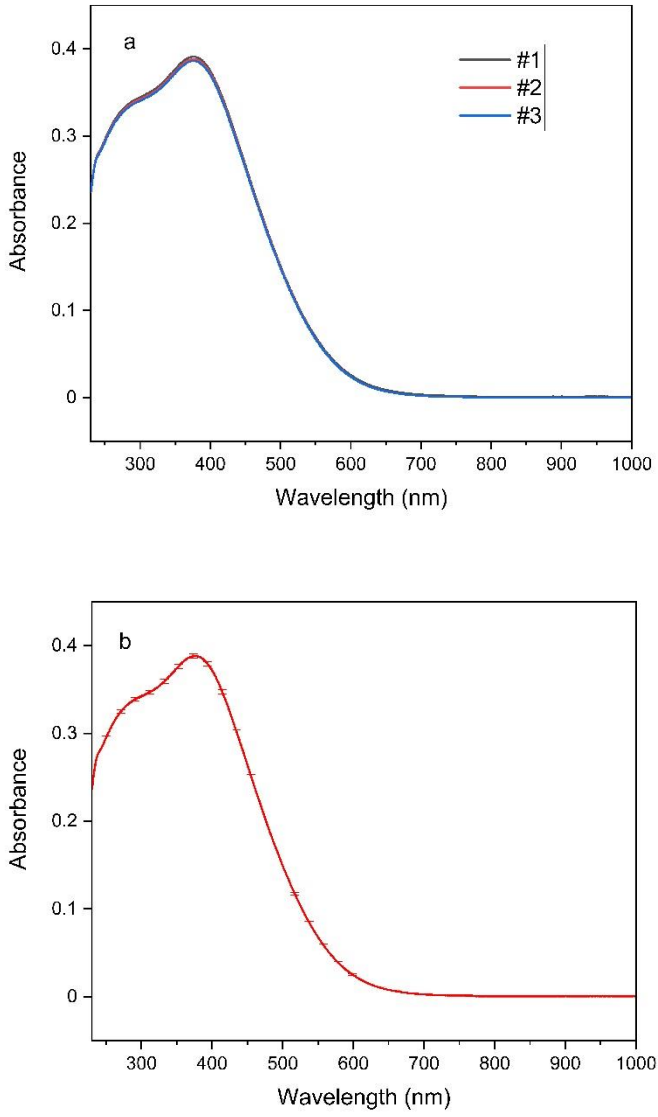

Figure A.3.3. (a) Three consecutive (#1,2 and 3) recorded UV-Vis absorption spectra of 0.07 mol.L^{-1} Tb(III) in 4 mol.L^{-1} K_2CO_3 solution at pH=14 (2h electrolysis time). Blank solution without terbium was used as reference sample for baseline correction. A path length of 0.1 mm was used. **(b)** The average of these spectra with standard deviation included. The absorbance is calculated 0.3833 ± 0.0025 at 365 nm.

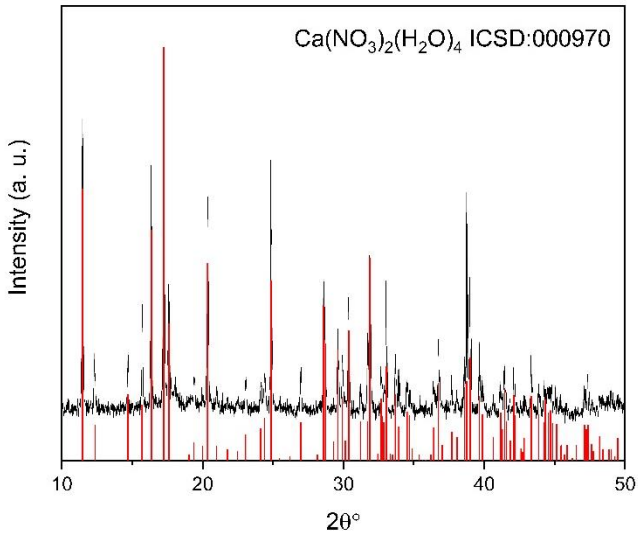

Figure A.3.4. X-Ray Diffractogram of precipitation collected in nitrate media, after a 0.01 mol.L^{-1} Tb(III) in 3 mol.L^{-1} $Ca(NO_3)_2$ solution was electrolyzed for 2 hours. The main phase is $Ca(NO_3)_2{\cdot}4H_2O$.

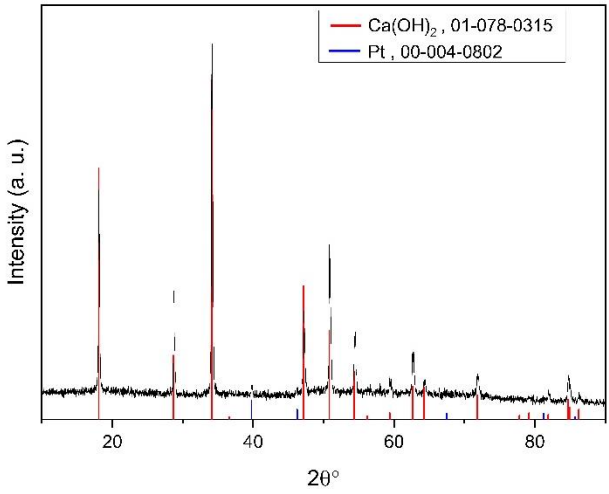

Figure A.3.5. X-Ray Diffractogram of the deposition collected on Pt-wire counter electrode in nitrate solution (0.01 mol.L^{-1} Tb(III) in 3 mol.L^{-1} $Ca(NO_3)_2$) electrolysed for 2 hours. The main phase is $Ca(OH)_2$. The Pt diffraction peaks are due to the substrate.

Supplementary information for Chapter 4

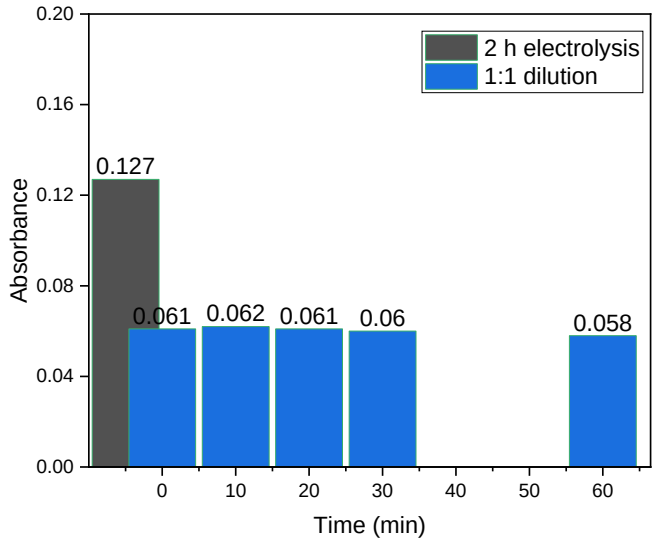

Figure A.4.1. UV-Vis absorbance at the wavelength of 365 nm, after 1:1 (v:v) dilution of Tb(IV) at 10, 20, 30 and 60 min after the dilution.

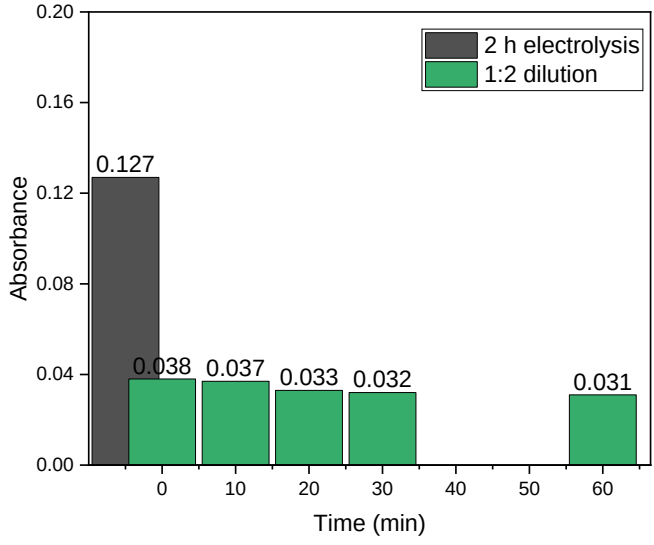

Figure A.4.2. UV-Vis absorbance at the wavelength of 365 nm, after 1:2 (v:v) dilution of Tb(IV) at 10, 20, 30 and 60 min after the dilution.

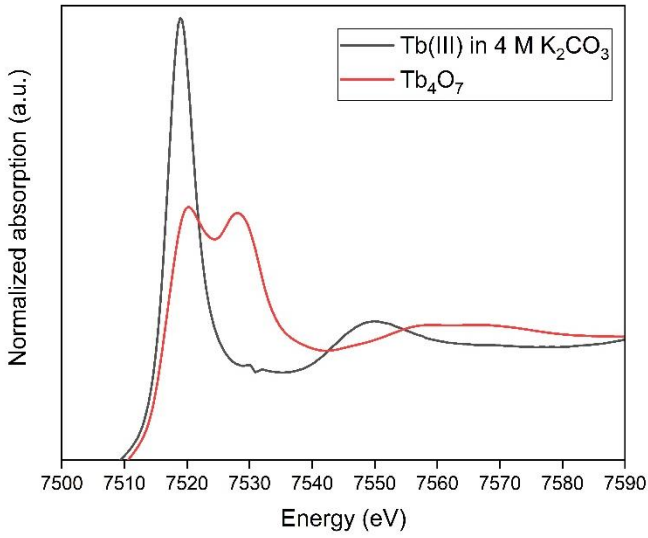

Figure A.4.3. XANES spectra of references Tb_4O_7 for Tb(IV), and Tb(III) in 4 mol.L^{-1} K_2CO_3 before electrolysis.

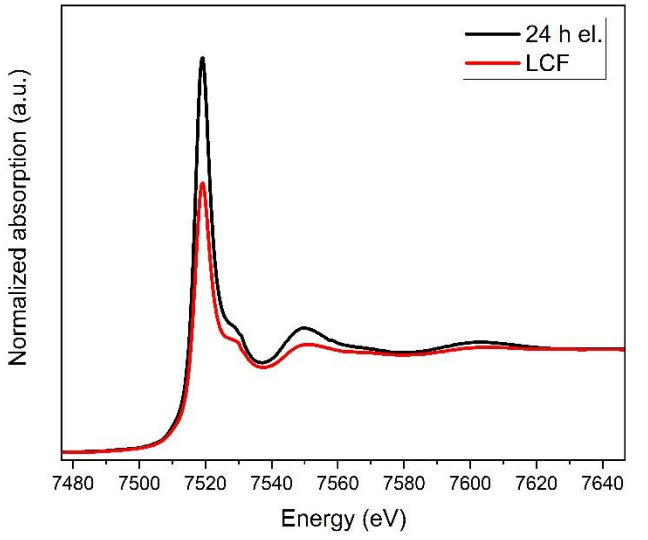

Figure A.4.4. Linear combination fitting using Tb_4O_7 and Tb(III) in carbonate as reference.

Supplementary information for Chapter 5

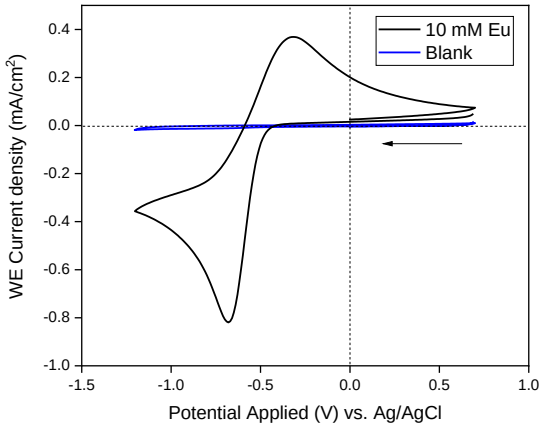

Figure A.5.1. Cyclic voltammogram recorded at 100 mV/s scan rate in 1 mol.L^{-1} $NaClO_4$, blank measurement without europium(III), and with 10 mmol.L^{-1} europium(III) added.

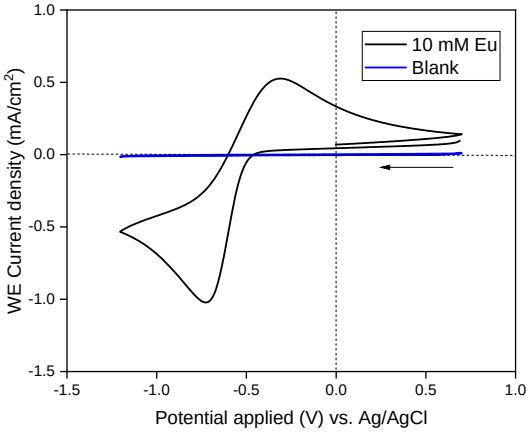

Figure A.5.2. Cyclic voltammogram recorded at 100 mV/s scan rate in 0.1 mol.L^{-1} $CaCl_2$, blank measurement without europium(III), and with 10 mmol.L^{-1} europium(III) added.

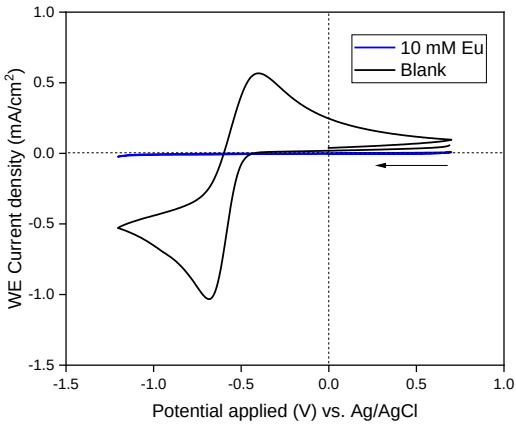

Figure A.5.3. Cyclic voltammogram recorded at 100 mV/s scan rate in 0.1 mol.L^{-1} $Ca(NO_3)_2$, blank measurement without europium(III), and with 10 mmol.L^{-1} europium(III) added.

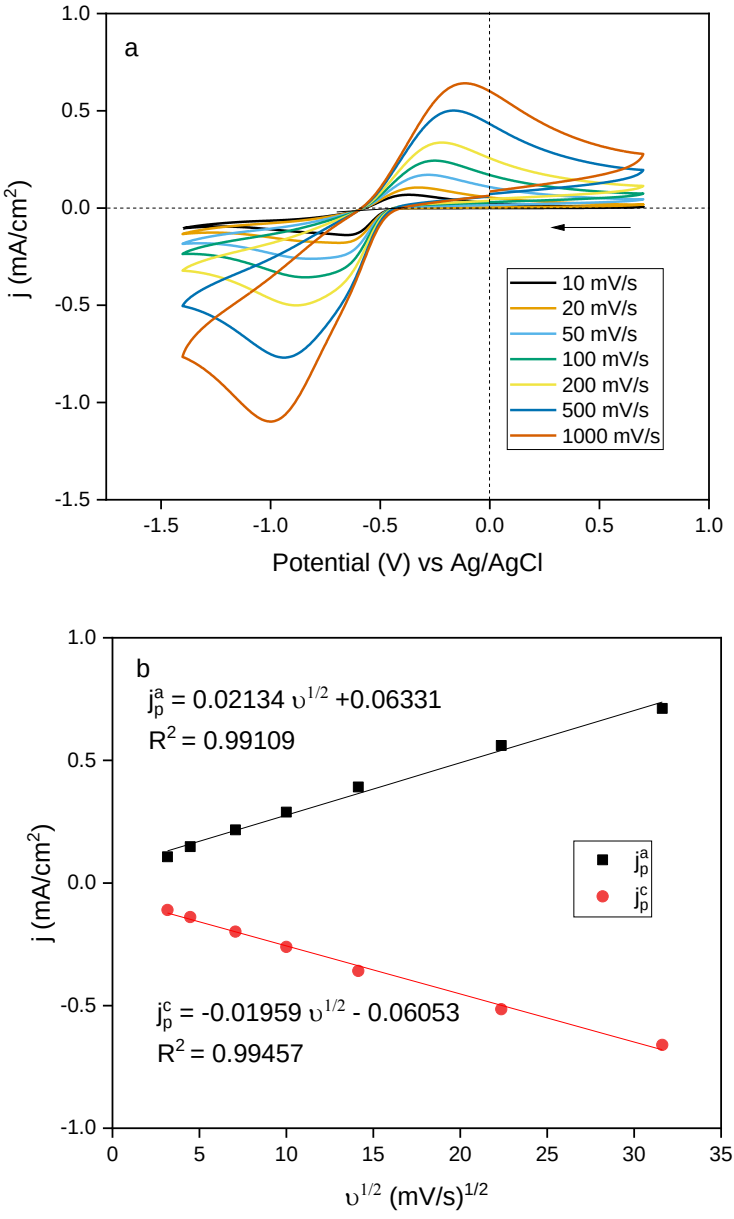

Figure A.5.4. a) Cyclic voltammograms (second cycles) of 10 mmol.L^{-1} Eu(III) in 3 mol.L^{-1} $CaCl_2$ at various scan rates b) Anodic and cathodic peak densities with respect to the square root at these scan rates.

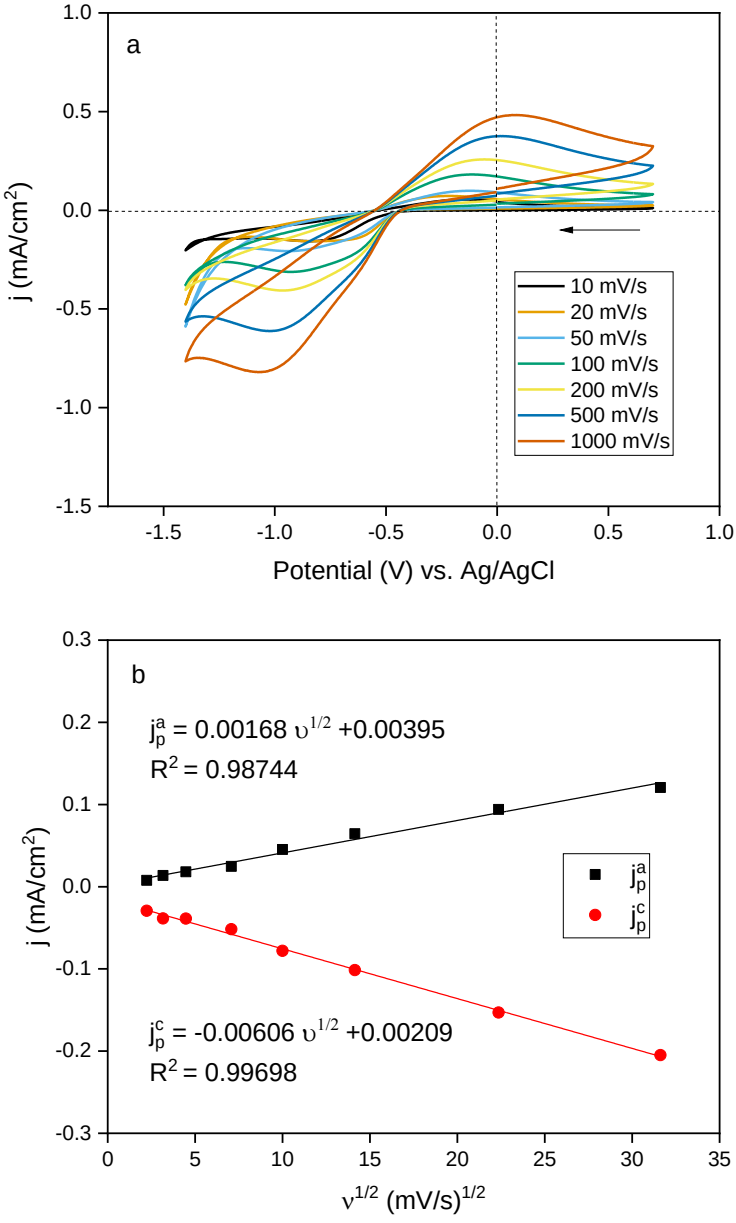

Figure A.5.5. a) Cyclic voltammograms (second cycles) of 10 mmol.L^{-1} Eu(III) in 3 mol.L^{-1} $Ca(NO_3)_2$ at various scan rates b) Anodic and cathodic peak densities with respect to the square root at these scan rates.

Scientific output

Peer reviewed journal articles

Arman, M.O., Geboes, B., Van Hecke, K. et al. Electrochemical oxidation of terbium(III) in aqueous media: influence of supporting electrolyte on oxidation potential and stability. *J Appl Electrochem* **52**, 583–593 (2022). https://doi.org/10.1007/s10800-021-01651-0

Conference contributions

7th International Symposium on Medical Radioisotopes (ISMERAD 7), Liège (Belgium), 09/05/2019.

Poster presentation: Electrochemical oxidation of terbium – the future of high purity Tb-161 for medical applications

European Nuclear Young Generation Forum (ENYGF19), Ghent (Belgium), 23-27 June 2019.

Oral presentation: Investigation of the redox chemistry of terbium in aqueous media using electrochemistry

71st Annual Meeting of the International Society of Electrochemistry (Online), 2-4 September 2020.

Oral presentation: Electrolyte influence on the electrochemical oxidation of terbium and its stabilization in aqueous media

19th Radiochemical Conference - RadChem 2022, Marianske Lazne (Czech Republic), 15-20 May 2022.

Oral presentation: Electrochemical oxidation of terbium(III) in aqueous media towards purification of medical Tb-161

References

(1) World Health Organization. *Assessing National Capacity for the Prevention and Control of Noncommunicable Diseases: Report of the 2019 Global Survey*; 2020.

(2) Euratom Supply Agency. *Supply of medical radioisotopes*. https://euratom-supply.ec.europa.eu/activities/supply-medical-radioisotopes_en (accessed 2023-02-20).

(3) Miller, K. D.; Nogueira, L.; Devasia, T.; Mariotto, A.; Yabroff, K.; Jemal, A.; Kramer, J.; Siegel, R. Cancer Treatment and Survivorship Statistics, 2022. *CA Cancer J Clin* **2022**, *72* (5), 409–436. https://doi.org/10.3322/caac.21731.

(4) World Nuclear Association. *Radioisotopes in Medicine*. https://world-nuclear.org/information-library/non-power-nuclear-applications/radioisotopes-research/radioisotopes-in-medicine.aspx (accessed 2023-02-05).

(5) Kostelnik, T. I.; Orvig, C. Radioactive Main Group and Rare Earth Metals for Imaging and Therapy. *Chem Rev* **2019**, *119* (2), 902–956. https://doi.org/10.1021/acs.chemrev.8B00294.

(6) Elisa Crestoni, M. Radiopharmaceuticals for Diagnosis and Therapy. In *Reference Module in Chemistry, Molecular Sciences and Chemical Engineering*; Elsevier Inc., 2018; pp 1–12. https://doi.org/10.1016/b978-0-12-409547-2.14205-2.

(7) Davison, N.; Quirk, J. A.; Wills, C.; Dixon, C.; Waddell, P. G.; Dawson, J. A.; Lu, E. Elucidating Solution-State Coordination Modes of Multidentate Neutral Amine Ligands with Group-1 Metal Cations: Variable-Temperature NMR Studies. *Inorg Chem* **2022**, *61* (38), 15204–15212. https://doi.org/10.1021/acs.inorgchem.2c02457

(8) Wangler, B.; Schirrmacher, R.; Bartenstein, P.; Wangler, C. Chelating Agents and Their Use in Radiopharmaceutical Sciences. *Mini-Reviews in Medicinal Chemistry* **2011**, *11* (11), 968–983. https://doi.org/10.2174/138955711797068445.

(9) Price, E. W.; Orvig, C. Matching Chelators to Radiometals for Radiopharmaceuticals. *Chem Soc Rev* **2014**, *43* (1), 260–290. https://doi.org/10.1039/C3CS60304K.

(10) Mishiro, K.; Hanaoka, H.; Yamaguchi, A.; Ogawa, K. Radiotheranostics with Radiolanthanides: Design, Development Strategies, and Medical Applications. *Coord Chem Rev* **2019**, *383*, 104–131. https://doi.org/10.1016/j.ccr.2018.12.005.

(11) Rigby, A.; Blower, J. E.; Blower, P. J.; Terry, S. Y. A.; Abbate, V. Targeted Auger Electron-Emitter Therapy: Radiochemical Approaches for Thallium-201 Radiopharmaceuticals. *Nucl Med Biol* **2021**, *98–99*, 1–7. https://doi.org/10.1016/j.nucmedbio.2021.03.012.

(12) Guidoccio, F.; Mazzarri, S.; Orsini, F.; Erba, P. A.; Mariani, G. Reactor-Produced Therapeutic Nuclides. In *Nuclear Oncology: From Pathophysiology to Clinical Applications*; 2017; pp 173–198. https://doi.org/10.1007/978-3-319-26236-9_36.

(13) Barca, C.; Griessinger, C. M.; Faust, A.; Depke, D.; Essler, M.; Windhorst, A. D.; Devoogdt, N.; Brindle, K. M.; Schäfers, M.; Zinnhardt, B.; Jacobs, A. H. Expanding Theranostic Radiopharmaceuticals for Tumor Diagnosis and Therapy. *Pharmaceuticals* **2022**, *15* (13). https://doi.org/10.3390/ph15010013.

(14) Kilbourn, M. R.; Scott, P. J. H. *Handbook of Radiopharmaceuticals: Methodology and Applications*, Second edi.; John Wiley & Sons, Ltd, 2021. https://doi.org/10.1002/9781119500575.

(15) Cutler, C. S.; Hennkens, H. M.; Sisay, N.; Huclier-Markai, S.; Jurisson, S. S. Radiometals for Combined Imaging and Therapy. *Chem Rev* **2013**, *113* (2), 858–883. https://doi.org/10.1021/cr3003104.

(16) Van de Voorde, M.; Van Hecke, K.; Cardinaels, T.; Binnemans, K. Radiochemical Processing of Nuclear-Reactor-Produced Radiolanthanides for Medical Applications. *Coord Chem Rev* **2019**, *382*, 103–125. https://doi.org/10.1016/j.ccr.2018.11.007.

(17) Holman, B. L.; Tumeh, S. S. Single-Photon Emission Computed Tomography (SPECT): Applications and Potential. *The Journal of the American Medical Association* **1990**, *263* (4), 561–564. https://doi.org/10.1001/jama.1990.03440040100036.

(18) Pimlott, S. L.; Sutherland, A. Molecular Tracers for the PET and SPECT Imaging of Disease. *Chem Soc Rev* **2011**, *40* (1), 149–162. https://doi.org/10.1039/b922628c.

(19) Ametamey, S. M.; Honer, M.; Schubiger, P. A. Molecular Imaging with PET. *Chem Rev* **2008**, *108* (5), 1501–1516. https://doi.org/10.1021/cr0782426.

(20) Qaim, S. M.; Spahn, I. Development of Novel Radionuclides for Medical Applications. *J Labelled Comp Radiopharm* **2017**, *61* (3), 126–140. https://doi.org/10.1002/jlcr.3578.

(21) Türler, A. Matched Pair Theranostics. *Chimia (Aarau)* **2019**, *73* (11), 947–949. https://doi.org/10.2533/chimia.2019.947.

(22) Sadler, A. W. E.; Hogan, L.; Fraser, B.; Rendina, L. M. Cutting Edge Rare Earth Radiometals: Prospects for Cancer Theranostics. *EJNMMI Radiopharm Chem* **2022**, *7* (21). https://doi.org/10.1186/S41181-022-00173-0.

(23) Hertz, B. Dr. Saul Hertz (1905–1950) Discovers the Medical Uses of Radioactive Iodine: The First Targeted Cancer Therapy. In *Thyroid Cancer - Advances in Diagnosis and Therapy*; IntechOpen, 2016. https://doi.org/10.5772/64609.

(24) Yordanova, A.; Eppard, E.; Kürpig, S.; Bundschuh, R. A.; Schönberger, S.; Gonzalez-Carmona, M.; Feldmann, G.; Ahmadzadehfar, H.; Essler, M. Theranostics in Nuclear Medicine Practice. *Onco Targets Ther* **2017**, *10*, 4821–4828. https://doi.org/10.2147/OTT.S140671.

(25) Qaim, S. M.; Scholten, B.; Neumaier, B. New Developments in the Production of Theranostic Pairs of Radionuclides. *J Radioanal Nucl Chem* **2018**, *318*, 1493–1508. https://doi.org/10.1007/s10967-018-6238-x.

(26) Rösch, F. Radiolanthanides in Endoradiotherapy: An Overview. *Radiochim Acta* **2007**, *95* (6), 303–311. https://doi.org/10.1524/ract.2007.95.6.303.

(27) Teo, R. D.; Termini, J.; Gray, H. B. Lanthanides: Applications in Cancer Diagnosis and Therapy. *J Med Chem* **2016**, *59* (13), 6012–6024. https://doi.org/10.1021/acs.jmedchem.5b01975.

(28) Talip, Z.; Favaretto, C.; Geistlich, S.; Van Der Meulen, N. P. A Step-by-Step Guide for the Novel Radiometal Production for Medical Applications: Case Studies with ^{68}Ga, ^{44}Sc, ^{177}Lu and ^{161}Tb. *Molecules* **2020**, *25* (4). https://doi.org/10.3390/molecules25040966.

(29) Banerjee, S.; Pillai, M. R. A.; Knapp, F. F. Lutetium-177 Therapeutic Radiopharmaceuticals: Linking Chemistry, Radiochemistry, and Practical Applications. *Chem Rev* **2015**, *115* (8), 2934–2974. https://doi.org/10.1021/cr500171e.

(30) Hennrich, U.; Eder, M. [^{177}Lu]Lu-PSMA-617 (Pluvicto^{TM}): The First FDA-Approved Radiotherapeutical for Treatment of Prostate Cancer. *Pharmaceuticals* **2022**, *15* (1292). https://doi.org/10.3390/ph15101292.

(31) U.S. Food and Drug Administration. *FDA approves lutetium Lu 177 dotatate for treatment of GEP-NETS*. https://www.fda.gov/drugs/resources-information-approved-drugs/fda-approves-lutetium-lu-177-dotatate-treatment-gep-nets.

(32) U.S. Food and Drug Administration. *Quadramet® prescribing information*. https://www.accessdata.fda.gov/drugsatfda_docs/label/2017/020570s008lbl.pdf.

(33) Naskar, N.; Lahiri, S. Theranostic Terbium Radioisotopes: Challenges in Production for Clinical Application. *Front Med (Lausanne)* **2021**, *8*, 675014. https://doi.org/10.3389/fmed.2021.675014.

(34) Starovoitova, V. N.; Tchelidze, L.; Wells, D. P. Production of Medical Radioisotopes with Linear Accelerators. *Applied radiation and isotopes* **2014**, *85*, 39–44. https://doi.org/10.1016/j.apradiso.2013.11.122.

(35) Ma, D.; Ketring, A. R.; Ehrhardt, G. J.; Jia, W. Production of Radiolanthanides and Radiotherapy Research at MURR. *J Radioanal Nucl Chem* **1996**, *206* (1), 119–126. https://doi.org/10.1007/BF02040048.

(36) Beyer, G. J.; Čomor, J. J.; Daković, M.; Soloviev, D.; Tamburella, C.; Hagebø, E.; Allan, B.; Dmitriev, S. N.; Zaitseva, N. G.; Starodub, G. Y.; Molokanova, L. G.; Vranješ, S.; Miederer, M. Production Routes of the Alpha Emitting ^{149}Tb for Medical Application. *Radiochim Acta* **2002**, *90* (5), 247–252. https://doi.org/10.1524/ract.2002.90.5_2002.247.

(37) Currie, G.; Wheat, J.; Davidson, R.; Kiat, H. Radionuclide Production. *Radiographer* **2011**, *58* (3), 46–52. https://doi.org/10.1002/j.2051-3909.2011.tb00155.x.

(38) Srivastava, S. C.; Mausner, L. F. Therapeutic Radionuclides: Production, Physical Characteristics, and Applications. In *Therapeutic Nuclear Medicine*; Baum, R. P., Ed.; Springer Berlin, Heidelberg, 2013; pp 11–50. https://doi.org/10.1007/174_2012_782.

(39) Müller, C.; Zhernosekov, K.; Köster, U.; Johnston, K.; Dorrer, H.; Hohn, A.; van der Walt, N. T.; Türler, A.; Schibli, R. A Unique Matched Quadruplet of Terbium Radioisotopes for PET and SPECT and for α- and β^--Radionuclide Therapy: An in Vivo Proof-of-Concept Study with a New Receptor-Targeted Folate Derivative. *Journal of Nuclear Medicine* **2012**, *53* (12), 1951–1959. https://doi.org/10.2967/jnumed.112.107540.

(40) CERN Courier. *Terbium: a new 'Swiss army knife' for nuclear medicine*. https://cerncourier.com/a/terbium-a-new-swiss-army-knife-for-nuclear-medicine/ (accessed 2020-03-16).

(41) Grünberg, J.; Lindenblatt, D.; Dorrer, H.; Cohrs, S.; Zhernosekov, K.; Köster, U.; Türler, A.; Fischer, E.; Schibli, R. Anti-L1CAM Radioimmunotherapy Is More Effective with the Radiolanthanide Terbium-161 Compared to Lutetium-177 in an Ovarian Cancer Model. *Eur J Nucl Med Mol Imaging* **2014**, *41* (10), 1907–1915. https://doi.org/10.1007/s00259-014-2798-3.

(42) Müller, C.; Reber, J.; Haller, S.; Dorrer, H.; Bernhardt, P.; Zhernosekov, K.; Türler, A.; Schibli, R. Direct in Vitro and in Vivo Comparison of ^{161}Tb and ^{177}Lu Using a Tumour-Targeting Folate Conjugate. *Eur J Nucl Med Mol Imaging* **2014**, *41* (3), 476–485. https://doi.org/10.1007/s00259-013-2563-z.

(43) Rosar F, Maus S, Schaefer-Schuler A, Burgard C, Khreish F, E. S. New Horizons in Radioligand Therapy: ^{161}Tb-PSMA-617 in Advanced MCRPC. *Clin Nucl Med* **2023**, *48* (5), 433–434. https://doi.org/10.1097/RLU.0000000000004589.

(44) Al-Ibraheem, A.; Scott, A. M. ^{161}Tb-PSMA Unleashed: A Promising New Player in the Theranostics of Prostate Cancer. *Nucl Med Mol Imaging* **2023**, *57*, 168–171. https://doi.org/10.1007/s13139-023-00804-7.

(45) Baum, R. P.; Singh, A.; Kulkarni, H. R.; Bernhardt, P.; Rydén, T.; Schuchardt, C.; Gracheva, N.; Grundler, P. V; Köster, U.; Müller, D.; Pröhl, M.; Zeevaart, J. R.; Schibli, R.; Van Der Meulen, N. P.; Müller, C. First-in-Human Application of ^{161}Tb: A Feasibility Study Using ^{161}Tb-DOTATOC. *Journal of Nuclear Medicine* **2021**, *62* (10), 1391–1397. https://doi.org/10.2967/jnumed.120.258376.

(46) Lehenberger, S. M. Evaluation and Application of the Low Energy Electron Emitter ^{161}Tb, Technical University of Munich, 2010.

(47) Das, T.; Pillai, M. R. A. Options to Meet the Future Global Demand of Radionuclides for Radionuclide Therapy. *Nucl Med Biol* **2013**, *40* (1), 23–32. https://doi.org/10.1016/j.nucmedbio.2012.09.007.

(48) Nayak, D.; Lahiri, S. Application of Radioisotopes in the Field of Nuclear Medicine: I. Lanthanide Series Elements. *J Radioanal Nucl Chem* **1999**, *242* (2), 423–432. https://doi.org/10.1007/BF02345573.

(49) Vermeulen, K.; Van De Voorde, M.; Segers, C.; Coolkens, A.; Rodriguez Pérez, S.; Daems, N.; Duchemin, C.; Crabbé, M.; Opsomer, T.; Vargas, C. S.; Heinke, R.; Lambert, L.; Bernerd, C.; Burgoyne, A. R.; Cocolios, T. E.; Stora, T.; Ooms, M. Exploring the Potential of High-Molar-Activity Samarium-153 for Targeted Radionuclide Therapy with [^{153}Sm]Sm-DOTA-TATE. *Pharmaceutics* **2022**, *14* (2566). https://doi.org/10.3390/pharmaceutics14122566.

(50) Bayouth, J. E.; Macey, D. J.; Kasi, L. P.; V., F. F. *Dosimetry and toxicity of samarium-153-EDTMP administered for bone pain due to skeletal metastases*. Journal of Nuclear Medicine. https://pubmed.ncbi.nlm.nih.gov/7505819/ (accessed 2023-04-18).

(51) Simón, J.; Frank, R. K.; Crump, D. K.; Erwin, W. D.; Ueno, N. T.; Wendt, R. E. A Preclinical Investigation of the Saturation and Dosimetry of ^{153}Sm-DOTMP as a Bone-Seeking Radiopharmaceutical. *Nucl Med Biol* **2012**, *39* (6), 770–776. https://doi.org/10.1016/j.nucmedbio.2011.12.015.

(52) Sgouros, G.; Bodei, L.; McDevitt, M. R.; Nedrow, J. R. Radiopharmaceutical Therapy in Cancer: Clinical Advances and Challenges. *Nat Rev Drug Discov* **2020**, *19* (9), 589–608. https://doi.org/10.1038/S41573-020-0073-9.

(53) Kalef-Ezra, J. A.; Valakis, S. T.; Pallada, S. Samarium-153 EDTMP for Metastatic Bone Pain Palliation: The Impact of Europium Impurities. *Phys Med* **2015**, *31* (1), 104–107. https://doi.org/10.1016/j.ejmp.2014.10.078.

(54) Van de Voorde, M.; Duchemin, C.; Heinke, R.; Lambert, L.; Chevallay, E.; Schneider, T.; Van Stenis, M.; Cocolios, T. E.; Cardinaels, T.; Ponsard, B.; Ooms, M.; Stora, T.; Burgoyne, A. R. Production of Sm-153 with Very High Specific Activity for Targeted Radionuclide Therapy. *Front Med (Lausanne)* **2021**, *8*. https://doi.org/10.3389/fmed.2021.675221.

(55) Naseri, F.; Charkhi, A.; Salek, N.; Vosoughi, S. The Radio-Europium Impurities in [153Sm]-Edtmp Production: A Review of Isolation Methods. *Nucl Med Commun* **2021**, *42* (9), 951–963. https://doi.org/10.1097/mnm.0000000000001419.

(56) Gupta, B.; Malik, P.; Deep, A. Solvent Extraction and Separation of Tervalent Lanthanides and Yttrium Using Cyanex 923. *Solvent Extraction and Ion Exchange* **2007**, *21* (2), 239–258. https://doi.org/10.1081/SEI-120018948.

(57) Jensen, M. P.; Chiarizia, R.; Ulicki, J. S.; Spindler, B. D.; Murphy, D. J.; Hossain, M. M.; Roca-Sabio, A.; de Blas, A.; Rodríguez-Blas, T. Solvent Extraction Separation of Trivalent Americium from Curium and the Lanthanides. *Solvent Extraction and Ion Exchange* **2015**, *33* (4), 329–345. https://doi.org/10.1080/07366299.2015.1046292.

(58) Li, Z.; Binnemans, K. Hydration Counteracts the Separation of Lanthanides by Solvent Extraction. *AIChE Journal* **2020**, *66* (e16545). https://doi.org/10.1002/aic.16545.

(59) Shimojo, K.; Aoyagi, N.; Saito, T.; Okamura, H.; Kubota, F.; Goto, M.; Naganawa, H. Highly Efficient Extraction Separation of Lanthanides Using a Diglycolamic Acid Extractant. *Analytical Sciences* **2014**, *30* (2), 263–269. https://doi.org/10.2116/analsci.30.263.

(60) Atanassova, M. Synergistic Solvent Extraction and Separation of Lanthanide(III) Ions with 4-benzoyl-3-phenyl-5-isoxazolone and the Quaternary Ammonium Salt. *Solvent Extraction and Ion Exchange* **2009**, *27* (2), 159–171. https://doi.org/10.1080/07366290802674655.

(61) Atanassova, M. Effect of the 18-Crown-6 and Benzo-18-Crown-6 on the Solvent Extraction and Separation of Lanthanide(III) Ions with 8-Hydroxyquinoline. *Russian Journal of Inorganic Chemistry* **2007**, *52* (8), 1304–1311. https://doi.org/10.1134/S0036023607080244.

(62) Sivaraman, N.; Kumar, R.; Subramaniam, S.; Vasudeva Rao, P. R. Separation of Lanthanides Using Ion-Interaction Chromatography with HDEHP Coated Columns. *J Radioanal Nucl Chem* **2002**, *252* (3), 491–495. https://doi.org/10.1023/A:1015894418606.

(63) Roosen, J.; Binnemans, K. Adsorption and Chromatographic Separation of Rare Earths with EDTA- and DTPA-Functionalized Chitosan Biopolymers. *J Mater Chem A Mater* **2013**, *2* (5), 1530–1540. https://doi.org/10.1039/c3Ta14622g.

(64) Raut, N. M.; Jaison, P. G.; Aggarwal, S. K. Comparative Evaluation of Three α-Hydroxycarboxylic Acids for the Separation of Lanthanides by Dynamically Modified Reversed-Phase High-Performance Liquid Chromatography. *J Chromatogr A* **2002**, *959* (1–2), 163–172. https://doi.org/10.1016/s0021-9673(02)00447-8.

(65) Zu, J.; Pan, X.; Han, G.; Xue, Y.; Diao, J.; Liu, S. Selective Adsorption of ^{99}Tc and Recovery of Lanthanides at Different Acidity by PS-TMMA Resin with Double Functional Groups. *J Radioanal Nucl Chem* **2023**, *332* (2), 399–407. https://doi.org/10.1007/S10967-022-08754-8.

(66) Karol, P. J. Rare Earth Separations Using Cation-Exchange Column Chromatography : Comparison of -Hydroxyisobutyric Acid and -Hydroxy Methylbutyric Acid as Eluants. *J Chromatogr A* **1973**, *79*, 287–291. https://doi.org/10.1016/S0021-9673(01)85299-7.

(67) Lie, J.; Liu, J. C. Selective Separation of Lanthanide Group in Spent NiMH Battery Acidic Leaching Solutions. *Sep Purif Technol* **2023**, *307*. https://doi.org/10.1016/j.seppur.2022.122671.

(68) Zhao, X.; Wong, M.; Mao, C.; Trieu, T. X.; Zhang, J.; Feng, P.; Bu, X. Size-Selective Crystallization of Homochiral Camphorate Metal− Organic Frameworks for Lanthanide Separation. *J Am Chem Soc* **2014**, *136*, 56. https://doi.org/10.1021/ja5067306.

(69) Lu, H.; Guo, X.; Wang, Y.; Diefenbach, K.; Chen, L.; Wang, J. Q.; Lin, J.; Wang, S. Size-Dependent Selective Crystallization Using an Inorganic Mixed-Oxoanion System for Lanthanide Separation. *Dalton Transactions* **2019**, *48* (34), 12808–12811. https://doi.org/10.1039/c9dt02387a.

(70) Yang, H.; Peng, F.; Schier, D. E.; Markotic, S. A.; Zhao, X.; Hong, A. N.; Wang, Y.; Feng, P.; Bu, X. Selective Crystallization of Rare-Earth Ions into Cationic Metal-Organic Frameworks for Rare-Earth Separation. *Angewandte Chemie International Edition* **2021**, *60* (20), 11148–11152. https://doi.org/10.1002/anie.202017042.

(71) Luo, H. M.; Boll, R. A.; Bell, J. R.; Dai, S. Facile Solvent Extraction Separation of Th-227 and Ac-225 Based on Room-Temperature Ionic Liquids. *Radiochim Acta* **2012**, *100* (10), 771–777. https://doi.org/10.1524/ract.2012.1950.

(72) Gujar, R. B.; Ansari, S. A.; Murali, • M S; Mohapatra, • P K; Manchanda, V. K. Comparative Evaluation of Two Substituted Diglycolamide Extractants for "Actinide Partitioning." https://doi.org/10.1007/s10967-010-0467-y.

(73) Narasimhan, D. V. S.; Mani, R. S. Chemical and Radiochemical Evaluation of the Purity Of99mTc Extracted by MEK. *Journal of Radioanalytical Chemistry* **1976**, *33* (1), 81–100. https://doi.org/10.1007/BF02519685.

(74) Martini, P.; Boschi, A.; Cicoria, G.; Zagni, F.; Corazza, A.; Uccelli, L.; Pasquali, M.; Pupillo, G.; Marengo, M.; Loriggiola, M.; Skliarova, H.; Mou, L.; Cisternino, S.; Carturan, S.; Melendez-Alafort, L.; Uzunov, N. M.; Bello, M.; Alvarez, C. R.; Esposito, J.; Duatti, A. In-House Cyclotron Production of High-Purity Tc-99m and Tc-99m Radiopharmaceuticals. *Applied Radiation and Isotopes* **2018**, *139*, 325–331. https://doi.org/10.1016/j.apradiso.2018.05.033.

(75) Uzunov, N. M.; Melendez-Alafort, L.; Bello, M.; Cicoria, G.; Zagni, F.; De Nardo, L.; Selva, A.; Mou, L.; Rossi-Alvarez, C.; Pupillo, G.; Di Domenico, G.; Uccelli, L.; Boschi, A.; Groppi, F.; Salvini, A.; Taibi, A.; Duatti, A.; Martini, P.; Pasquali, M.; Loriggiola, M.; Marengo, M.; Strada, L.; Manenti, S.; Rosato, A.; Esposito, J. Radioisotopic Purity and Imaging Properties of Cyclotron-Produced 99mTc Using Direct 100Mo(p,2n) Reaction. *Phys Med Biol* **2018**, *63* (18). https://doi.org/10.1088/1361-6560/aadc88.

(76) Martini, P.; Boschi, A.; Cicoria, G.; Uccelli, L.; Pasquali, M.; Duatti, A.; Pupillo, G.; Marengo, M.; Loriggiola, M.; Esposito, J. A Solvent-Extraction Module for Cyclotron Production of High-Purity Technetium-99m. *Applied Radiation and Isotopes* **2016**, *118*, 302–307. https://doi.org/10.1016/j.apradiso.2016.10.002.

(77) Boschi, A.; Martini, P.; Pasquali, M.; Uccelli, L. Recent Achievements in Tc-99m Radiopharmaceutical Direct Production by Medical Cyclotrons. *Drug Dev Ind Pharm* **2017**, *43* (9), 1402–1412. https://doi.org/10.1080/03639045.2017.1323911.

(78) Chattopadhyay, S.; Barua, L.; De, A.; Saha Das, S.; Kuniyil, R.; Bhaskar, P.; Pal, S. S.; Kumar Sarkar, S.; Das, M. K. A Computerized Compact Module for Separation of (99m)Tc-Radionuclide from Molybdenum. *Applied Radiation and Isotopes* **2012**, *70* (11), 2631–2637. https://doi.org/10.1016/j.apradiso.2012.07.013.

(79) Martini, P.; Boschi, A.; Cicoria, G.; Uccelli, L.; Pasquali, M.; Duatti, A.; Pupillo, G.; Marengo, M.; Loriggiola, M.; Esposito, J. A Solvent-Extraction Module for Cyclotron Production of High-Purity Technetium-99m. *Applied Radiation and Isotopes* **2016**, *118*, 302–307. https://doi.org/10.1016/j.apradiso.2016.10.002.

(80) Martini, P.; Adamo, A.; Syna, N.; Boschi, A.; Uccelli, L.; Weeranoppanant, N.; Markham, J.; Pascali, G. Perspectives on the Use of Liquid Extraction for Radioisotope Purification. *Molecules* **2019**, *24* (2). https://doi.org/10.3390/molecules24020334.

(81) Lahiri, S.; Mukhopadhyay, B. Liquid-Liquid Extraction of Carrier-Free Radioisotopes Produced in α-Particle Activated Molybdenum Target by HDEHP and TBP. *Applied Radiation and Isotopes* **1997**, *48* (7), 925–929. https://doi.org/10.1016/S0969-8043(97)00017-1.

(82) Freiser, H.; Morrison, G. H. Solvent Extraction in Radiochemical Separations. *Annual Review of Nuclear and Particle Science* **1959**, *9*, 221–244.

(83) Cutler, C. S.; Wilder, S. L.; Embree, M. F. Separation Method for Carrier-Free Radiolanthanides. CA2742764A1, November 6, 2009.

(84) Van de Voorde, M. Supported Ionic Liquid Phases for Extraction and Separation of Medical Radiolanthanides: Towards Purification of Medical Samarium-153. PhD Thesis, KU Leuven, 2019.

(85) Lehenberger, S.; Barkhausen, C.; Cohrs, S.; Fischer, E.; Grünberg, J.; Hohn, A.; Köster, U.; Schibli, R.; Türler, A.; Zhernosekov, K. The Low-Energy $\beta^-$and Electron Emitter ^{161}Tb as an Alternative to ^{177}Lu for Targeted Radionuclide Therapy. *Nucl Med Biol* **2011**, *38* (6), 917–924. https://doi.org/10.1016/j.nucmedbio.2011.02.007.

(86) Dadachova, E.; Mirzadeh, S.; Smith, S. V.; Knapp, F. . F.; Hetherington, E. L. Radiolabeling Antibodies with Holmium-166. *Applied Radiation and Isotopes* **1997**, *48* (4), 477–481.

(87) Kumar, P.; Jaison, P. G.; Rao, D. R. M.; Telmore, V. M.; Sarkar, A.; Aggarwal, S. K. Determination of Lanthanides and Yttrium in High Purity Dysprosium by Rp-Hplc Using δ-Hydroxyisobutyric Acid as an Eluent. *J Liq Chromatogr Relat Technol* **2013**, *36* (11), 1513–1527. https://doi.org/10.1080/10826076.2012.692148.

(88) Lebedev, N. A.; Novgorodov, A. F.; Misiak, R.; Brockmann, J.; Rösch, F. Radiochemical Separation of No-Carrier-Added ^{177}Lu as Produced via the ^{176}Ybn,γ^{177}Yb→^{177}Lu Process. *Applied Radiation and Isotopes* **2000**, *53* (3), 421–425. https://doi.org/https://doi.org/10.1016/S0969-8043(99)00284-5.

(89) *Extraction Chromatography*; Braun, T., Ghersini, G., Eds.; Elsevier, 1975.

(90) Monroy-Guzman, F.; Salinas, E. J. Separation of Micro-Macrocomponent Systems: ^{149}Pm – Nd, ^{161}Tb-Gd, ^{166}Ho-Dy and ^{177}Lu-Yb by Extraction Chromatography. *J. Mex. Chem. Soc.* **2015**, *59* (2), 143–150.

(91) Horwitz, E. P.; McAlister, D. R.; Bond, A. H.; Barrans, R. E.; Williamson, J. M. A Process for the Separation of ^{177}Lu from Neutron Irradiated ^{176}Yb Targets. *Applied Radiation and Isotopes* **2005**, *63* (1), 23–36. https://doi.org/10.1016/j.apradiso.2005.02.005.

(92) Siekierski, S.; Fidelis, I. Extraction Chromatography of Lanthanides. In *Journal of Chromatography Library*; Braun, T. ; G. G., Ed.; Elsevier, 1975; Vol. 2, pp 226–253. https://doi.org/10.1016/S0301-4770(08)60974-4.

(93) Jelinek, L.; Wei, Y.; Arai, T.; Kumagai, M. Selective Eu(III) Electro-Reduction and Subsequent Separation of Eu(II) from Rare Earths(III) via HDEHP Impregnated Resin. *Solvent Extraction and Ion Exchange* **2007**, *25* (4), 503–513. https://doi.org/10.1080/07366290701415911.

(94) Van de Voorde, M.; Van Hecke, K.; Binnemans, K.; Cardinaels, T. Supported Ionic Liquid Phases for the Separation of Samarium and Europium in Nitrate Media: Towards Purification of Medical Samarium-153. *Sep Purif Technol* **2020**, *232*. https://doi.org/10.1016/j.seppur.2019.115939.

(95) Atanasyants, A. G.; Seryogin, A. N. The Reaction of the Electrochemical Reduction Eu (III) + e- → Eu(II) in Hydrochloric Solution. *Hydrometallurgy* **1995**, *37* (3), 367–374. https://doi.org/10.1016/0304-386X(94)00036-3.

(96) Zelić, M. Electrochemical Reduction of Europium (3+) at Increasing Concentrations of Different Salts. Part I . Voltammetric Measurements. *Croatica Chemica Acta* **2003**, *76* (3), 241–248.

(97) Jelinek, L.; Arai, T.; Yuezhou, W.; Kumagai, M. Direct Spectroscopic Determination of Europium (II) Concentration during Europium (III) Electro-Reduction in Hydrochloric Acid Medium. *Journal of Rare Earths* **2007**, *25* (1), 1–5. https://doi.org/10.1016/S1002-0721(07)60033-7.

(98) Van De Voorde, M.; Geboes, B.; Vander Hoogerstraete, T.; Van Hecke, K.; Cardinaels, T.; Binnemans, K. Stability of Europium(II) in Aqueous Nitrate Solutions. *Dalton Transactions* **2019**, *48*, 14758–14768. https://doi.org/10.1039/c9dt03139a.

(99) Bulhões, L. O. de S.; Rabockai, T. Electrochemical Reduction of Lanthanides in Propylene Carbonate. *Electrochim Acta* **1982**, *27* (8), 1071–1073. https://doi.org/10.1016/0013-4686(82)80111-4.

(100) Chakravarty, R.; Chakraborty, S.; Khan, M. S.; Ram, R.; Sarma, H. D.; Dash, A. An Electrochemical Approach for Removal of Radionuclidic Contaminants of Eu from ^{153}Sm for Effective Use in Metastatic Bone Pain Palliation. *Nucl Med Biol* **2018**, *58*, 8–19. https://doi.org/10.1016/j.nucmedbio.2017.11.010.

(101) Cotton, S. *Lanthanide and Actinide Chemistry*; Woollins, D., Crabtree, B., Atwood, D., Meyer, G., Eds.; John Wiley & Sons, Ltd: Uppingham, Rutland, 2006. https://doi.org/10.1002/0470010088.

(102) Wadsworth, Earl.; Duke, F. R.; Goetz, C. A. Present Status of Cerium(IV)-Cerium(III) Potentials. *Anal Chem* **1957**, *29* (12), 1824–1825. https://doi.org/10.1021/ac60132a046.

(103) Smith, G. F.; Getz, C. A.; Frederick Smith, G.; Getz, C. A. Cerate Oxidimetry. *Industrial and Engineering Chemistry, Analytical Edition* **1938**, *10* (4), 191–195. https://doi.org/10.1021/ac50120A006.

(104) Binnemans, K. Applications of Tetravalent Cerium Compounds. In *Handbook on the Physics and Chemistry of Rare Earths*; Gschneidner, K. A., Bunzli, J.-C. G., Pecharsky, V. K., Eds.; Elsevier, 2006; Vol. 36, pp 281–392. https://doi.org/https://doi.org/10.1016/S0168-1273(06)36003-5.

(105) Hobart, D. E.; Samhoun, K.; Young, J. P.; Norvell, V. E.; Mamantov, G.; Peterson, J. R. Stabilization of Praseodymium(IV) and Terbium(IV) in Aqueous Carbonate Solution. *Inorganic and Nuclear Chemistry Letters* **1980**, *16* (5), 321–328. https://doi.org/10.1016/0020-1650(80)80069-9.

(106) Hobart, D. E. Electrochemical and Spectroscopic Studies of Some Less Stable Oxidation States of Selected Lanthanide and Actinide Elements, Dissertation, University of Tennessee, 1981.

(107) Hobart, D. E.; Samhoun, K.; Peterson, J. R. Spectroelectrochemical Studies of the Actinides: Stabilization of Americium(IV) in Aqueous Carbonate Solution. *Radiochim Acta* **1982**, *31*, 139–145. https://doi.org/10.1524/ract.1982.31.34.139.

(108) Propst, R. C. Electrochemical Oxidation of Terbium(3) at the Conducting Glass Electrode. *Journal of Inorganic and Nuclear Chemistry* **1974**, *36* (5), 1085–1094. https://doi.org/10.1016/0022-1902(74)80218-6.

(109) Varlashkin, P. G.; Begun, G. M.; Peterson, J. R. On the Nature of Tetravalent Terbium in Carbonate-Hydroxide Solutions. *Journal of the Less Common Metals* **1985**, *109* (1), 123–134. https://doi.org/10.1016/0022-5088(85)90112-2.

(110) Li, X.; Dong, W.; Qi, Y.; Wang, D.; Yang, R. Studies on the Stabilization of Terbium(IV) in Aqueous Tetrametaphosphate Solution. *Polyhedron* **1991**, *10* (13), 1479–1483. https://doi.org/10.1016/S0277-5387(00)86069-6.

(111) Sayed, S. A.; Rabie, K. A.; Salama, I. E. Studies on Europium Separation from a Middle Rare Earth Concentrate by in Situ Zinc Reduction Technique. *Sep Purif Technol* **2005**, *46* (3), 145–154. https://doi.org/10.1016/j.seppur.2005.05.006.

(112) Donohue, T. Photochemical Separation of Europium from Lanthanide Mixtures in Aqueous Solution. *J Chem Phys* **1977**, *67* (11), 5402–5404. https://doi.org/10.1063/1.434656.

(113) Qiu, L. F.; Kang, X. H.; Wang, T. S. A Study on Photochemical Separation of Rare Earths: The Separation of Europium from an Industrial Concentrate Material of Samarium, Europium, and Gadolinium. *Sep Sci Technol* **1991**, *26* (2), 199–221. https://doi.org/10.1080/01496399108050467.

(114) Myasoedov, B. F.; Kulyako, Yu. M.; Sklyarenko, I. S. Electrochemical Reduction of Europium in Acetonitrile. *Journal of Inorganic and Nuclear Chemistry* **1975**, *37* (1), 113–117. https://doi.org/https://doi.org/10.1016/0022-1902(75)80136-9.

(115) Myasoedov, B. F.; Kulyako, Yu. M. M.; Sklyarenko, I. S. Electrochemical Reduction of Americium and Some Rare Earth Elements in Acetonitrile. *Journal of Inorganic and Nuclear Chemistry* **1976**, *38* (4), 827–830. https://doi.org/https://doi.org/10.1016/0022-1902(76)80365-X.

(116) Rabockai, T. Electrochemical Reduction of Ytterbium in Perchloric Media. *J Electroanal Chem Interfacial Electrochem* **1977**, *76* (1), 83–89. https://doi.org/https://doi.org/10.1016/S0022-0728(77)80008-9.

(117) Steeman, E.; Temmerman, E.; Verbeek, F. Electrochemical Reduction of the Lanthanide Ions: Part I. First Reduction Step of Ytterbium(III) in Acidic 1 M $NaClO_4$ Solution. *J Electroanal Chem Interfacial Electrochem* **1978**, *89* (1), 97–111. https://doi.org/https://doi.org/10.1016/S0022-0728(78)80035-7.

(118) Ferro, S.; De Battisti, A. Electrochemistry of the Aqueous Europium(III)/Europium(II) Redox Couple at Conductive Diamond Electrodes. *Journal of Electroanalytical Chemistry* **2002**, *533*, 177–180. https://doi.org/10.1016/S0022-0728(02)01073-2.

(119) Jelinek, L.; Wei, Y.; Arai, T.; Kumagai, M. Study on Separation of Eu(II) from Trivalent Rare Earths via Electro-Reduction and Ion Exchange. *J Alloys Compd* **2008**, *451*, 341–343. https://doi.org/10.1016/j.jallcom.2007.04.139.

(120) Schwantes, J. M.; Sudowe, R.; Nitsche, H.; Hoffman, D. C. Applications of Solvent Extraction in the High-Yield Multi-Process Reduction/Separation of Eu from Excess Sm. *J Radioanal Nucl Chem* **2008**, *276* (2), 543–548. https://doi.org/10.1007/s10967-008-0539-4.

(121) Van de Voorde, M.; Van Hecke, K.; Binnemans, K.; Cardinaels, T.; Voorde, M. Van De; Hecke, K. Van; Binnemans, K.; Cardinaels, T. Separation of Samarium and Europium by Solvent Extraction with an Undiluted Quaternary Ammonium Ionic Liquid: Towards High-Purity Medical Samarium-153. *RSC Adv* **2018**, *8* (36), 20077–20086. https://doi.org/10.1039/C8RA03279C.

(122) Binnemans, K.; Jones, P. T. Perspectives for the Recovery of Rare Earths from End-of-Life Fluorescent Lamps. *Journal of Rare Earths* **2014**, *32* (3), 195–200. https://doi.org/10.1016/S1002-0721(14)60051-X.

(123) Wang, X.; Chang, H.; Xie, J.; Zhao, B.; Liu, B.; Xu, S.; Pei, W.; Ren, N.; Huang, L.; Huang, W. Recent Developments in Lanthanide-Based Luminescent Probes. *Coord Chem Rev* **2014**, *273–274*, 201–212. https://doi.org/10.1016/j.ccr.2014.02.001.

(124) Van de Voorde, M.; Van Hecke, K.; Binnemans, K.; Cardinaels, T. Separation of Samarium and Europium by Solvent Extraction with an Undiluted Quaternary Ammonium Ionic Liquid: Towards High-Purity Medical Samarium-153. *RSC Adv* **2018**, *8* (36), 20077–20086. https://doi.org/10.1039/C8RA03279C.

(125) Zuo, Y.; Liu, Y.; Chen, J.; Li, D. Q. The Separation of Cerium(IV) from Nitric Acid Solutions Containing Thorium(IV) and Lanthanides (III) Using Pure [C8mim]PF6 as Extracting Phase. *Ind Eng Chem Res* **2008**, *47* (7), 2349–2355. https://doi.org/10.1021/ie071486w.

(126) Kedari, C. S.; Pandit, S. S.; Ramanujam, A. In Situ Electro-Oxidation and Liquid-Liquid Extraction of Cerium(IV) from Nitric Acid Medium Using Tributyl Phosphate and 2-Ethylhexyl Hydrogen 2-Ethylhexyl Phosphonate. *J Radioanal Nucl Chem* **1997**, *222* (1–2), 141–147. https://doi.org/10.1007/BF02034260.

(127) Borai, E. H.; Shahr El-Din, A. M.; El Afifi, E. M.; Aglan, R. F.; Abo-Aly, M. M. Subsequent Separation and Selective Extraction of Thorium (IV), Iron (III), Zirconium (IV) and Cerium (III) from Aqueous Sulfate Medium. *South African Journal of Chemistry* **2016**, *69*, 148–156. https://doi.org/10.17159/0379-4350/2016/v69a18.

(128) Rabockai, T.; Luis, L. O. Electrochemical Reduction of Eu3+ in Aqueous Ethylene Glycol Solutions. *Electrochim Acta* **1980**, *25* (8), 1041–1042. https://doi.org/10.1016/0013-4686(80)87012-5.

(129) Zhao, H. L.; You, Q. C.; Chun, A. M. Electrochemical Oxidation of Ce(III) to Ce(IV) in Mixed Acid (H_2SO_4 and CH_3SO_3H). *Adv Mat Res* **2012**, *588–589*, 90–94. https://doi.org/10.4028/www.scientific.net/amr.588-589.90.

(130) Kiekens, P.; Steen, L.; Donche, H.; Temmerman, E. Kinetics of Ce(IV) Reduction at Gold, Carbon and Iridium Electrodes. *Electrochim Acta* **1981**, *26* (7), 841–845. https://doi.org/10.1016/0013-4686(81)85043-8.

(131) Gupta, R.; Gamare, J.; Jayachandran, K.; Gupta, S. K.; Lohithakshan, K. V.; Kamat, J. V. Electrochemical, Thermodynamic and Spectroscopic Investigations of Ce^{III} in a 1-Ethyl-3-Methylimidazolium Ethyl Sulfate (EMIES) Ionic Liquid. *Eur J Inorg Chem* **2015**, *2015* (26), 4396–4401. https://doi.org/10.1002/ejic.201500671.

(132) Knecht, L. A. Oxidation of Cerium(III) to Cerium(IV) Using a Mixture of Hot Concentrated Perchloric and Sulfuric Acids. *Anal Chim Acta* **1967**, *39* (C), 349–355. https://doi.org/10.1016/S0003-2670(01)80514-6.

(133) Piro, N. A.; Robinson, J. R.; Walsh, P. J.; Schelter, E. J. The Electrochemical Behavior of Cerium(III/IV) Complexes: Thermodynamics, Kinetics and Applications in Synthesis. *Coord Chem Rev* **2014**, *260* (1), 21–36. https://doi.org/10.1016/j.ccr.2013.08.034.

(134) Modiba, P.; Crouch, A. M. Electrochemical Study of Cerium(IV) in the Presence of Ethylenediaminetetraacetic Acid (EDTA) and Diethylenetriaminepentaacetate (DTPA) Ligands. *J Appl Electrochem* **2008**, *38* (9), 1293–1299. https://doi.org/10.1007/s10800-008-9558-7.

(135) Gompa, T. P.; Ramanathan, A.; Rice, N. T.; La Pierre, H. S. The Chemical and Physical Properties of Tetravalent Lanthanides: Pr, Nd, Tb, and Dy. *Dalton Transactions* **2020**, *49* (45), 15945–15987. https://doi.org/10.1039/d0dt01400a.

(136) Frederick Smith, G.; Getz, C. A. Cerate Oxidimetry. *Industrial and Engineering Chemistry, Analytical Edition* **1938**, *10* (4), 191–195.

(137) Wei, H.; Li, Y.; Zhang, Z.; Xue, T.; Kuang, S.; Liao, W. Selective Extraction and Separation of Ce (IV) and Th (IV) from RE(III) in Sulfate Medium Using Di(2-Ethylhexyl)-N-Heptylaminomethylphosphonate. *Solvent Extraction and Ion Exchange* **2017**, *35* (2), 117–129. https://doi.org/10.1080/07366299.2017.1292025.

(138) Sedneva, T. A. Cerium(III) Electrooxidation in Nitric Acid Solutions of Rare-Earth Elements. *Russian Journal of Applied Chemistry* **2005**, *78* (6), 907–911. https://doi.org/10.1007/s11167-005-0418-5.

(139) Van De Voorde, M.; Van Hecke, K.; Binnemans, K.; Cardinaels, T. Separation of Samarium and Europium by Solvent Extraction with an Undiluted Quaternary Ammonium Ionic Liquid: Towards High-Purity Medical Samarium-153. *RSC Adv* **2018**, *8* (36), 20077–20086. https://doi.org/10.1039/c8ra03279c.

(140) Yörükoğlu, A.; Girgin, İ. Recovery of Europium by Electrochemical Reduction from Sulfate Solutions. *Hydrometallurgy* **2002**, *63* (1), 85–91. https://doi.org/10.1016/S0304-386X(01)00215-8.

(141) Peppard, D. F.; Horwitz, E. P.; Mason, G. W. Comparative Liquid-Liquid Extraction Behaviour of Europium (II) and Europium (III). *Journal of Inorganic and Nuclear Chemistry* **1962**, *24* (4), 429–439. https://doi.org/10.1016/0022-1902(62)80039-6.

(142) Ying, Y.; Ru-Dong, Y. Synthesis and Characterization of Tetravalent Terbium Complexes of Alkali Terbium Hexaoxidoiodates. *Polyhedron* **1992**, *11* (8), 963–966. https://doi.org/10.1016/S0277-5387(00)83348-3.

(143) Josse, M.; Dubois, M.; El-Ghozzi, M.; Cellier, J.; Avignant, D. Anti-$KSbF_6$ Structure of $CaTbF_6$ and $CdTbF_6$: A Confirmation of the Singular Crystal Chemistry of Tb^{4+} in Fluorides. *Acta Crystallogr B* **2005**, *61* (1), 1–10. https://doi.org/10.1107/S0108768104026928.

(144) Wang, D.; Qiu, G.; Jin, X.; Hu, X.; Chen, G. Z. Electrochemical Metallization of Solid Terbium Oxide. *Angewandte Chemie International Edition* **2006**, *45* (15), 2384–2388. https://doi.org/10.1002/anie.200503571.

(145) Avignant, D.; Largeau, E.; Gaumet, V.; Dugat, P.; El-Ghozzi, M. Recent Progress in Tetravalent Terbium Chemistry. *J Alloys Compd* **1998**, *275–277*, 1–5. https://doi.org/10.1016/S0925-8388(98)00262-X.

(146) Qiang, S.; Zhijian, W.; Chongli, G. Solvent Extraction of Terbium(III,IV) Periodate Complexes with Quaternary Amine. *Solvent Extraction and Ion Exchange* **1995**, *13* (2), 275–288. https://doi.org/10.1080/07366299508918274.

(147) Qiang, S.; Zhijian, W.; Chongli, G. Solvent Extraction of Tetravalent Terbium Tb(IV) and Other Trivalent Rare Earths with Quaternary Amine. In *International solvent extraction conference*; Melbourne, 1996; Vol. I, pp 605–610.

(148) Rice, N. T.; Popov, I. A.; Russo, D. R.; Bacsa, J.; Batista, E. R.; Yang, P.; Telser, J.; La Pierre, H. S. Design, Isolation, and Spectroscopic Analysis of a Tetravalent Terbium Complex. *J Am Chem Soc* **2019**, *141* (33), 13222–13233. https://doi.org/10.1021/jacs.9b06622.

(149) Willauer, A. R.; Palumbo, C. T.; Scopelliti, R.; Zivkovic, I.; Douair, I.; Maron, L.; Mazzanti, M. Stabilization of the Oxidation State +IV in Siloxide-Supported Terbium Compounds. *Angewandte Chemie - International Edition* **2020**, *59* (9), 3549–3553. https://doi.org/10.1002/anie.201914733.

(150) Palumbo, C. T.; Zivkovic, I.; Scopelliti, R.; Mazzanti, M. Molecular Complex of Tb in the +4 Oxidation State. *J Am Chem Soc* **2019**, *141* (25), 9827–9831. https://doi.org/10.1021/jacs.9b05337.

(151) Rao, R. R.; Milliken, S. B.; Robinson, S. L.; Mann, C. K. Anodic Oxidation of Lithium, Cadmium, Silver, and Tetrabutylammonium Nitrates. *Anal Chem* **1970**, *42* (9), 1076–1080. https://doi.org/10.1021/ac60291a006.

(152) Mishima, H.; Iwasita, T.; Macagno, V. A.; Giordano, M. C. The Electrochemical Oxidation of Nitrate Ion on Platinum from Silver Nitrate in Acetonitrile Solutions—I. Kinetic Analysis. *Electrochim Acta* **1973**, *18* (4), 287–292. https://doi.org/10.1016/0013-4686(73)80030-1.

(153) Colombi, M.; Fiori, G.; Formaro, L. Electrochemical Study of the Anodic Oxidation of Nitrate Ion on a Platinum Electrode in Acetic Acid. *J Electroanal Chem Interfacial Electrochem* **1973**, *44* (1), 21–24. https://doi.org/10.1016/S0022-0728(73)80510-8.

(154) Moeller, T. *Inorganic Chemistry*; John Wiley & Sons, New York, 1953.

(155) Lehenberger, S.; Barkhausen, C.; Cohrs, S.; Fischer, E.; Grünberg, J.; Hohn, A.; Köster, U.; Schibli, R.; Türler, A.; Zhernosekov, K. The Low-Energy β-and Electron Emitter161Tb as an Alternative To177Lu for Targeted Radionuclide Therapy. *Nucl Med Biol* **2011**, *38* (6), 917–924. https://doi.org/10.1016/j.nucmedbio.2011.02.007.

(156) Gracheva, N.; Müller, C.; Talip, Z.; Heinitz, S.; Köster, U.; Zeevaart, J. R.; Vögele, A.; Schibli, R.; Van Der Meulen, N. P. Production and Characterization of No-Carrier-Added 161 Tb as an Alternative to the Clinically-Applied 177 Lu for Radionuclide Therapy. *EJNMMI Radiopharm Chem* **2019**, *4* (12). https://doi.org/10.1186/s41181-019-0063-6.

(157) Lehenberger, S.; Barkhausen, C.; Cohrs, S.; Fischer, E.; Grünberg, J.; Hohn, A.; Köster, U.; Schibli, R.; Türler, A.; Zhernosekov, K. The Low-Energy $\beta^-$and Electron Emitter ^{161}Tb as an Alternative to ^{177}Lu for Targeted Radionuclide Therapy. *Nucl Med Biol* **2011**, *38* (6), 917–924. https://doi.org/10.1016/j.nucmedbio.2011.02.007.

(158) Grünberg, J.; Lindenblatt, D.; Dorrer, H.; Cohrs, S.; Zhernosekov, K.; Köster, U.; Türler, A.; Fischer, E.; Schibli, R. Anti-L1CAM Radioimmunotherapy Is More Effective with the Radiolanthanide Terbium-161 Compared to Lutetium-177 in an Ovarian Cancer Model. *Eur J Nucl Med Mol Imaging* **2014**, *41* (10), 1907–1915. https://doi.org/10.1007/s00259-014-2798-3.

(159) Arman, M. O.; Geboes, B.; Van Hecke, K.; Binnemans, K.; Cardinaels, T. Electrochemical Oxidation of Terbium(III) in Aqueous Media: Influence of Supporting Electrolyte on Oxidation Potential and Stability. *J Appl Electrochem* **2022**, *52* (3), 583–593. https://doi.org/10.1007/s10800-021-01651-0.

(160) Li, W. P.; Smith, C. J.; Cutler, C. S.; Hoffman, T. J.; Ketring, A. R.; Jurisson, S. S. Aminocarboxylate Complexes and Octreotide Complexes with No Carrier Added 177Lu, 166Ho and 149Pm. *Nucl Med Biol* **2003**, *30* (3), 241–251. https://doi.org/10.1016/S0969-8051(02)00418-3.

(161) Smirnov, V. V; Karavan, M. D.; Logunov, M. V; Tananaev, I. G.; Myasoedov, B. F. Original Russian Text © I. *Radiochemistry* **2018**, *60* (5), 404–419. https://doi.org/10.1134/S1066362218050028.

(162) Kuzovkina, E. V; Lavrinovich, E. A.; Novikov, A. P.; Stepanova, E. S.; Karavan, M. D.; Smirnov, I. V. Kinetics of Americium and Europium Extraction by Tert-Butylthiacalix[4]Arene from Alkaline Media. https://doi.org/10.1007/s10967-017-5165-6.

(163) Smirnov, V. V; Karavan, M. D.; Logunov, M. V; Tananaev, I. G.; Myasoedov, B. F. Extraction of Radionuclides from Alkaline and Carbonate Media. *Radiochemistry* **2018**, *60* (5), 404–419. https://doi.org/10.1134/S1066362218050028.

(164) Myasoedov, B. F.; Lebedev, I. A.; Khizhnyak, P. L.; Timofeev, G. A. Electrochemical Oxidation of Americium and Californium in Carbonate Solutions*. **1986**, *122*, 189–193.

(165) Karalova, Z. I.; Lavrinovich, E. A.; Myasoedov, B. F. Use of Actinides in Uncommon Oxidation States. **1992**, *159* (2), 259–266.

(166) Smirnov, I. V; Stepanova, E. S.; Ivenskaya, N. M.; Karavan, M. D.; Zaripov, S. R.; Sofiya, •; Kleshnina, R.; Solovieva, S. E.; Antipin, I. S. Cesium and Americium Extraction from Carbonate-Alkaline Media with O-Substituted p-Alkylcalix[8]Arenes. *J Radioanal Nucl Chem* **2017**, *317* (1257–1265). https://doi.org/10.1007/s10967-017-5505-6.

(167) Valentinovich Boyarintsev, A.; Valerievna Kostikova, G.; Stepanov, S. I.; Shoustikov, A. A.; Chekmarev, A. M.; Tsivadze, A. Y.; Illarionovich Stepanov, S.; Aleksandrovich Shoustikov, A.; Mihailovich Chekmarev, A.; Yusupovich Tsivadze, A. Separation of Uranium(VI) and Americium(III) by Extraction from Na2CO3-H2O2 Solutions Using Methyltrioctylammonium Carbonate in Toluene. *Solvent Extraction and Ion Exchange* **2021**, *39* (7), 745–763. https://doi.org/10.1080/07366299.2021.1876993.

(168) Clifford, W. E.; Bullwinkel, E. P.; McClaine, L. A.; Noble, P. The Solvent Extraction of Uranium (VI) from Carbonate Solutions. *J Am Chem Soc* **1958**, *80* (12), 2959–2961. https://doi.org/10.1021/ja01545a014.

(169) Boyarintsev, A. V.; Perevalov, S. A.; Stepanov, S. I.; Chekmarev, A. M. Liquid–Liquid Extraction of Neptunium(VI) and Neptunium(V) from Carbonate Solutions by Methyltrioctylammonium Carbonate in Toluene. *J Radioanal Nucl Chem* **2020**, *327* (1), 385–393. https://doi.org/10.1007/s10967-020-07487-w.

(170) Karalova, Z. K.; Myasoedov, B. F.; Bukina, T. V; Rodionova, L. M. The Use of Decylamine for the Extraction of Actinides and Lanthanides from Carbonate Solutions. *Radiokhimiya* **1985**, *27* (1), 47–49.

(171) Karalova, Z. K.; Myasoedov, B. F.; Rodionova, L. M.; Kuznetsova, S. A. Extraction of Transplutonium Elements from Carbonate Solutions with Alkylpyrocatechol. *Radiokhimiya* **1981**, *25* (2), 187–191.

(172) Sherry, H. S.; Marinsky, J. A. Carbonate and Bicarbonate Complexes of Neodymium and Europium. *Inorg Chem* **1964**, *3* (3), 330–335. https://doi.org/10.1021/ic50013a006.

(173) Sherry, H. S.; Marinsky, J. A. Carbonate Complexes of the Lighter Lanthanides. *Inorg Chem* **1963**, *2* (5), 957–959. https://doi.org/10.1021/ic50009a019.

(174) Joly, Y. X-Ray Absorption near-Edge Structure Calculations beyond the Muffin-Tin Approximation. *Phys Rev B* **2001**, *63*, 125120-1-125120–10. https://doi.org/10.1103/PhysRevB.63.125120.

(175) Hedin, L.; I. Lundqvist, B.; Lundqvist, S. Local Exchange-Correlation Potentials. *Solid State Commun* **1971**, *9* (9), 537–541. https://doi.org/10.1016/0038-1098(71)90141-4.

(176) Saito, N.; Sekine, T. Anion Exchange Behaviour of Yttrium . *Nature* **1957**, *180* (4589), 753. https://doi.org/10.1038/180753A0.

(177) Misumi, S.; Taketatsu, T. Anion Exchange Studies of Beryllium(II), Cerium(IV), Thorium(IV) and Uranium(VI) Carbonate Complex Ions. *Bull Chem Soc Jpn* **1958**, *32* (8), 876–879.

(178) Taketatsu, T. The Dissolution and Anion Exchange Behavior of Rare Earth and Other Metallic Elements in Potassium Bicarbonate, Potassium Carbonate and Ammonium Carbonate Solutions. *Bull Chem Soc Jpn* **1963**, *36* (5), 549–553. https://doi.org/10.1246/BCSJ.36.549.

(179) Taketatsu, T. Anion-Exchange Separation of Rare Earth Elements and Thorium from Uranium with Carbonate Solutions. *Talanta* **1963**, *10* (10), 1077–1082. https://doi.org/10.1016/0039-9140(63)80146-0.

(180) Gärtner, R. S.; Witkamp, G. J. Regeneration of Mixed Solvent by Ion Exchange Resin: Selective Removal of Chloride and Sulfate. *Sep Sci Technol* **2005**, *40* (12), 2391–2410. https://doi.org/10.1080/01496390500267442.

(181) Michiba, K.; Tahara, T.; Nakai, I.; Miyawaki, R.; Matsubara, S. Crystal Structure of Hexagonal RE(CO3)OH. *Zeitschrift fur Kristallographie* **2011**, *226* (6), 518–530. https://doi.org/10.1524/zkri.2011.1222.

(182) Dixey, R. J. C.; Saines, P. J. Optimization of the Magnetocaloric Effect in Low Applied Magnetic Fields in LnOHCO3 Frameworks. *Inorg Chem* **2018**, *57* (20), 12543–12551. https://doi.org/10.1021/acs.inorgchem.8B01549.

(183) Asprey, L. B.; Cunningham, B. B. Unusual Oxidation States of Some Actinide and Lanthanide Elements. *Progress in Inorganic Chemistry* **1960**, *2*, 267–302. https://doi.org/10.1002/9780470166031.ch6.

(184) Schumacher, P. D.; Doyle, J. L.; Schenk, J. O.; Clark, S. B. Electroanalytical Chemistry of Lanthanides and Actinides. *Rev Anal Chem* **2013**, *32* (2), 159–171. https://doi.org/10.1515/revac-2012-0032.

(185) Eller, P. G.; Penneman, R. A. Stabilization of Actinides and Lanthanides in High Oxidation States. *Journal of The Less-Common Metals* **1987**, *127*, 19–33. https://doi.org/10.1016/0022-5088(87)90354-7.

(186) Mikheev, N. B.; Auerman, L. N.; Rumer, I. A.; Kamenskaya, A. N.; Kazakevich, M. Z. The Anomalous Stabilisation of the Oxidation State 2+ of Lanthanides and Actinides. *Russian Chemical Reviews* **1992**, *61* (10), 990–998. https://doi.org/10.1070/rc1992v061n10abeh001011.

(187) Payne G. F.; Peterson J. R. Oxidation Studies of Selected Lanthanides in Acetonitrile. *Journal of The Less-Common Metals* **1986**, *126*, 371–377.

(188) Gibilaro, M.; Massot, L.; Chamelot, P.; Cassayre, L.; Taxil, P. Electrochemical Extraction of Europium from Molten Fluoride Media. *Electrochim Acta* **2009**, *55* (1), 281–287. https://doi.org/10.1016/j.electacta.2009.08.052.

(189) Huang, W.; Tian, L.; She, C.; Jiang, F.; Zheng, H.; Li, W.; Wu, G.; Long, D.; Li, Q. Electrochemical Behavior of Europium(III)-Europium(II) in LiF-NaF-KF Molten Salt. *Electrochim Acta* **2014**, *147*, 114–120. https://doi.org/10.1016/j.electacta.2014.08.119.

(190) Kuznetsov, S. A. Electrochemical Study of Stabilization Higher Oxidation States of D- and f-Metals in Molten Salts. *Int J Electrochem Sci* **2016**, *11* (8), 6580–6596. https://doi.org/10.20964/2016.08.53.

(191) Yamagata, M.; Katayama, Y.; Miura, T. Electrochemical Behavior of Samarium, Europium, and Ytterbium in Hydrophobic Room-Temperature Molten Salt Systems. *J Electrochem Soc* **2006**, *153*, E5–E9. https://doi.org/10.1149/1.2136088.

(192) Morais, C. A.; Ciminelli, V. S. T. Recovery of Europium by Chemical Reduction of a Commercial Solution of Europium and Gadolinium Chlorides. *Hydrometallurgy* **2001**, *60* (3), 247–253. https://doi.org/10.1016/S0304-386X(01)00156-6.

(193) Willauer, A. R.; Palumbo, C. T.; Fadaei-Tirani, F.; Zivkovic, I.; Douair, I.; Maron, L.; Mazzanti, M. Accessing the +IV Oxidation State in Molecular Complexes of Praseodymium. *J Am Chem Soc* **2020**, *142* (12), 5538–5542. https://doi.org/10.1021/jacs.0c01204.

(194) Van Den Bogaert, B.; Gheeraert, L.; Leblebici, M. E.; Binnemans, K.; Van Gerven, T. Photochemical Recovery of Europium from Non-Aqueous Solutions. *Phys. Chem. Chem. Phys* **2016**, *18*, 29961–29968. https://doi.org/10.1039/c6cp06329b.

(195) Van Den Bogaert, B.; Meerbeeck, L. Van; Binnemans, K.; Van Gerven, T. Influence of Irradiance on the Photochemical Reduction of Europium(III). *Green Chemistry* **2016**, *18*, 4198–4204. https://doi.org/10.1039/c6gc00541a.

(196) Hirai, T.; Komasawa, I. Separation of Europium from Samarium and Gadolinium by Combination of Electrochemical Reduction and Solvent Extraction. *Journal of Chemical Engineering of Japan*. 1992, pp 644–648. https://doi.org/10.1252/jcej.25.644.

(197) Sayed, S. A.; Rabie, K. A.; Salama, I. E. Studies on Europium Separation from a Middle Rare Earth Concentrate by in Situ Zinc Reduction Technique. *Sep Purif Technol* **2005**, *46* (3), 145–154. https://doi.org/10.1016/J.SEPPUR.2005.05.006.

(198) Härk, E.; Jäger, R.; Lust, K.; Kasuk, H.; Lust, E. The Kinetics of Electroreduction of Europium(III) Cations at Bismuth Single-Crystal Electrode. *Journal of Solid State Electrochemistry* **2012**, *16* (3), 921–926. https://doi.org/10.1007/s10008-011-1443-3.

(199) Henstridge, M. C.; Wang, Y.; Limon-Petersen, J. G.; Laborda, E.; Compton, R. G. An Experimental Comparison of the Marcus-Hush and Butler-Volmer Descriptions of Electrode Kinetics Applied to Cyclic Voltammetry. The One Electron Reductions of Europium (III) and 2-Methyl-2-Nitropropane Studied at a Mercury Microhemisphere Electrode. *Chem Phys Lett* **2011**, *517* (1–3), 29–35. https://doi.org/10.1016/j.cplett.2011.10.004.

(200) Ferro, S.; De Battisti, A. Electrochemistry of the Aqueous Europium(III)/Europium(II) Redox Couple at Conductive Diamond Electrodes. *Journal of Electroanalytical Chemistry* **2002**, *533* (1–2), 177–180. https://doi.org/10.1016/S0022-0728(02)01073-2.

(201) Bertelsen, E. R.; Kovach, N. C.; Trewyn, B. G.; Antonio, M. R.; Shafer, J. C. Electrochemical Reduction of Europium(III) Using Tetra-n-Octyl Diglycolamide Functionalized Ordered Mesoporous Carbon Microelectrodes. *J Mater Chem C Mater* **2020**, *8* (20), 6689–6700. https://doi.org/10.1039/D0TC00824A.

(202) Adin, A.; Sykes, A. G. The Kinetics of the Oxidation of Europium(II) with Vanadium(III) and Chromium(III) in Aqueous Perchloric Acid Solutions. *Journal of Chemical Society* **1966**, 1230–1236.

(203) Frank Kinard, W.; Philp, R. H. Electrochemical Studies of the Eu(III)/(II) Reaction by Conventional and Kalousek Polarography. *J Electroanal Chem Interfacial Electrochem* **1970**, *25* (3), 373–379. https://doi.org/10.1016/S0022-0728(70)80099-7.

(204) Rabockai, T.; Jordan, I. Electrochemistry of Europium in Aqueous and Aqueous Formamide Solutions. *Anal Lett* **1974**, *7* (10), 647–658. https://doi.org/10.1080/00032717408059025.

(205) Rabockai, T. The Influence of Temperature on the Diffusion Coefficient of Europium in Aqueous Formamide Solutions. *Electrochim Acta* **1977**, *22* (4), 489–490. https://doi.org/10.1016/0013-4686(77)85106-2.

(206) Timmer, B.; Sluyters-Rehbach, M.; Sluyters, J. H. On the Impedance of Galvanic Cells XIX. The Potential Difference of the Faradaic Impedance in the Case of an Irreversible Electrode Reaction; Experimental Verification for the Redox Couple Eu3+/Eu2+ in 1 M NaClO4 and the Mechanism of the Zn2+/Zn(Hg) React. *J Electroanal Chem* **1967**, *14*, 181–191.

(207) Kumari, A.; Jha, M. K.; Pathak, D. D.; Chakravarty, S.; Lee, J. Processes Developed for the Separation of Europium (Eu) from Various Resources. *Separation and Purification Reviews* **2019**, *48* (2), 91–121. https://doi.org/10.1080/15422119.2018.1454959.

(208) Rabockai, T.; Luis, L. O. Electrochemical Reduction of Eu^{3+} in Aqueous Ethylene Glycol Solutions. *Electrochim Acta* **1980**, *25* (8), 1041–1042. https://doi.org/10.1016/0013-4686(80)87012-5.

(209) Rabockai, T.; De S. Bulhões, L. O.; Luis, L. O. Electrochemical Reduction of Eu^{3+} in Aqueous Ethylene Glycol Solutions. *Electrochim Acta* **1980**, *25* (8), 1041–1042. https://doi.org/10.1016/0013-4686(80)87012-5.

(210) Jagadeeswara Rao, C.; Venkatesan, K. A.; Nagarajan, K.; Srinivasan, T. G.; Vasudeva Rao, P. R. Electrochemical Behavior of Europium (III) in N-Butyl-N-Methylpyrrolidinium Bis(Trifluoromethylsulfonyl)Imide. *Electrochim Acta* **2009**, *54* (20), 4718–4725. https://doi.org/10.1016/j.electacta.2009.03.074.

(211) Cetnarska, M.; Stroka, J. Electrode Processes of the Eu(III)/Eu(II) System in Water + Hexamethylphosphortriamide Mixtures. *J Electroanal Chem Interfacial Electrochem* **1987**, *234*, 263–275. https://doi.org/10.1016/0022-0728(87)80177-8.

(212) Tanaka, F.; Yamashita, S. Luminescence Lifetimes of Aqueous Europium Chloride, Nitrate, Sulfate, and Perchlorate Solutions. Studies on the Nature of the Inner Coordination Sphere of the Europium(III) Ion. *Inorg Chem* **1984**, *23* (14), 2044–2046. https://doi.org/10.1021/ic00182a013.

(213) Rard, J. A. Chemistry and Thermodynamics of Europium and Some of Its Simpler Inorganic Compounds and Aqueous Species. *Chem Rev* **1985**, *85* (6), 555–582. https://doi.org/10.1021/cr00070a003.

(214) Garcia, J.; Allen, M. J. Developments in the Coordination Chemistry of Europium(II). *Eur J Inorg Chem* **2012**, *29*, 4550–4563. https://doi.org/10.1002/ejic.201200159.

(215) Friesen, S.; Krickl, S.; Luger, M.; Nazet, A.; Hefter, G.; Buchner, R. Hydration and Ion Association of La3+ and Eu3+ Salts in Aqueous Solution. *Physical Chemistry Chemical Physics* **2018**, *20* (13), 8812–8821. https://doi.org/10.1039/c8cp00248g.

(216) Bard, A. J.; Faulkner, L. R. *Electrochemical Methods Fundamentals and Applications*; John Wiley & Sons, Ltd, 2001.

(217) da Silva, D. A. C.; Pinzón C, M. J.; Messias, A.; Fileti, E. E.; Pascon, A.; Franco, D. V.; Da Silva, L. M.; Zanin, H. G. Effect of Conductivity, Viscosity, and Density of Water-in-Salt Electrolytes on the Electrochemical Behavior of Supercapacitors: Molecular Dynamics Simulations and in Situ Characterization Studies. *Mater. Adv* **2022**, *3*, 611–623. https://doi.org/10.1039/d1ma00890k.

(218) Treimer, S.; Tanga, A.; Johnson, D. C. A Consideration of the Application of Koutecký-Levich Plots in the Diagnoses of Charge-transfer Mechanisms at Rotated Disk Electrodes. *Electroanalysis* **2002**, *14* (3), 165–171. https://doi.org/10.1002/1521-4109(200202)14:3<165::AID-ELAN165>3.0.CO;2-6.

(219) Štulíková, M. Is Nitrate Really an Inert Electrolyte? A Brief Review. *Talanta* **1991**, *38* (7), 805–807. https://doi.org/10.1016/0039-9140(91)80205-e.

(220) Vermeulen, K.; Van de Voorde, M.; Segers, C.; Coolkens, A.; Rodriguez Pérez, S.; Daems, N.; Duchemin, C.; Crabbé, M.; Opsomer, T.; Saldarriaga Vargas, C.; Heinke, R.; Lambert, L.; Bernerd, C.; Burgoyne, A. R.; Cocolios, T. E.; Stora, T.; Ooms, M. Exploring the Potential of High-Molar-Activity Samarium-153 for Targeted Radionuclide Therapy with [153Sm]Sm-DOTA-TATE. *Pharmaceutics* **2022**, *14* (12). https://doi.org/10.3390/pharmaceutics14122566.

(221) Islami-Rad, S. Z.; Shamsaei, M.; Gholipour-Peyvandi, R.; Ghannadi-Maragheh, M. Reactor Production and Purification of 153 Sm Radioisotope via Nat Sm Target Irradiation 1. *Radiochemistry* **2011**, *53* (6), 542–544. https://doi.org/10.1134/S1066362211060129.

(222) U.S. Food and Drug Administration. *Quadramet ^{R} prescribing information*. https://www.accessdata.fda.gov/drugsatfda_docs/label/2017/020570s008lbl.pdf (accessed 2023-03-17).

(223) Ponsard, B. Production of Radioisotopes in the BR2 High-Flux Reactor for Applications in Nuclear Medicine and Industry. *J Labelled Comp Radiopharm* **2007**, *50* (5–6), 333–337. https://doi.org/10.1002/jlcr.1377.

(224) Deelstra, H.; Verbeek, F. The Separation of the Lanthanides and Yttrium by Cation Exchange Elution with Ammonium α-Hydroxyisobutyrate and Lactate. *J Chromatogr A* **1965**, *17*, 558–566. https://doi.org/10.1016/S0021-9673(00)99910-2.

(225) Shilov, V. P.; Gogolev, A. V.; Fedoseev, A. M.; Perminov, V. P. Mechanism of Cerium(III) Oxidation with Ozone in Sulfuric Acid Solutions. *Radiochemistry* **2014**, *56* (4), 400–403. https://doi.org/10.1134/S1066362214040079.

(226) Robinson, J. R.; Carroll, P. J.; Walsh, P. J.; Schelter, E. J. The Impact of Ligand Reorganization on Cerium(III) Oxidation Chemistry. *Angewandte Chemie - International Edition* **2012**, *51* (40), 10159–10163. https://doi.org/10.1002/anie.201203481.

(227) Piro, N. A.; Robinson, J. R.; Walsh, P. J.; Schelter, E. J. The Electrochemical Behavior of Cerium(III/IV) Complexes: Thermodynamics, Kinetics and Applications in Synthesis. *Coord Chem Rev* **2014**, *260* (1), 21–36. https://doi.org/10.1016/j.ccr.2013.08.034.

(228) Jones, A. S. The Reduction of Ytterbium (III) to Ytterbium (II), 2007.

(229) Davis, D. D.; Stevenson, K. L.; King, G. K. Photolysis of Europium(II) Perchlorate in Aqueous Acidic Solution. *Inorg Chem* **1977**, *16* (3), 670–673. https://doi.org/10.1021/ic50169a036.

(230) Steeman, E.; Temmerman, E.; Verbeek, F. Electrochemical Reduction of the Lanthanide Ions: Part II. Second Reduction Step of Europium(III), Ytterbium(III) and Samarium(III) in Acidic Tetramethylammonium Perchlorate Solution. *J Electroanal Chem Interfacial Electrochem* **1978**, *89* (1), 113–122. https://doi.org/https://doi.org/10.1016/S0022-0728(78)80036-9.

(231) Mowafy, E. A.; Mohamed, D. Extraction Behavior of Trivalent Lanthanides from Nitric Acid Medium by Selected Structurally Related Diglycolamides as Novel Extractants. *Sep Purif Technol* **2014**, *128*, 18–24. https://doi.org/10.1016/j.seppur.2014.03.005.

(232) Adachi, G. Y.; Tomokiyo, K.; Sorita, K.; Shiokawa, J. Luminescence of Divalent Europium Complexes with Crown Ethers and Polyethylene Glycols. *J Chem Soc Chem Commun* **1980**, No. 19, 914–915. https://doi.org/10.1039/C39800000914.

(233) Kuda-Wedagedara, A. N. W.; Wang, C.; Martin, P. D.; Allen, M. J. Aqueous Eu^{II}-Containing Complex with Bright Yellow Luminescence. *J Am Chem Soc* **2015**, *137* (15), 4960–4963. https://doi.org/10.1021/jacs.5b02506.

(234) Pourmand, A.; Dauphas, N. Distribution Coefficients of 60 Elements on TODGA Resin: Application to Ca, Lu, Hf, U and Th Isotope Geochemistry. *Talanta* **2010**, *81* (3), 741–753. https://doi.org/10.1016/j.talanta.2010.01.008.